EPA-600/2-76-280
October 1976

Environmental Protection Technology Series

PARTICULATE SIZING TECHNIQUES FOR CONTROL DEVICE EVALUATION: CASCADE IMPACTOR CALIBRATIONS

Industrial Environmental Research Laboratory
Office of Research and Development
U.S. Environmental Protection Agency
Research Triangle Park, North Carolina 27711

RESEARCH REPORTING SERIES

Research reports of the Office of Research and Development, U.S. Environmental Protection Agency, have been grouped into five series. These five broad categories were established to facilitate further development and application of environmental technology. Elimination of traditional grouping was consciously planned to foster technology transfer and a maximum interface in related fields. The five series are:

1. Environmental Health Effects Research
2. Environmental Protection Technology
3. Ecological Research
4. Environmental Monitoring
5. Socioeconomic Environmental Studies

This report has been assigned to the ENVIRONMENTAL PROTECTION TECHNOLOGY series. This series describes research performed to develop and demonstrate instrumentation, equipment and methodology to repair or prevent environmental degradation from point and non-point sources of pollution. This work provides the new or improved technology required for the control and treatment of pollution sources to meet environmental quality standards.

EPA REVIEW NOTICE

This document is available to the public through the National Technical Information Service, Springfield, Virginia 22161.

EPA-600/2-76-280
October 1976

PARTICULATE SIZING TECHNIQUES FOR CONTROL DEVICE EVALUATION: CASCADE IMPACTOR CALIBRATIONS

by

Kenneth M. Cushing, George E. Lacey,
Joseph D. McCain, and Wallace B. Smith

Southern Research Institute
2000 Ninth Avenue, South
Birmingham, Alabama 35205

Contract No. 68-02-0273
ROAP No. 21ADM-011
Program Element No. 1AB012

EPA Project Officer: D. Bruce Harris

Industrial Environmental Research Laboratory
Office of Energy, Minerals, and Industry
Research Triangle Park, NC 27711

Prepared for

U.S. ENVIRONMENTAL PROTECTION AGENCY
Office of Research and Development
Washington, DC 20460

FOREWORD

As part of a program to evaluate pollution control devices for stationary sources, the Process Measurement Branch, Industrial Environmental Research Laboratory, Environmental Protection Agency, has contracted Southern Research Institute to improve the state of the art for making particle size measurements. Although this work is continuing, the completion of this initial contract represents the attainment of a significant milestone because it has lead to the understanding and solution of several important problems related to particle sizing. This work has resulted in several reports which describe the development of prototype systems and procedures for making particle size measurements in industrial flue gases.

This final report includes the results of a calibration study which was done to evaluate and quantify the behavior of cascade impactors and to determine the accuracy of theories for predicting their performance. The data included in this report are unique and should be beneficial to cascade impactor users and manufacturers.

Sabert Oglesby, Jr.
Vice President
Southern Research Institute

ABSTRACT

A calibration study of five commercially available cascade impactors has been conducted to determine sizing parameters and wall losses. A Vibrating Orifice Aerosol Generator was used to produce monodisperse ammonium fluorescein aerosol particles 18 micrometers to 1 micrometer in diameter. A pressurized Collison Nebulizer System was used to disperse Dow Corning Polystyrene Latex (PSL) spheres 2 micrometers to 0.46 micrometer in diameter. When ammonium fluorescein was used the mass collected by each impactor surface was determined using absorption spectrophotometry of washes from the various surfaces. When sizing with the PSL spheres a Climet Instruments Model 208A Particle Analyzer was used to determine particle number concentrations at the inlet and outlet of the test impactor. Results are reported showing stage collection efficiency as a function of the square root of the Stokes number, stage collection efficiency as a function of particle size, and impactor wall losses (total, nozzle, and inlet cone) as a function of particle size. It has been determined that the values of the Stokes number for the 50% collection efficiency are not generally the same for each impactor stage. A table of these values is presented. Published theories do not successfully predict these $\sqrt{\psi}_{50}$ values, so empirical calibration is required before these devices can be accurately used in the field or laboratory.

CONTENTS

FIGURES

FIGURES (CONT'D)

FIGURES (CONT'D)

FIGURES (CONT'D)

FIGURES (CONT'D)

FIGURES (CONT'D)

FIGURES (CONT'D)

TABLES

LIST OF ABBREVIATIONS AND SYMBOLS

ABBREVIATIONS

ACFM -- Actual Cubic Feet Per Minute
C -- Cunningham Slip Correction Factor, dimensionless
C_v -- Vibrating Orifice Generator Solution Concentration
D_p -- Particle Diameter, cm
d_p -- Vibrating Orifice Generator Dry Particle Diameter, cm
D_{p50} -- Particle Diameter at 50% Collection Efficiency
D_j -- Impactor Stage Jet Diameter, cm
F -- Vibrating Orifice Generator Crystal Oscillation Frequency, Hz
LPM -- Liters Per Minute
PCNS -- Pressurized Collison Nebulizer System
Q -- Vibrating Orifice Generator Solution Flowrate, cm^3/min
RE -- Reynolds Number, $\rho V_j D_j/\mu$ or $\rho V_j\ 2W/\mu$
S -- Impactor Jet to Plate Spacing, cm
T -- Impactor Jet Throat Length, cm
V_j -- Impactor Jet Velocity, cm/sec
VOAG -- Vibrating Orifice Aerosol Generator
W -- Impactor Jet Slot Width, cm

Symbols

ρ -- Gas Density, gm/cm^3
$P\rho$ -- Density of Particle
μ -- Gas Viscosity, poise
ψ -- Stokes Number, dimensionless
$\sqrt{\psi}_{50}$ -- Square Root of Stokes Number at 50% Collection Efficiency

ACKNOWLEDGMENTS

The cooperation, helpful suggestions and overall interest shown by the Project Officer, D. Bruce Harris, during this three year study is gratefully acknowledged.

SECTION 1

INTRODUCTION

This final report for EPA Contract Number 68-02-0273 presents a comprehensive description of the methods and results of a two year evaluation and calibration study of five commercially available cascade impactors. These cascade impactors and their manufacturers are listed below:

1.) Andersen Mark III Stack Sampler (Andersen)
Andersen 2000, Inc.
Atlanta, Georgia 30320

2.) Brink Model BMS-11 Cascade Impactor (Brink)
Monsanto Enviro-Chem Systems, Inc.
St. Louis, Missouri 63166

3.) MRI Model 1502 Inertial Cascade Impactor (MRI)
Meteorology Research, Inc.
Altadena, California 91001

4.) Sierra Model 226 Source Cascade Impactor (Sierra)
Sierra Instruments, Inc.
Carmel Valley, California 93924

5.) University of Washington Mark III Source Test Cascade Impactor (U. of W.)
Pollution Control Systems, Inc.
Renton, Washington 98055

The normal 5-stage Brink impactor has been modified by Southern Research Institute to include an inline cyclone precollector, a "0" stage, and a "6" stage.

Table 1 includes the operational parameters of the five cascade impactors used in this study. The Brink was the only impactor tested with two types of collection media. The Sierra impactor was the only one systematically tested at two different flowrates.

The Andersen impactor is used with glass fiber substrates supplied by the manufacturer. For the Brink impactor a small disc of glass fiber material was tested as well as a thin grease

TABLE 1

Cascade Impactor Calibration Study
Operational Parameters

Laboratory Conditions - 73°F/22°C 29.5" Hg/750 mm Hg

Aerosol Particles - Ammonium Fluorescein Density - 1.35 gm/cm^3
- Polystyrene Latex Density - 1.00 gm/cm^3

Impactor	No. of Stages	Substrate Material	Nominal Sampling Flowrate
Andersen	8	Pre-cut glass fiber filter mats	0.5 ACFM/ 14.16 LPM
Brink (Modified)	7	Glass fiber filter inserts	0.03 ACFM/ .85 LPM
Brink (Modified)	7	Greased collection plates	0.03 ACFM/ .85 LPM
MRI	7	Greased collection plates	0.5 ACFM/ 14.16 LPM
Sierra	6	Pre-cut glass fiber filter mats	0.5 ACFM/ 14.16 LPM
Sierra	6	Pre-cut glass fiber filter mats	0.25ACFM/ 7.08 LPM
U of Washington	7	Greased collection plates	0.5 ACFM/ 14.16 LPM

layer. The MRI and U. of W. impactors are used with thin films of grease on the collection plates. The Sierra is supplied with pre-cut glass fiber mats.

The individual stage parameters for the Andersen, Brink, MRI, Sierra, and U. of W. are listed in Table 2 through Table 6, respectively. Even though the critical interior dimensions of each impactor were supplied by the manufacturer, a measurement of each quantity was also performed as a check. This was necessary because differences in a jet diameter, for example, can have a major influence on the collection characteristics of an impactor stage. The Cumulative Fraction of the Impactor Pressure Drop at each Stage was measured at the nominal flowrate; however, this relationship should be valid at all practical flowrates for which each impactor could be used. The Reynolds number and jet velocities are based on the nominal flowrates given for each impactor in Table 1.

To the user of an inertial cascade impactor the most important consideration is the degree to which the data that is obtained will duplicate the actual particulate size distribution which is sampled. In order to transform the mass collected by several impaction stages into a size distribution, an accurate knowledge of the relationship between collection efficiency and particulate size for each stage is essential.

Theoretically, cascade impactor operation can be described by the theory of impaction from a jet. The end result of such a calculation is impaction efficiency versus particle size. Impaction efficiency is defined as the fraction of particles of a certain size in the jet which impact on a collection plate. This value can be obtained theoretically or experimentally under ideal conditions. The collection efficiency of an impactor stage, however, is the ratio of the mass (or number) of particles of a certain size collected on an impaction surface to the total mass (or number) of particles of the same size in a jet impinging on that surface. The collection efficiency is the product of the theoretical impaction efficiency and the adhesion efficiency.[3] The adhesion efficiency is the fraction of the number of particles which adhere to the surface after touching it by the impaction process. This depends in a large part on the surface characteristics of the particle and collection surface. Thus, there will be disagreement between the theoretical impaction efficiency and the experimentally determined collection efficiency in the cases where particle bounce, reentrainment, electrostatic effects, wall losses and non-ideal geometry have an effect. For this reason, the theory of impaction may not be sufficiently accurate in predicting impactor performance.

TABLE 2

Cascade Impactor Stage Parameters

Andersen Mark III Stack Sampler

Stage No.	No. of Jets	D_j-Jet Diameter (cm)	S-Jet to Plate Distance (cm)	$\frac{S}{D_j}$	Reynolds Number	Jet Velocity (m/sec)	Cumulative Fraction of Impactor Pressure Drop at each stage
1	264	.1638	.254	1.55	45	0.4	0.0
2	264	.1253	.254	2.03	59	0.8	0.0
3	264	.0948	.254	2.68	78	1.3	0.0
4	264	.0759	.254	3.35	98	2.0	0.0
5	264	.0567	.254	4.48	131	3.6	0.0
6	264	.0359	.254	7.08	206	9.0	0.2
7	264	.0261	.254	9.73	284	17.1	0.3
8	156	.0251	.254	10.12	500	31.5	1.0

TABLE 3

Cascade Impactor Stage Parameters

Modified Brink Model B Cascade Impactor

Stage No.	No. of Jets	D_j-Jet Diameter (cm)	S-Jet to Plate Distance (cm)	$\frac{S}{D_j}$	Reynolds Number	Jet Velocity (m/sec)	Cumulative Fraction of Impactor Pressure Drop at each stage
0	1	.3598	1.016	2.82	326	1.4	0.0
1	1	.2439	0.749	3.07	481	3.0	0.0
2	1	.1755	0.544	3.10	669	6.0	0.0
3	1	.1375	0.424	3.08	853	9.7	0.0
4	1	.0930	0.277	2.98	1263	21.2	0.065
5	1	.0726	0.213	2.93	1617	35.3	0.255
6	1	.0573	0.191	3.33	2049	58.8	1.000

TABLE 4

Cascade Impactor Stage Parameters

MRI Model 1502 Inertial Cascade Impactors

Stage No.	No. of Jets	D_j-Jet Diameter (cm)	S-Jet to Plate Distance (cm)	$\frac{S}{D_j}$	Reynolds Number	Jet Velocity (m/sec)	Cumulative Fraction of Impactor Pressure Drop at each stage
1	8	0.870	0.767	.88	281	0.5	0.0
2	12	0.476	0.419	.88	341	1.1	0.0
3	24	0.205	0.191	.96	411	3.2	0.0
4	24	0.118	0.191	1.61	684	8.9	0.0
5	24	0.084	0.191	2.27	973	18.2	0.045
6	24	0.052	0.191	3.60	1530	45.9	0.216
7	12	0.052	0.191	3.60	3059	102.3	1.000

TABLE 5

Cascade Impactor Stage Parameters

Sierra Model 226 Source Sampler

Stage No.	W-Jet Slit Width (cm)	Jet Slit Length (cm)	S-Jet to Plate Distance (cm)	$\frac{S}{W}$	Reynolds Number (@14.16 lpm)	Jet Velocity (m/sec) (@14.16 lpm)	Cumulative Fraction of Impactor Pressure Drop at each Stage
1	0.3590	5.156	0.635	1.77	602	1.3	0.0
2	0.1988	5.152	0.318	1.60	602	2.3	0.0
3	0.1147	3.882	0.239	2.08	800	5.4	0.0
4	0.0627	3.844	0.239	3.81	808	10.0	0.154
5	0.0358	3.869	0.239	6.68	802	17.4	0.308
6	0.0288	2.301	0.239	8.30	1348	36.9	1.000

TABLE 6

Cascade Impactor Stage Parameters

University of Washington Mark III Source Test Cascade Impactor

Stage No.	No. of Jets	D_j-Jet Diameter (cm)	S-Jet to Plate Distance (cm)	$\frac{S}{D_j}$	Reynolds Number	Jet Velocity (m/sec)	Cumulative Fraction of Impactor Pressure Drop at each Stage
1	1	1.842	1.422	.78	1073	0.9	0.0
2	6	0.577	0.648	1.12	565	1.5	0.0
3	12	0.250	0.318	1.27	653	4.1	0.0
4	90	0.0808	0.318	3.94	269	5.2	0.019
5	110	0.0524	0.318	6.07	340	10.2	0.057
6	110	0.0333	0.318	9.55	535	25.4	0.189
7	90	0.0245	0.318	12.98	929	60.0	1.000

The theory of the impaction process has been developed by several researchers[1,5] to a state where the efficiency of impaction can be determined as a function of the particle size (D_p), Reynolds Number (Re), jet diameter or width (D_j,W), the jet to plate distance (S), and the jet throat length (T).

$$E = E\ (D_p,\ Re,\ S/D_j,\ T/D_j)$$

It is common practice to relate the particle size D_p to the square root of the Stokes number, $\sqrt{\psi}$. The Stokes number as defined by Fuchs[4] is the ratio of the particle stopping distance, ℓ, (the distance a particle will travel in air when given an initial velocity, V_o) to the jet diameter or width (D_j or W).

$$\psi = \ell/D_j$$

or
$$\psi = D_p^{\,2}\ \frac{C\rho_p V_o}{18\ \mu\ D_j}$$

C = Cunningham Slip Factor,

D_j = Jet Diameter (cm),

ρ_p = Particle Density (gm/cm^3),

μ = Gas Viscosity (poise), and

V_o = Jet Velocity (cm/sec).

By this procedure, the square root of the Stokes number $\sqrt{\psi}$ is used in impaction theories as a dimensionless quantity proportional to particle size.

$$\sqrt{\psi} = D_p\ \left(\frac{C\rho_p\ V_o}{18\ \mu\ D_j}\right)^{\frac{1}{2}}$$

This parameter is useful in presenting impactor calibration data because data from all stages of an impactor can be placed on a single graph, and under many circumstances would in theory lie along a common curve. The value of $\sqrt{\psi}$ at 50% collection efficiency, $\sqrt{\psi_{50}}$, defines the impaction stage D_{50}, the particle size at which half the particles of that size are collected and half are passed to the next stage. Thus, D_{50} is used as the effective stage cut diameter.

Recently Marple[5] has been able to construct theoretical impaction efficiency curves for several values of the jet to plate distance, jet Reynolds Number, and jet throat length. Figure 1 shows the results of these calculations for both round and rectangular jet impactors. The value of the square root of the Stokes number used by Marple, $\sqrt{STK}$, differs from that presented in this paper, $\sqrt{\psi}$, by a factor of $\sqrt{2}$. It can be seen from Figure 1 that for certain ranges of Re, S/D_j; S/W, or T/S; or T/W, the magnitude of $\sqrt{\psi_{50}}$ is sensitive to these parameters. This is a possible explanation for the unpredictability of commercial impactor behavior; e.g., compare Tables 2 through 6 and Figure 1.

During the course of this investigation several types of measurements were made. Wall losses for each impactor were measured when sampling ammonium fluorescein aerosols. Stage collection efficiencies for each impactor were determined for particle sizes from 15 micrometers diameter to approximately 0.4 micrometers. When sampling ammonium fluorescein aerosols it was possible to measure the collection efficiencies both corrected and uncorrected for wall losses. Because of the method used to sample polystyrene spheres, the collection efficiency data includes wall losses in the collection efficiency of the stage being tested.

Section 3 contains a description of the experimental procedures and the results are given in Section 4.

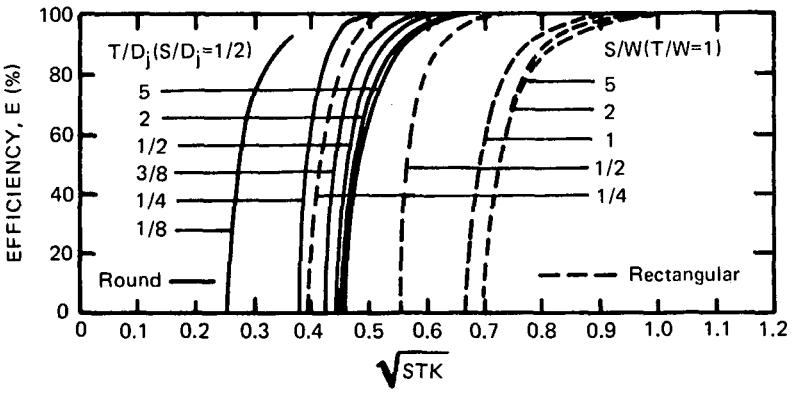

(a) EFFECT OF JET TO PLATE DISTANCE (Re=3,000)

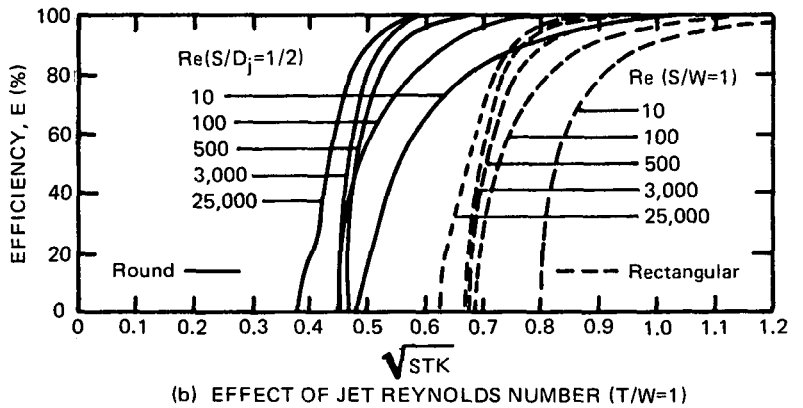

(b) EFFECT OF JET REYNOLDS NUMBER (T/W=1)

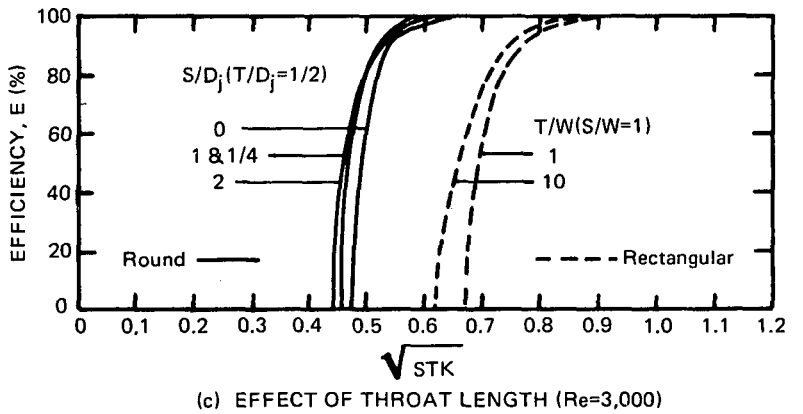

(c) EFFECT OF THROAT LENGTH (Re=3,000)

Figure 1. Theoretical impactor efficiency curves for rectangular and round impactors showing the effect of jet-to-plate distance S, Reynolds number Re, and throat length T.[5] Note that $\sqrt{STK} = D_p(C\rho_p V_0/9\ \mu D_j)^{\frac{1}{2}}$, whereas $\sqrt{\psi} = D_p(C\rho_p V_0/18\ \mu D_j)^{\frac{1}{2}}$.

SECTION 2

CONCLUSIONS

Five commercially available cascade impactors have been calibrated during this study. The method of calibration and the presentation of the results should make this data useful to both the field operator of these devices as well as those interested in the theory of impactor design.

Based on this work several conclusions can be drawn.

1. The value of $\sqrt{\psi_{50}}$ for each stage of a multiple stage impactor may be different. Prior to the current awareness of the importance of impactor calibration, it was the practice of many cascade impactor manufacturers and users to assume that the value of $\sqrt{\psi_{50}}$ for every stage was identical. In many cases the experimental value determined by Ranz and Wong[1] was used. Attempts to perform calibrations were not comprehensive. The theories of cascade impactor operation at this time do not describe the behavior of cascade impactors accurately enough to make it unnecessary to calibrate each device empirically. It is hoped that the data presented here will aid in the development of theoretical expressions which will better predict the behavior of cascade impactors.

2. The stage collection efficiencies are sensitive to the type of impactor collection substrate which is used. This is evident in the comparison of the Brink Cascade Impactor data using glass fiber collection substrates and greased collection plates. This strong dependence of collection efficiency on stage collection substrate material has also been explicitly illustrated and discussed by Willeke[2] and Rao.[3]

3. In the majority of cases the stage collection efficiency never reaches 100% for any particle size but reaches a maximum value that usually falls between 80% and 95%. This implies that some greatly oversized particles will reach every stage beyond the first stage. Unless suitable compensation can be made for the presence of these oversized particles, their presence will tend to bias the apparent particle size distribution toward higher than actual concentrations of fine particles and reduced concentrations of large particles. These errors probably tend to be more significant for the fine particle end of the distribution.

4. Ideally, an impactor stage should reach 100% collection efficiency for some particle size and stay at that value for all larger particle sizes. In practice, however, this is not the case as demonstrated by this study. In general the stage collection efficiency reaches a maximum less than 100% and then rolls off and decreases for particles larger than a certain size. This is attributed to the fact that these larger particles strike the plate with appreciable momentum, bounce, and are thus carried to a lower stage. The use of grease on the collection plates as well as a reduction in the impactor flowrate tends to decrease the magnitude of this problem. The Sierra impactor data illustrate the increase in collection efficiency which resulted from a decrease in sampling flowrate and concomitant reduction in bounce and cascading of large particles to lower stages. This study shows that in some cases the maximum efficiency was almost doubled by lowering the flowrate. A discussion of this phenomenon has also been presented by Rao.[3]

SECTION 3

DESCRIPTION OF EXPERIMENTAL PROCEDURES

Laboratory evaluation of the cascade impactors tested during this study involved the use of two types of particle generation systems, a Vibrating Orifice Aerosol Generator (VOAG) and a Pressurized Collison Nebulizer System (PCNS). The VOAG was used to generate monodisperse ammonium fluorescein particles with diameters from 18 micrometers to 1 micrometer. The PCNS was used to disperse three sizes of monodisperse Dow Corning Polystyrene Latex (PSL) spheres, 2.02 micrometers, 0.82 micrometer, and 0.46 micrometer diameter.

The VOAG used in this study was designed and built at Southern Research Institute, although similar devices have been reported by several authors previously[6,7,8], and a commercial unit is available from Thermo Systems, Inc.*

Figure 2 is a schematic diagram showing the operating principle of the VOAG. A solution of known concentration (in our case, a solution of fluorescein ($C_{20}H_{12}O_5$) in 0.1N NH_4OH is forced through a small orifice (5, 10, 15, or 20 μm diameter). The orifice is attached to a piezoelectric ceramic which, under electrical stimulation, will vibrate at a known frequency. This vibration imposes periodic perturbations on the liquid jet causing it to break up into uniformly-sized droplets. Knowing the liquid flow rate and the perturbation frequency, the droplet size can be readily calculated. The solvent evaporates from the droplets leaving the non-volatile solute as a spherical residue. The final dry particle size can be calculated from the droplet size through the known concentration of the liquid solution.

To calculate the dry particle size, the expression

$$d_p = \left(\frac{QC_v}{10\pi F}\right)^{1/3} \quad \text{is used,}$$

*Thermo Systems, Inc., 2500 N. Cleveland, St. Paul, Minn. 55113

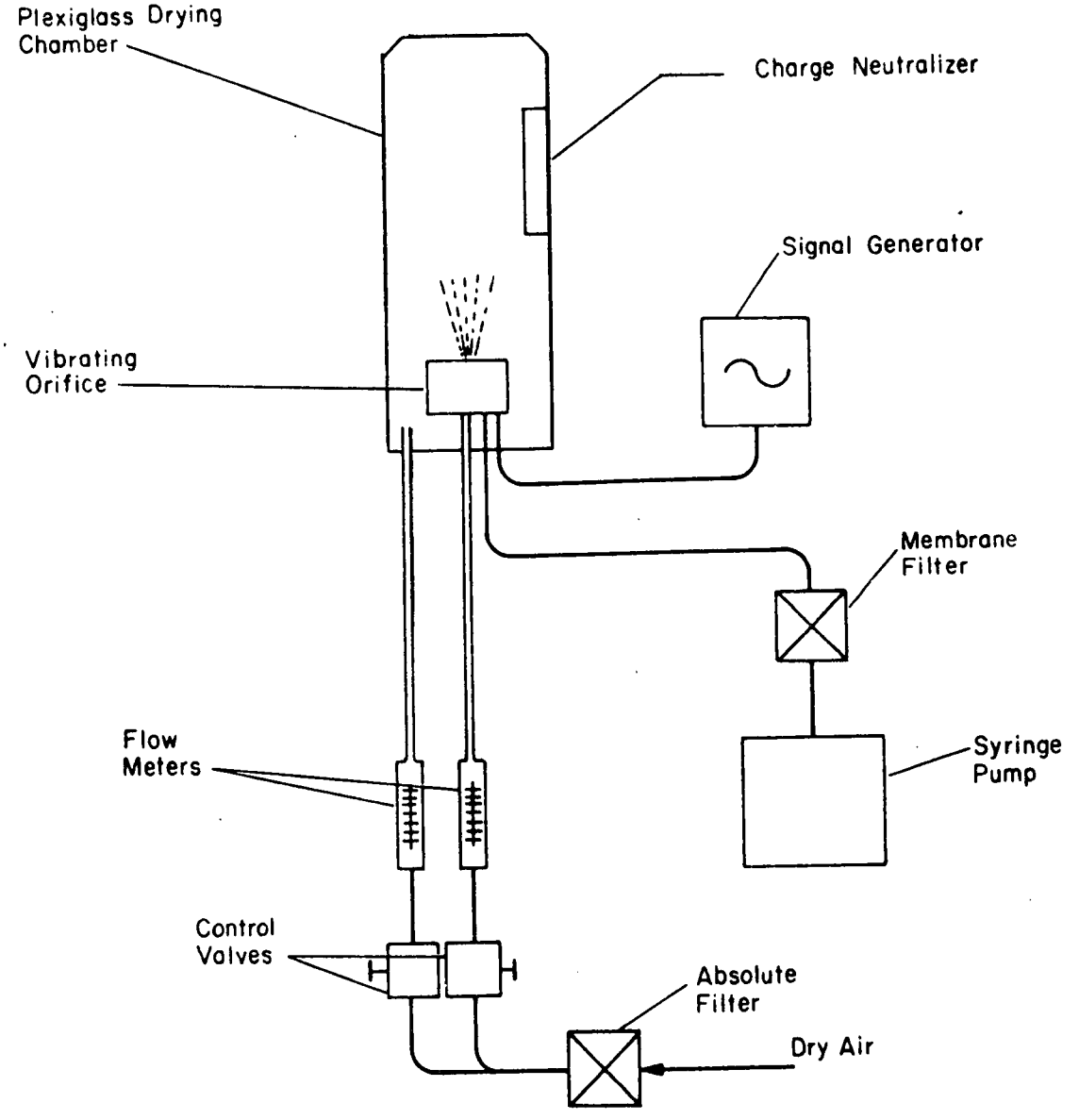

Figure 2. Schematic representation of the Vibrating Orifice Aerosol Generator.

where C_v is the solution concentration or $\frac{\text{volume of solute}}{\text{volume of solution}}$,

Q is the solution flow rate (cm^3/min), and

F is the perturbation frequency (Hz).

By the use of smaller orifices, one can obtain much higher operating frequencies. This in turn yields higher particle number concentrations and allows a shorter running time to collect the same mass per stage. The running time must be sufficiently long, however, to allow accurate determination of the stage collection efficiencies and wall losses. It was our experience that the 20 μm orifice was consistently easier to use in particle generation, primarily because of fewer clogging problems.

Prior to particle generation the orifices were washed in detergent with ultrasonic agitation and then rinsed several times in distilled water, also with ultrasonic agitation. After the filter and liquid handling system was flushed several times with the aerosol solution to be used, an orifice was placed, still wet with distilled water, or blown dry, into the crystal holder and the syringe pump turned on. A jet of air was played over the orifice to keep the surface clean until enough pressure was built up behind the orifice to form a jet.

After a stream of particles was generated, a determination of monodispersity had to be made. Two methods were used to accomplish this. By using a small, well-defined air jet to deflect the stream of particles, it was possible to tell when the aerosol was mono or polydisperse. Depending on particle size, the stream was deflected by the air at different angles, and if the aerosol was polydisperse, several streams could be seen at one time. By varying the crystal oscillation frequency, the system could be fine-tuned to give only a single deflected particle stream, thus indicating monodispersity. On several occasions, the aerosol tended to drift from monodispersity. To protect against this occurrence, periodic filter samples were taken and checked by optical microscopy. This also provided a good check on the sphericity of the aerosol because the final particles were investigated instead of the primary liquid droplets. The microscopy thus served as a check on proper drying, satellites, correct size, and multiplets. Polonium 210 alpha particle sources were placed near the air stream as charge neutralizers to reduce agglomeration and loss of particles due to electrostatic forces. A three-foot-high plexiglass cylinder was placed on the generator and dispersion and dilution air turned on to disperse, dilute and loft the particles into a plenum with several sampling ports. During each test, filter samples were drawn at intervals to insure continued monodispersity. Because of its nonhygroscopicity and physical[9]

properties, ammonium fluorescein was used throughout these studies as the test aerosol, although in theory, any material that will dissolve readily in an evaporable solvent could be used. Figure 3 shows one of the test aerosols generated with the VOAG. In general, it was found that about 4% to 8% by mass of the particles were of twice the volume (1.26 X diameter) of the primary particles. Solvent impurities limited the smallest size which could be generated with the VOAG using ammonium fluorescein to approximately 1 micrometer diameter. Thus optical microscopy was used as a secondary validation of particle size.

When it had been determined that particles of the correct size were being generated, each cascade impactor was allowed to sample from the plenum for the required length of time to collect a suitable sample. Nonisokinetic sampling was performed; however, it was determined by a series of tests that this did not affect the collection efficiency of the impactor stages as compared to isokinetic sampling results. It is likely that the nozzle losses were influenced however.

Several impactors tested are normally used with a greased substrate material on the collection plates. After several trials using Dow Corning High Vacuum Silicone Grease, Agar, K-Y Jelly, and Vaseline*, it was found that Vaseline was the most convenient material to use as a substrate medium for this study because it goes easily into solution in a small amount of benzene permitting easy separation of the particles from the substrate coating.

In all cases, a back-up filter was used to collect material not caught by the last impaction stage of each device. This allowed the calculation of the collection efficiency of all stages tested.

A pump and flow-metering device for each impactor insured repeatability in flow rate during each test. After several tests, it was determined that the Brink with bare plates did not perform satisfactorily due to severe particle bounce and reentrainment. Accordingly, testing of the Brink with bare plates was discontinued after sufficient data was taken to prove the unreliability of that configuration as a sizing device. Subsequently, only glass fiber substrates and greased plates were used with the Brink impactor.

At the conclusion of the sampling period, each impactor was carefully disassembled and all internal surfaces cleaned with a solution of 0.1N NH_4OH. Using a known amount of the solution, each plate and surface was washed to dissolve and rinse off the ammonium fluorescein particles. Where Vaseline was used, a small amount of benzene was poured over the greased collection plate in a small dish which was then placed in an ultrasonic cleaner. A small amount of agitation caused the

*Cheesborough-Pond's Inc. N.Y., N.Y. 10017

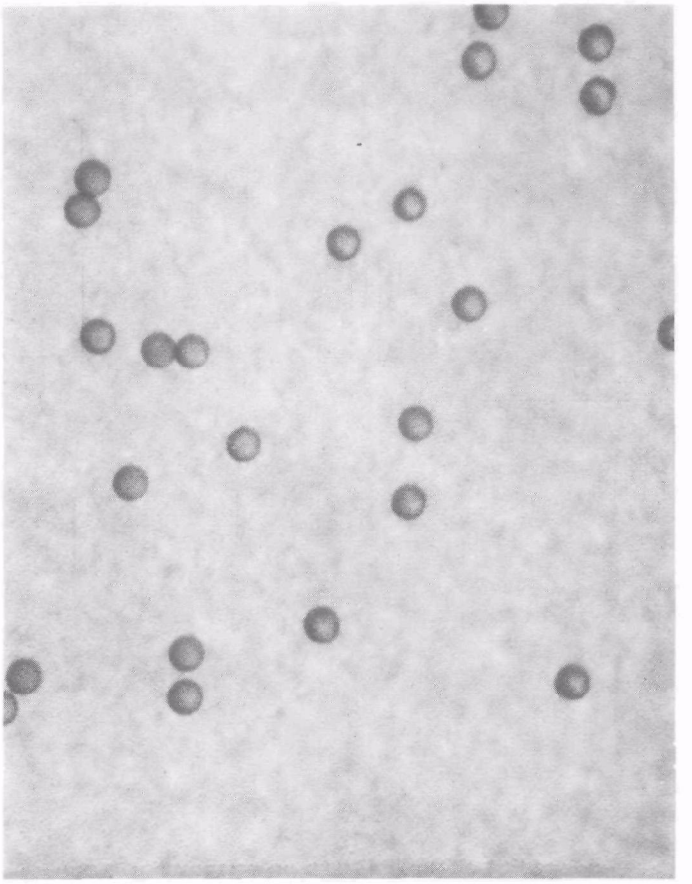

Figure 3. Ammonium fluorescein aerosol particles generated using the Vibrating Orifice Aerosol Generator.

Vaseline to dissolve and the ammonium fluorescein particles to become well mixed. Adding a known amount of 0.1N NH_4OH to the mixture with stirring caused the ammonium fluorescein to dissolve. After the benzene mixture floated to the top of the NH_4OH, the ammonium fluorescein solution was pipetted off.

The quantity of material on each surface was determined by absorption spectroscopy. Initially a Beckman Quartz Spectrophotometer, Model DU, and later a Bausch and Lomb Spectronic 88 Spectrophotometer, calibrated with solutions of known concentration of ammonium fluorescein, were used to measure the concentration of ammonium fluorescein in each wash. From knowledge of the amount of wash solution, the dilution factor, if any, and the absolute concentration, the mass of particles on each surface could be calculated. With the mass on each plate and surface known, the wall losses and stage collection efficiencies could be calculated.

A Pressurized Collison Nebulizer System similar to that reported by Calvert[10] was assembled as shown in Figure 4. A stream of dry dilution air is mixed with the nebulized suspension to reduce the aerosol concentration and to aid in drying. Valves placed upstream of the impactor allow variations in the flowrate. Three sizes of PSL particles were used (2.02 μm, 0.82 μm, and 0.46 micrometers diameter). Each impactor stage was tested at three flowrates near the nominal or designed impactor flowrate. Thus nine calibration points were obtained for each stage of each impactor. A Climet Instruments Model 208A Particle Analyzer was used to monitor the impactor inlet and outlet concentrations. Stages of each impactor were tested individually. This system was designed to allow two different air flow strategies depending on whether the impactor flowrate was higher or lower than the Climet inlet flowrate. Because of the limited availability of large PSL spheres, and because these data were supplementary to the ammonium fluorescein data, only the impactor stages for which information could be obtained with sizes of 2 micrometers diameter and smaller were tested. Generally these were the lower 3 or 4 impactor stages. For simplicity and convenience, mass flowmeters were used to measure the critical gas flowrates.

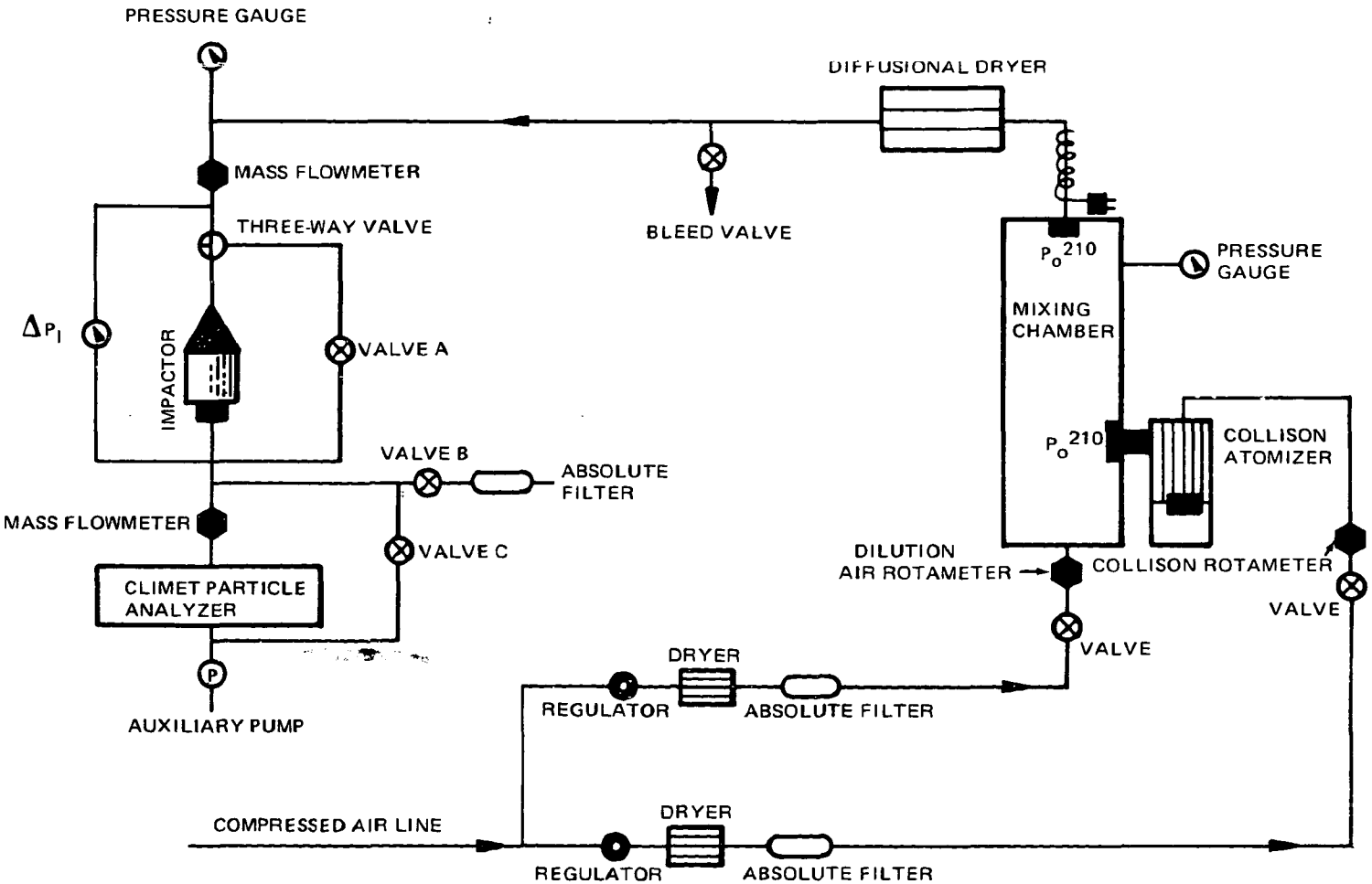

Figure 4. PSL calibration system for high and low flowrate impactor

SECTION 4

RESULTS OF THE CALIBRATION STUDY

WALL LOSSES

During the portion of the calibration procedure using ammonium fluorescein aerosols, data on wall losses were tabulated. By washing each cascade impactor surface after sampling a test aerosol, it was possible to obtain information on particle losses occurring in nozzles, inlet cones, jet plates, and other internal surfaces. These losses were calculated as percentages of the total amount of aerosol entering the impactor. Three types of wall losses were quantified: those occurring in the nozzles alone (Nozzle Wall Loss), those occurring in the inlet cone alone, where applicable (Inlet Cone Wall Loss), and those occurring in the nozzle, inlet cone, and other internal surfaces other than the collection substrates (Total Wall Loss).

The wall loss data are shown in Figures 5 through 11 for the seven impactor configurations tested as Percentage Wall Loss Versus Particle Diameter. Except for Figure 10, all wall loss data are based on the results of non-isokinetic sampling. The degree to which non-isokinetic sampling influenced the Nozzle Wall Loss is unknown.

In general, wall losses tend to decrease with particle size and are negligible for particles smaller than about 1-2 micrometers in diameter. The majority of the losses occur in the nozzles and inlet cones.

Wall losses can be attributed to particle settling, diffusion, electrostatic attraction, bounce, and reentrainment. Visual inspection of the nozzles and inlet cones indicate that the losses were predominantly due to settling. All impactors except the Brink were run in a horizontal position.

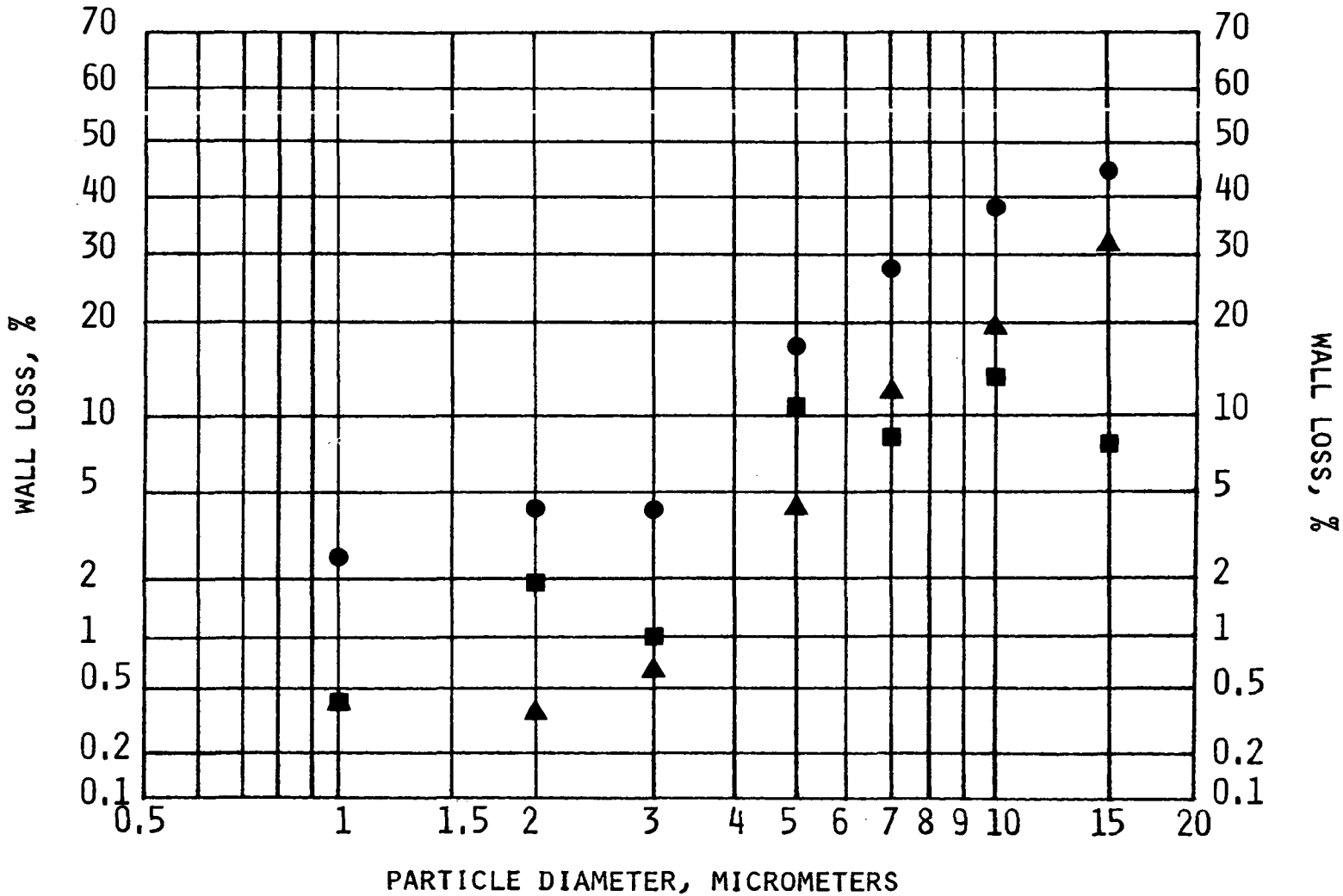

Figure 5. Impactor wall loss versus particle size. Andersen Mark III Stack Sampler. (14 LPM, 22°C, 29.5"Hg, 1.35 gm/cm^3) Nonisokinetic sampling. Total wall loss - ● Nozzle wall loss - ■ Inlet cone wall loss - ▲

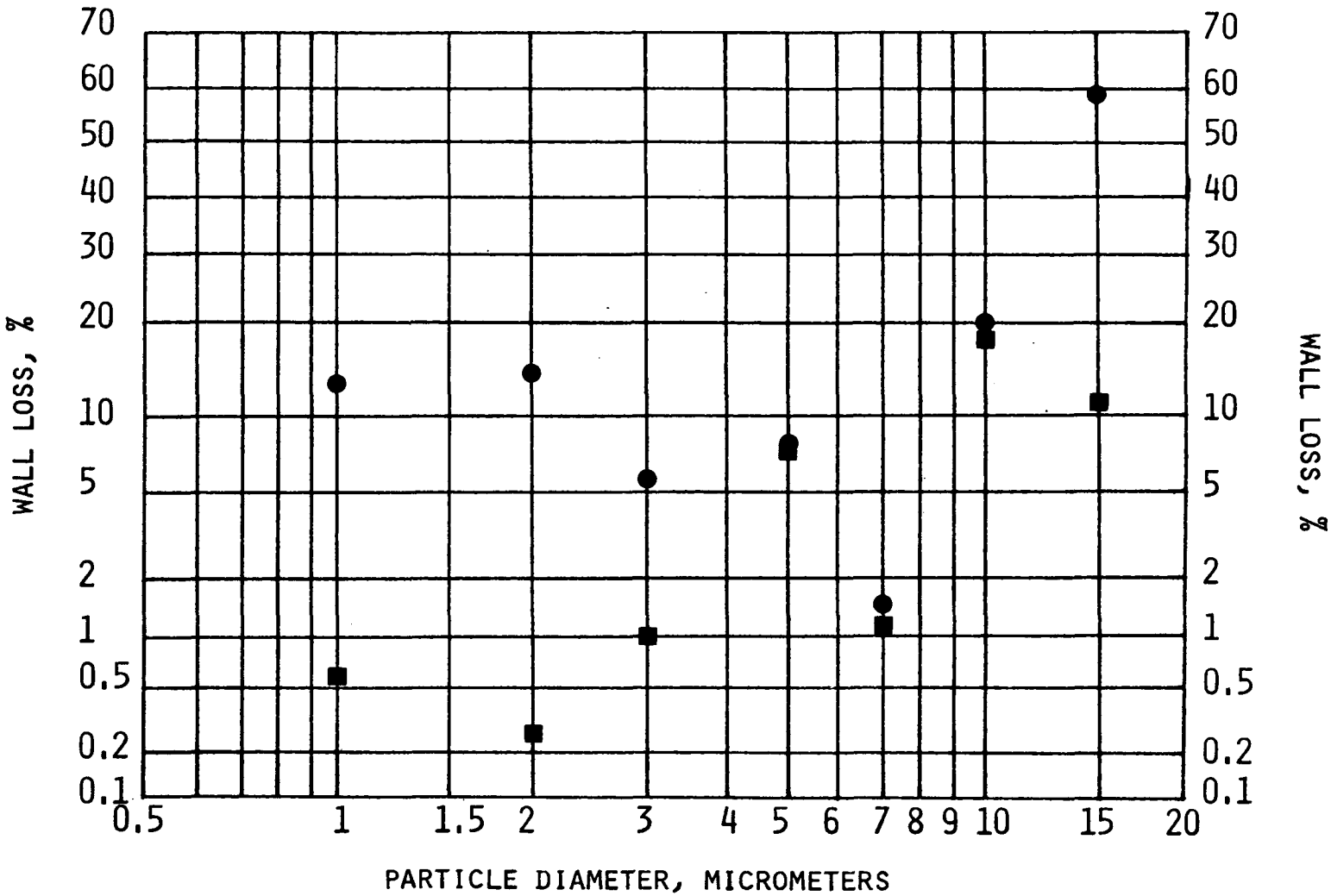

Figure 6. Impactor wall loss versus particle size. Modified Brink Model BMS-11 Cascade Impactor (Glass Fiber Substrates). (0.85 LPM, 22°C, 29.5" Hg, 1.35 gm/cm^3) Nonisokinetic sampling. Total wall loss - ● Nozzle wall loss - ■

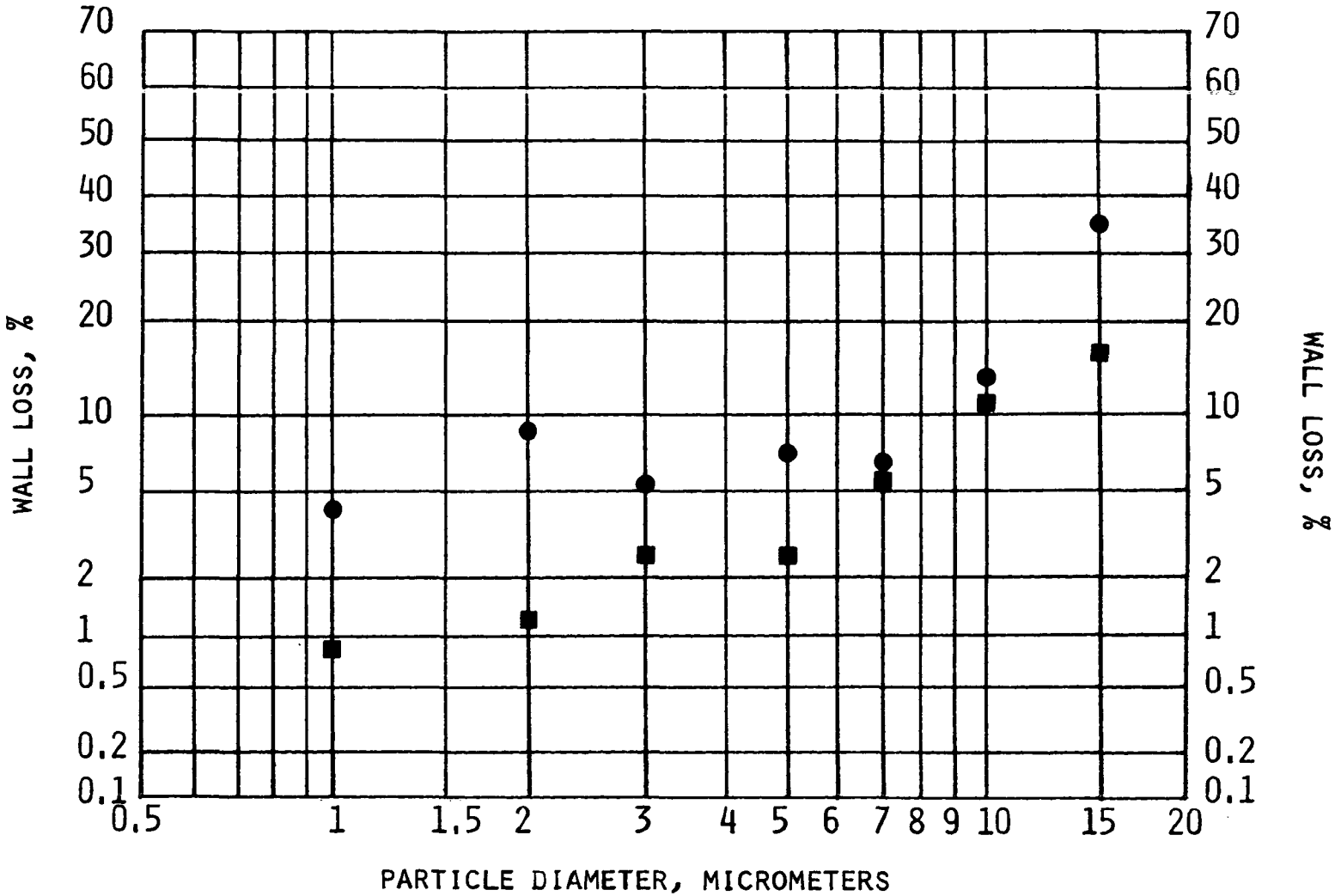

Figure 7. Impactor wall loss versus particle size. Modified Brink Model BMS-11 Cascade Impactor (Greased Collection Plates). (0.85 LPM, 22°C, 29.5"Hg, 1.35 gm/cm^3) Nonisokinetic sampling. Total wall loss - ● Nozzle wall loss - ■

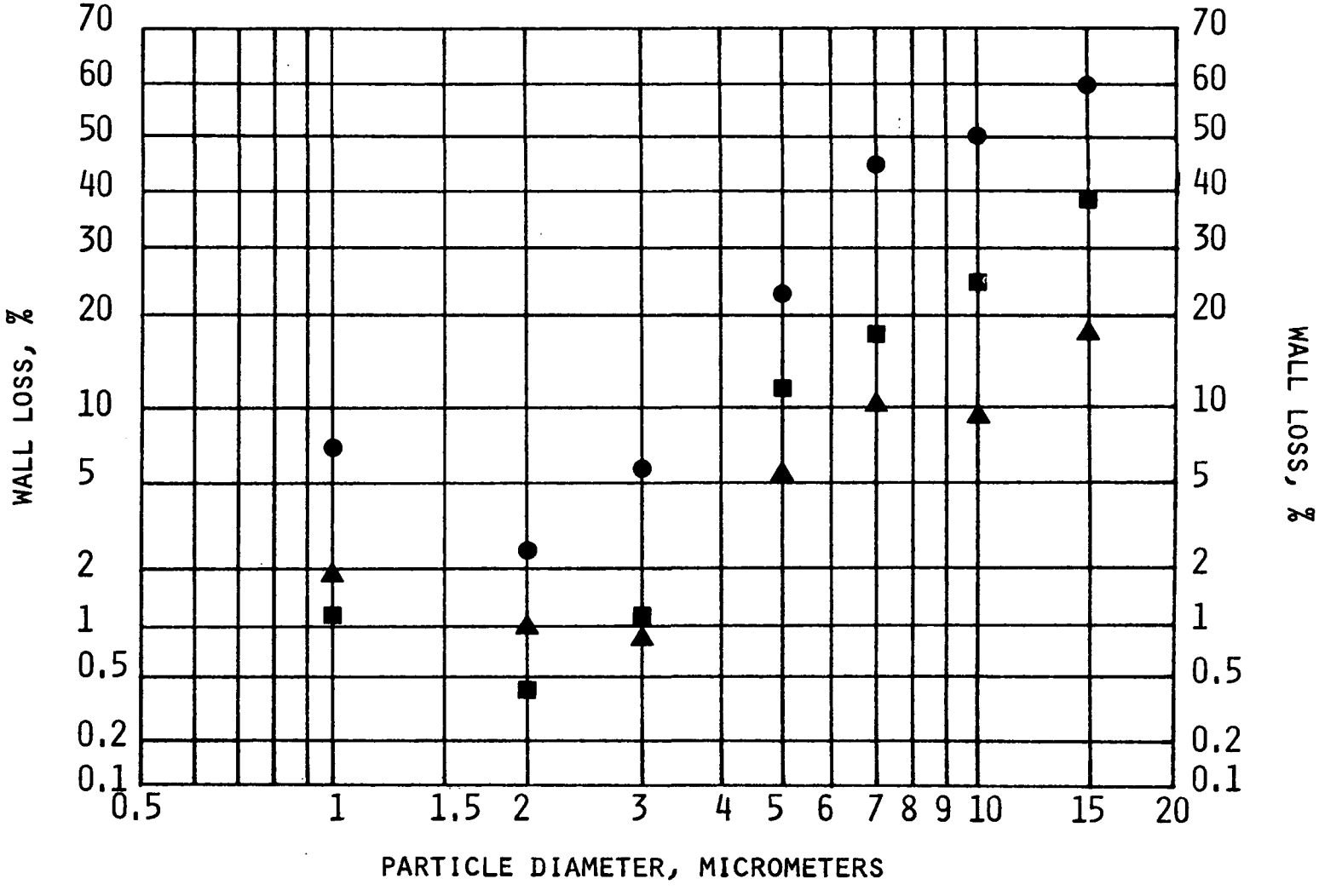

Figure 8. Impactor wall loss versus particle size. MRI Model 1502 Inertial Cascade Impactor. (14 LPM, 22°C, 29.5"Hg, 1.35 gm/cm^3) Noniso-kinetic sampling. Total wall loss - ● Nozzle wall loss - ■ Inlet cone wall loss - ▲

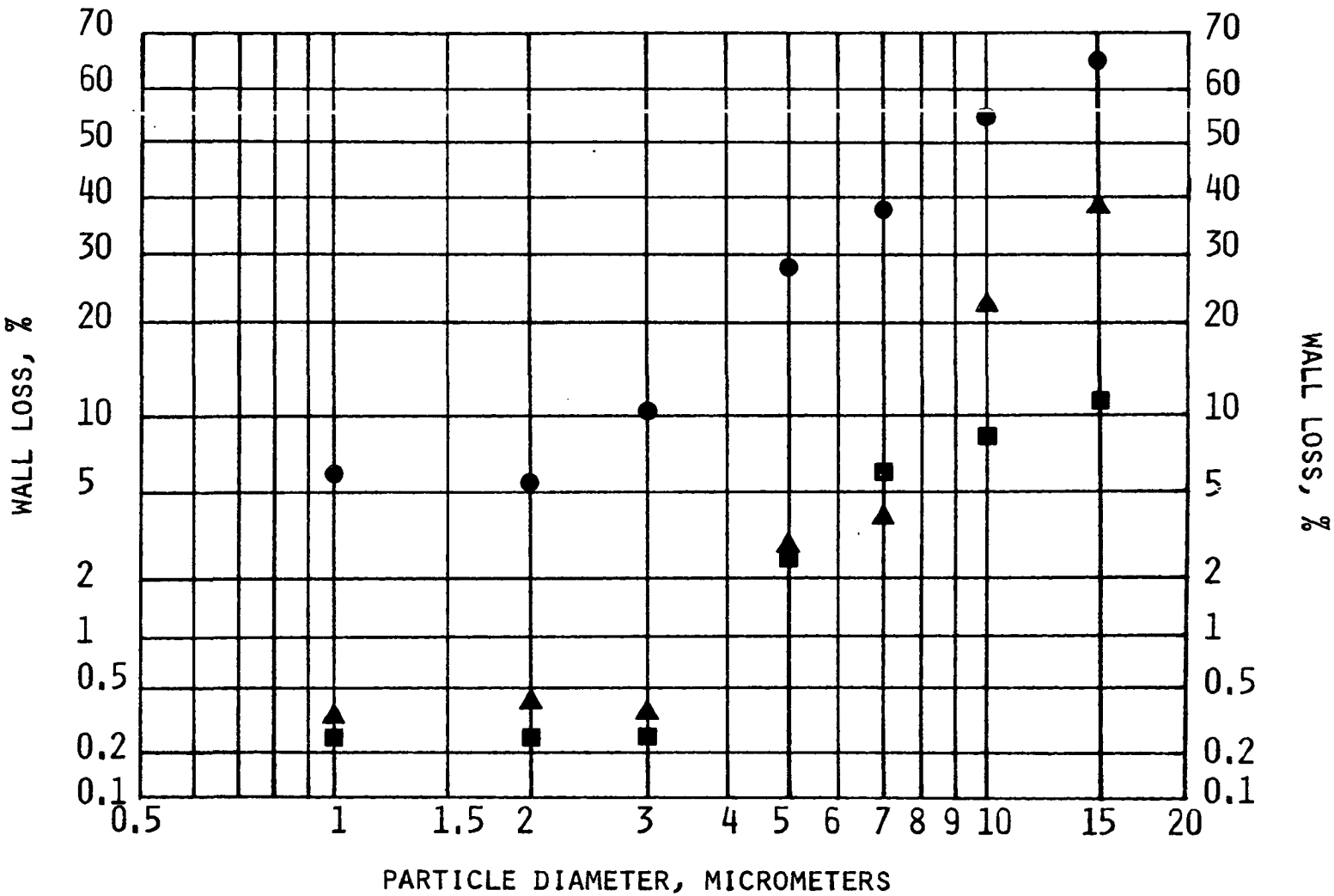

Figure 9. Impactor wall loss versus particle size. Sierra Model 226 Source Cascade Impactor. (14 LPM, 22°C, 29.5"Hg, 1.35 gm/cm^3) Nonisokinetic sampling. Total wall loss - ● Nozzle wall loss - ■ Inlet cone wall loss - ▲

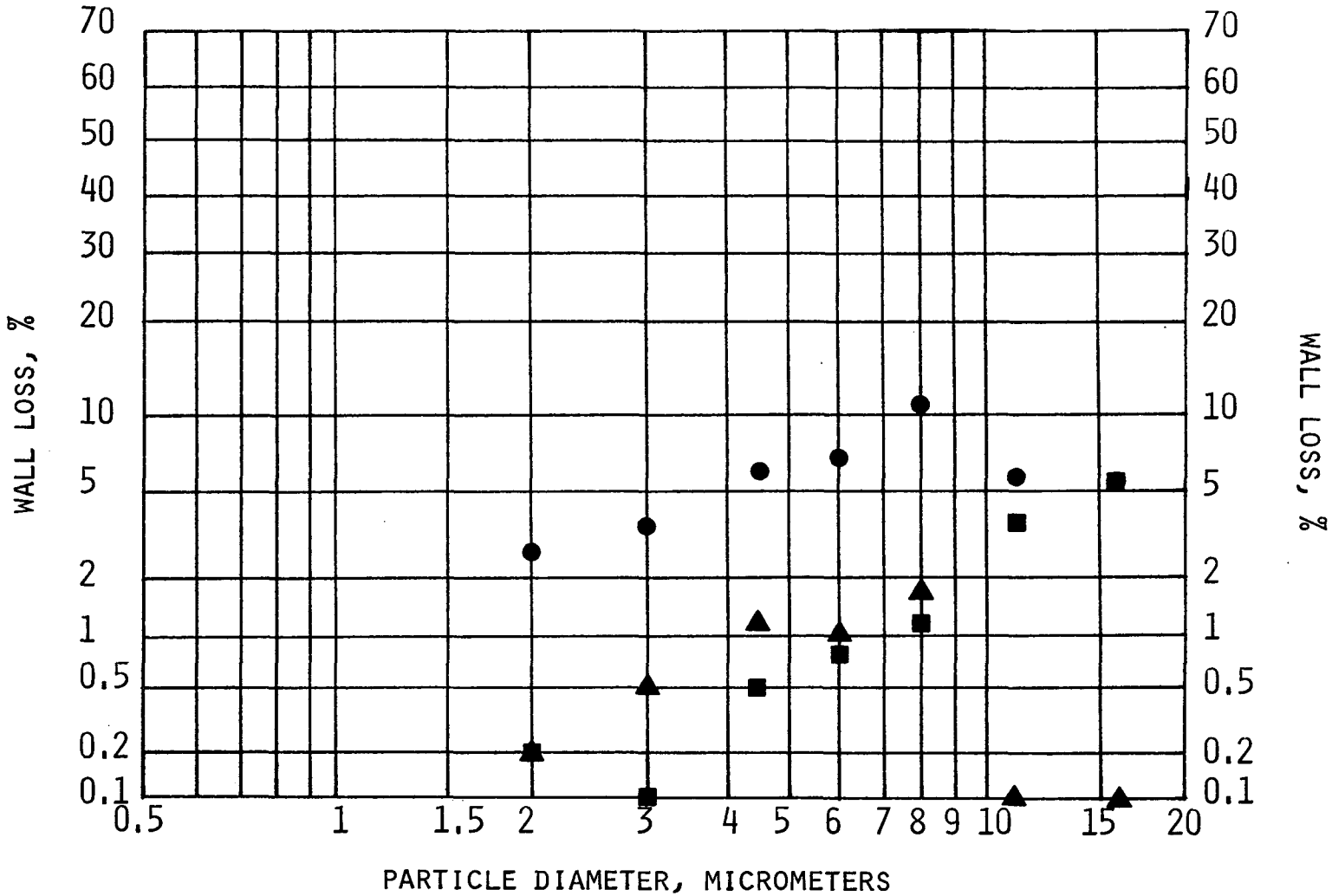

Figure 10. Impactor wall loss versus particle size. Sierra Model 226 Source Cascade Impactor. (7 LPM, 22°C, 29.5"Hg, 1.35 gm/cm^3) Isokinetic sampling. Total wall loss - ● Nozzle wall loss - ■ Inlet cone wall loss - ▲

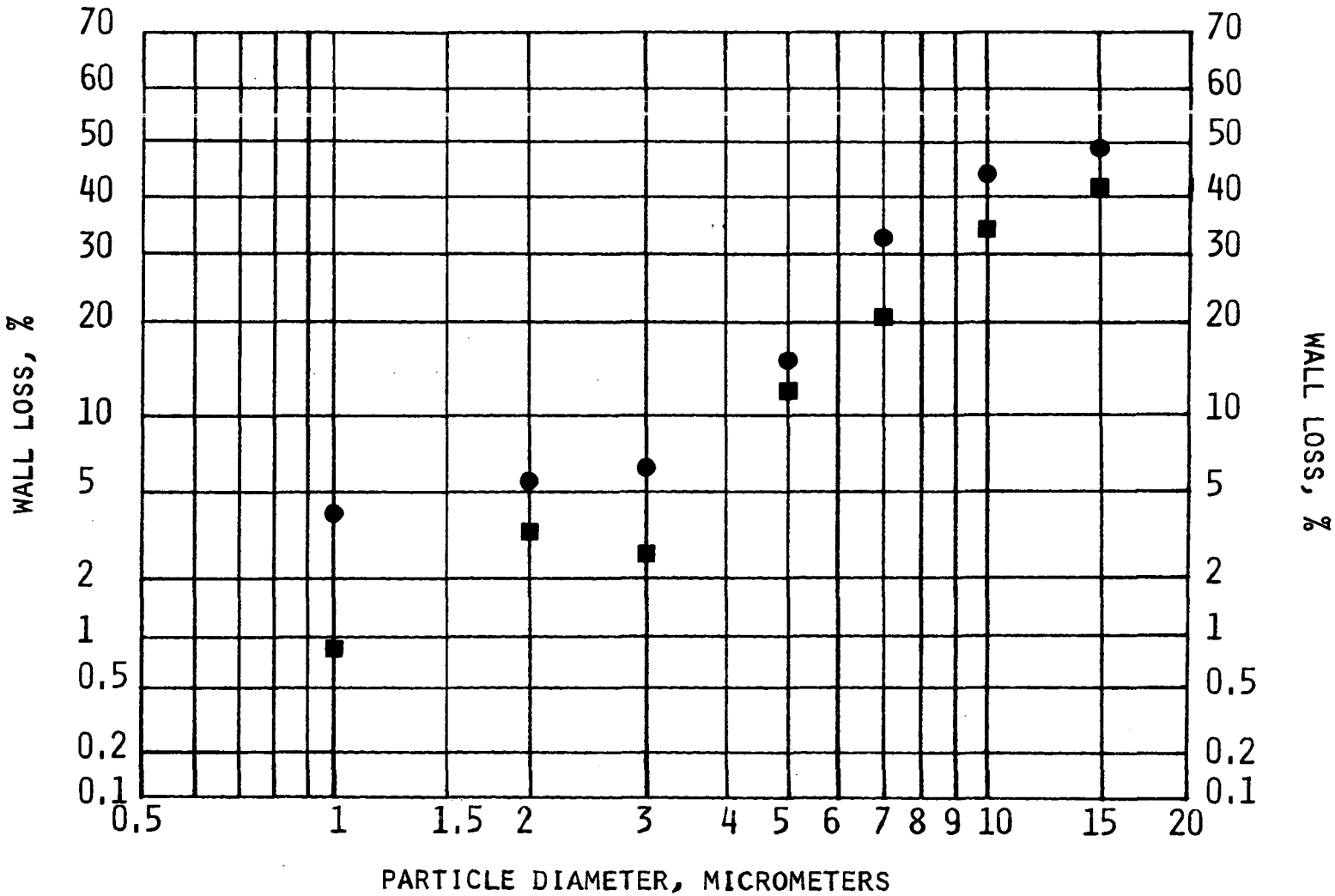

Figure 11. Impactor wall loss versus particle size. University of Washington Mark III Source Test Cascade Impactor. (14 LPM, 22°C, 29.5"Hg, 1.35 gm/cm^3) Nonisokinetic sampling. Total wall loss - ● Nozzle wall loss - ■

CALIBRATION DATA - EFFICIENCY VS. $\sqrt{\psi}$

Recall from the Introduction that if two or more impactor stages have the same Reynolds Number, jet to plate spacing, and jet throat length, then according to theory they should have the same particle collection efficiency for the same magnitude of the square root of the Stokes parameter. If these physical parameters differ, or if different collection substrate media are used, then these curves may not be identical. These differences are evident in Figures 12 through 26, which present in alphabetical order the Stage Collection Efficiency Versus $\sqrt{\psi}$ for each cascade impactor configuration. These efficiencies are based solely on the particles actually collected by an impaction surface and those found downstream of that surface. Particles on other surfaces such as the jet plate above the impaction surface were not included in the efficiency shown in these figures. These same impactor calibration data are shown, calculated on a different basis, in Figures 27 through 41. In these figures the ammonium fluorescein data have been corrected to include wall losses as follows:

The true collection efficiency is defined as the amount of material collected by an impaction stage divided by the amount of material incident on that stage. If material collected in jet nozzles, inlet cones, and jet stage surfaces is combined with the appropriate stage catch, the resulting collection efficiency is not a true collection efficiency as defined above. These "Corrected for Wall Loss" Stage Collection Efficiencies are useful in analyzing results from field tests where particulate collected on surfaces other than the impaction substrates is combined with the regular stage catches. For instance, the material collected in the nozzle, inlet cone, and 1st Jet Stage of the Andersen Mark III would be combined with the mass on the 1st Collection Substrate in order to obtain a total mass which would be presumed to have been caught on this collection substrate, if these wall losses had not occurred. Also, material on any lower jet stage would be combined with the appropriate collection substrate catch. Collection Efficiencies corrected in this way to include wall losses generally have higher magnitudes at all sizes.

The differences in $\sqrt{\psi_{50}}$ for the different impactor stages shown in the foregoing figures require that empirical calibrations be done. No existing theory is comprehensive enough to compensate for the variations in geometry and application techniques for single devices, among different devices, or among different users.

A difference can also be seen between the shapes of the empirical calibration curves and the curves predicted by Marple's theory. The empirical curves show a smooth tail which approaches zero for small values of $\sqrt{\psi}$. Marple's theory, however, predicts a sharp intersection between the efficiency curves and the abscissa. The "tails" are possibly due, at least in part, to the fact that the calibration aerosols cannot be made perfectly monodisperse, and always contain multiplets.[11] Such "tails" are probably unavoidable when using the VOAG, because these devices, at best, produce about 4% doublets at all times.

The graphs also indicate a more severe problem, common to all cascade impactors. On a majority of the stages the collection efficiency does not reach 100% at any value as would be expected theoretically. Also after reaching a maximum point, the curves fall off to lower efficiencies at higher $\sqrt{\psi}$ values. This means that some large particles will not be collected on upper stages and will be passed through the impactor to lower stages or even the back-up filter. An accurate knowledge of this type of behavior is essential to the proper design and application of cascade impactors.

The theoretical data of Marple[5] shown in Figure 1 indicates shifts in the square root of the Stokes Number, $\sqrt{\psi}$, which depend upon the jet to plate spacing ratio (S/D_j) and the Reynolds Number (Re). The values of $\sqrt{\psi}$ corresponding to a given particle collection efficiency increase for increasing Jet to Plate Spacing ratio and decrease for increasing Reynolds Number. Comparison of the values of these parameters as given in Tables 2 through 6 indicates that one would expect the Andersen Mark III behavior to be affected by these parameter variations to a greater extent than some of the other cascade impactors.

For the Andersen Mark III the values of the jet to plate spacing ratio change from about 1.5 to 10 between Stage 1 and 8. Theoretically this should cause the $\sqrt{\psi}$ curve to shift to larger values and become much steeper. The Reynolds Number changes from about 45 to 500 between stages 1 and 8. Theoretically this should cause a shift to the left in the $\sqrt{\psi}$ values as well as causing them to be steeper.

Although it is difficult to pinpoint the exact cause for the shifts in the Andersen data shown in Figures 12, 13, 14, 27, 28, and 29, the general shift to smaller $\sqrt{\psi}$ values and the corresponding increase in steepness could be due, in part, to a combination of these effects due to jet to plate spacing ratio and Reynolds Number.

The values of these parameters for the other impactors indicate that the effects would be much more difficult to separate and characterize because of the smaller changes in these values.

In Table 7 are presented the values of the square root of the Stokes number, at 50% Collection Efficiency, $\sqrt{\psi_{50}}$ for all impactor stages tested, both corrected and uncorrected for wall losses.

CALIBRATION DATA - EFFICIENCY VS. PARTICLE SIZE

The data presented in the previous section are shown in this section as Collection Efficiency Versus Particle Size. Figures 42 through 48 show these data uncorrected for wall losses while Figures 49 through 55 show the data corrected for wall losses. The same features of non-ideal impactor behavior discussed above are also evident in these graphs.

In Table 8 are presented the values of the particle diameter at 50% Collection Efficiency, $D_{p_{50}}$, for all impactor stages tested, both corrected and uncorrected for wall losses when operated at the conditions stated in Table 1 with unit density particles.

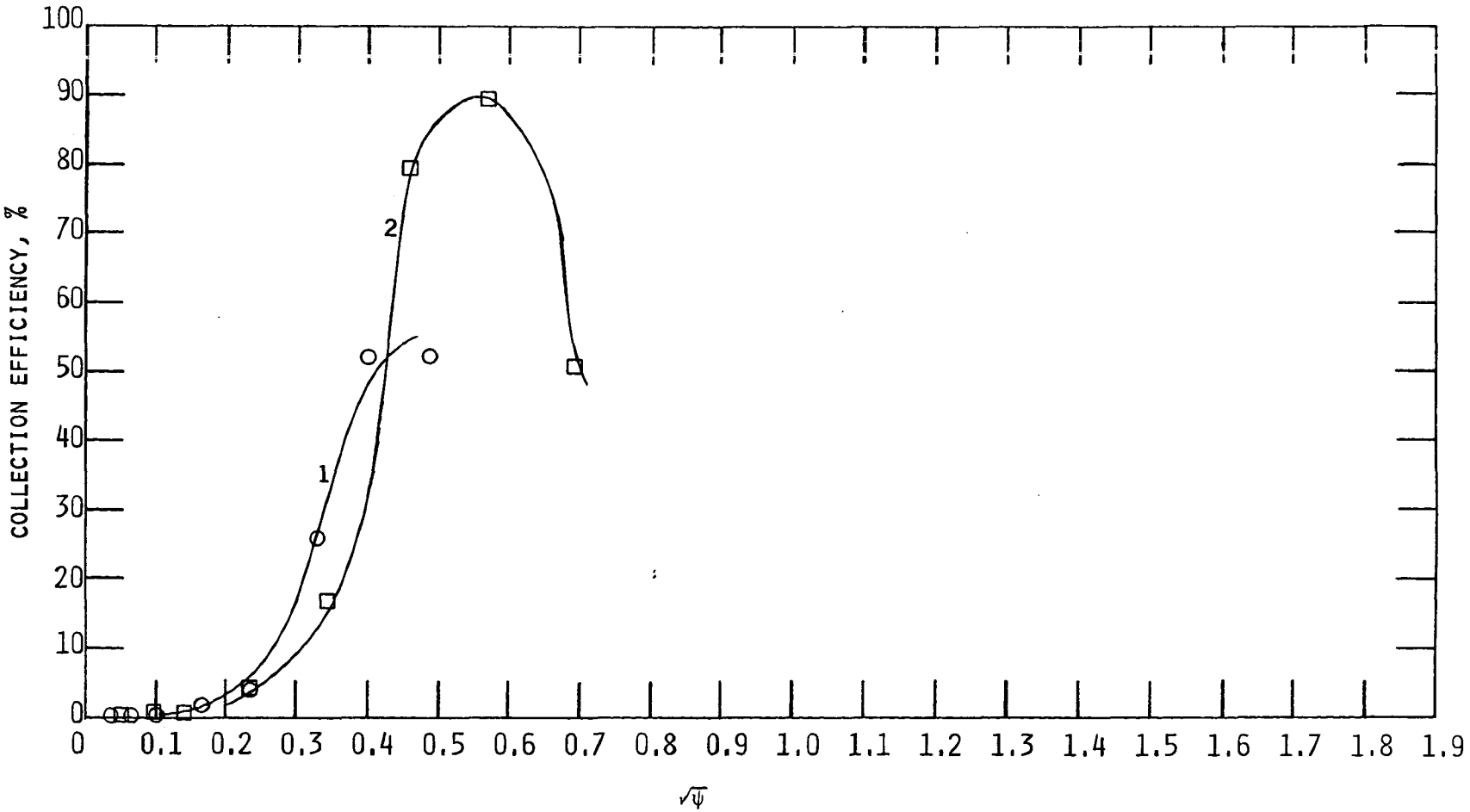

Figure 12. Collection efficiency (%) Versus $\sqrt{\psi}$
Andersen Mark III Stack Sampler
Stage 1 - Stage 2
Uncorrected for Wall Losses

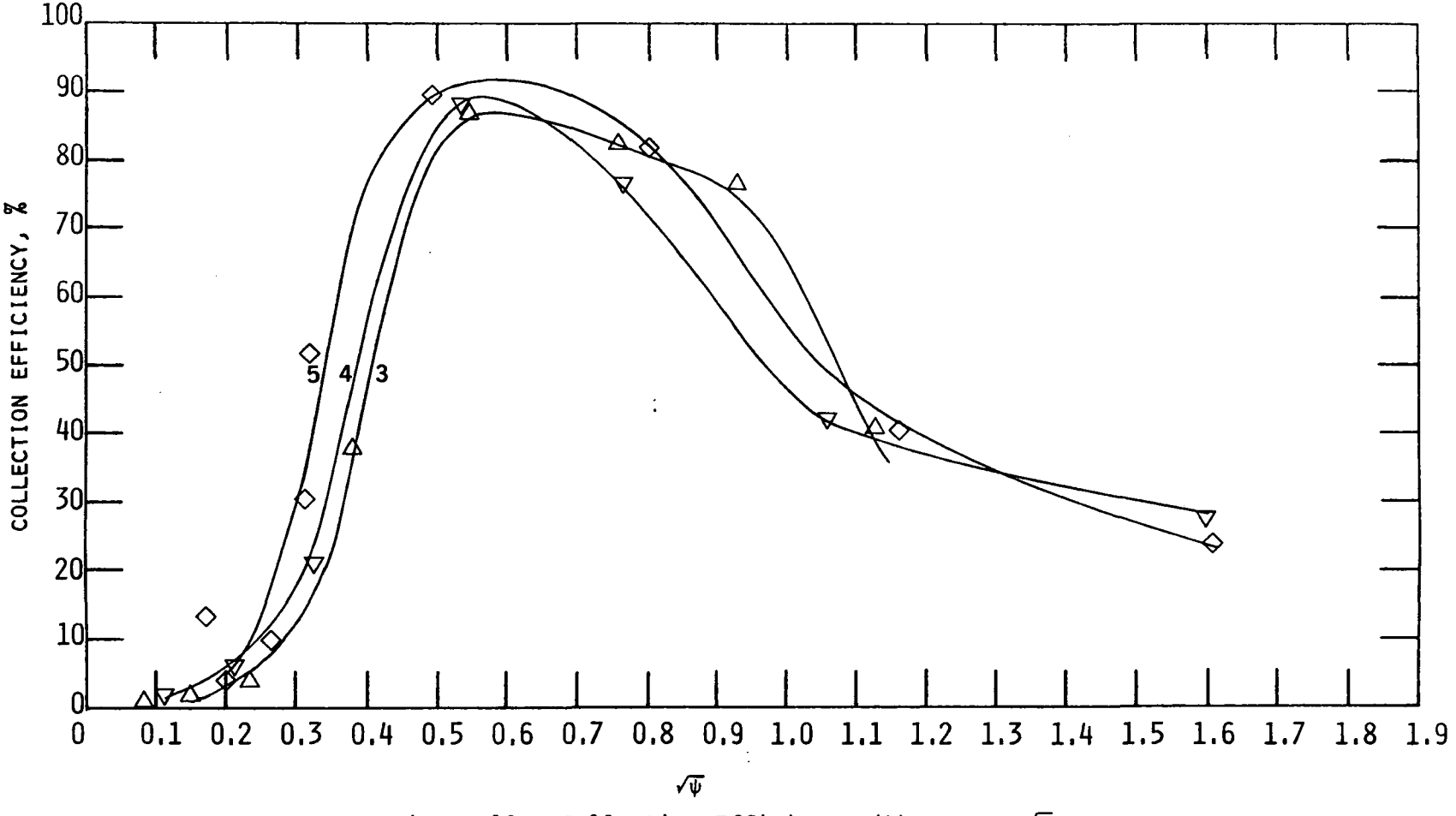

Figure 13. Collection Efficiency (%) Versus $\sqrt{\psi}$
Andersen Mark III Stack Sampler
Stage 3 - Stage 5
Uncorrected for Wall Losses

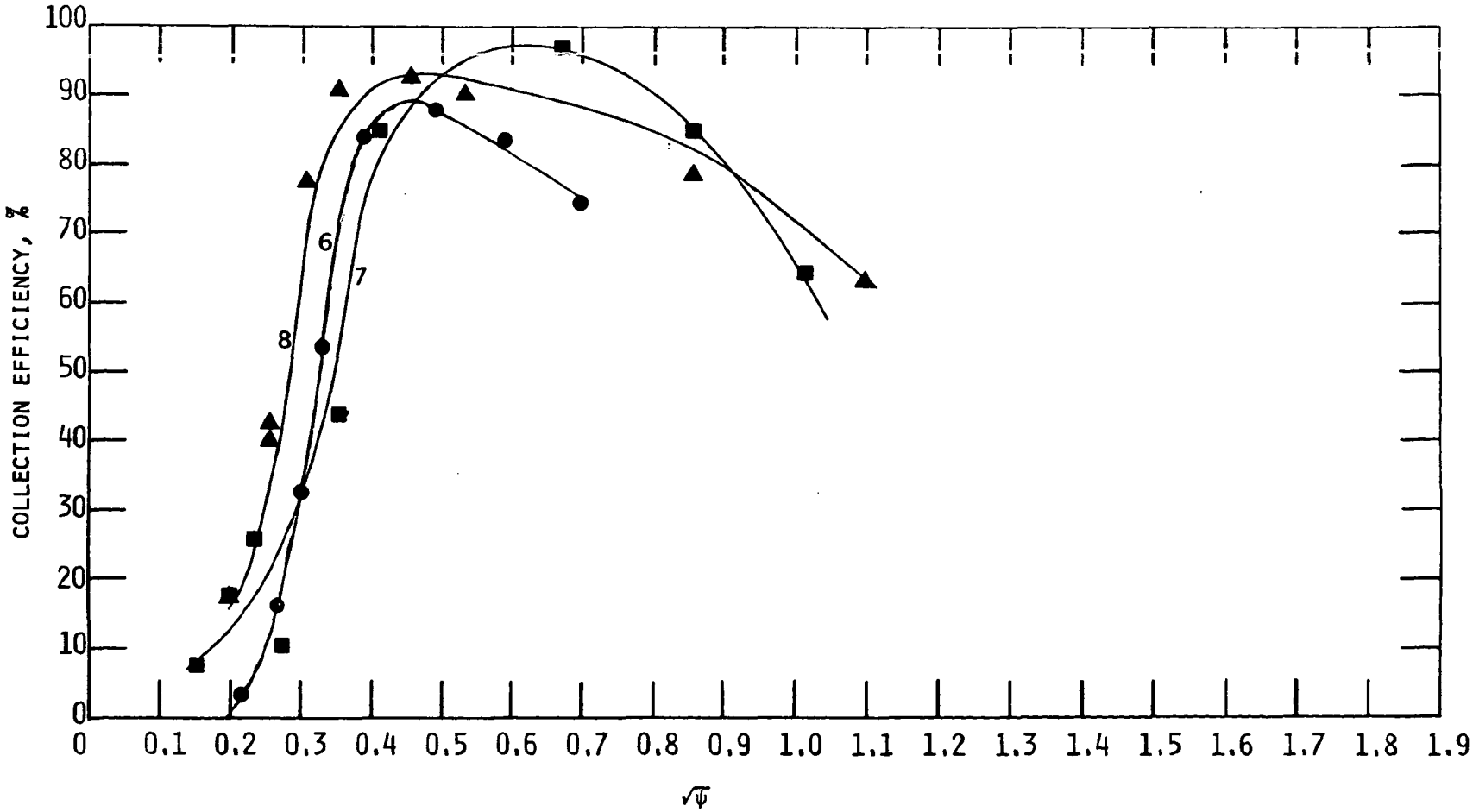

Figure 14. Collection Efficiency (%) Versus $\sqrt{\psi}$
Andersen Mark III Stack Sampler
Stage 6 - Stage 8
Uncorrected for Wall Losses

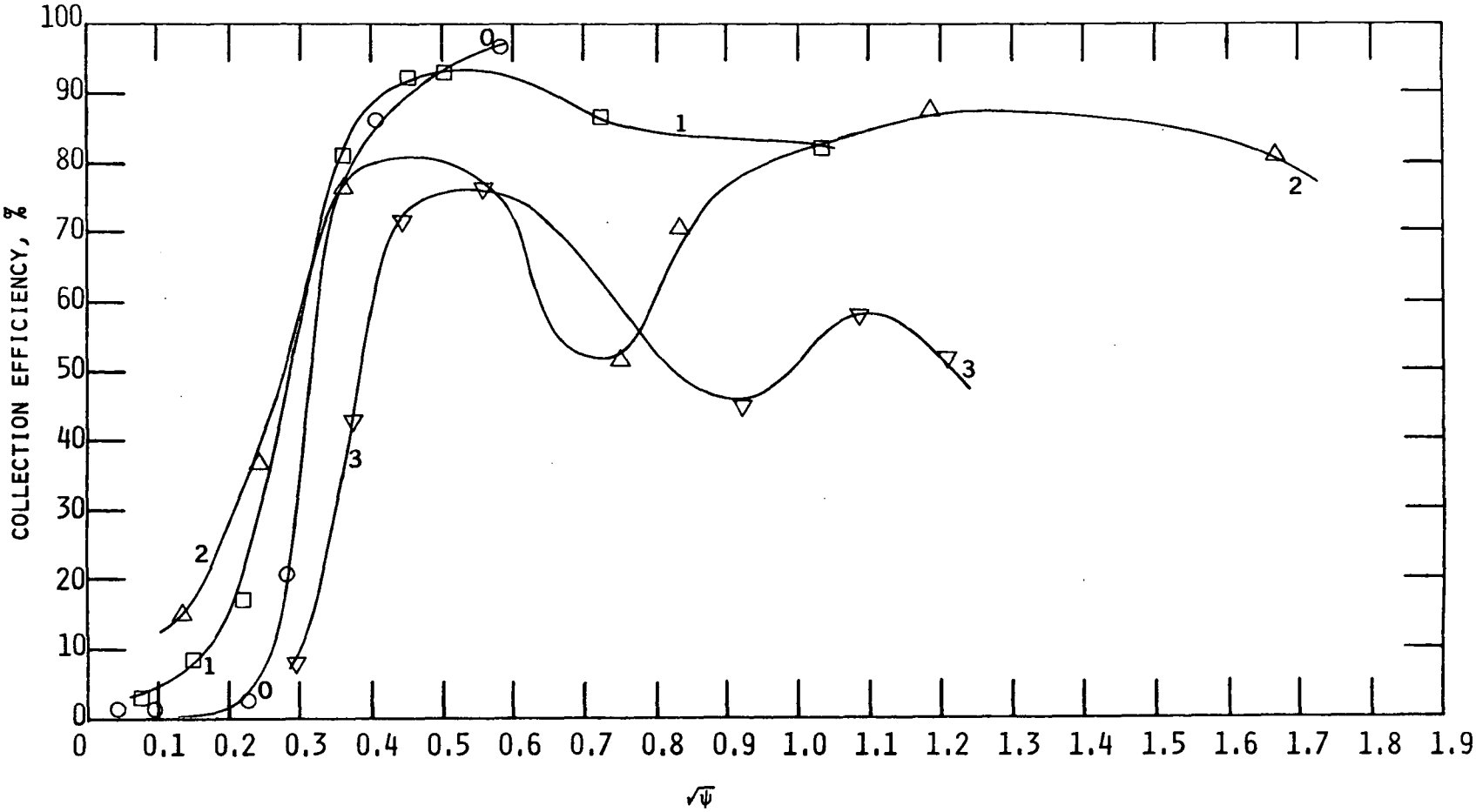

Figure 15. Collection Efficiency (%) Versus $\sqrt{\psi}$
Modified Brink BMS-11 Cascade Impactor
Stage 0 - Stage 3 (Glass Fiber Substrates)
Uncorrected for Wall Losses

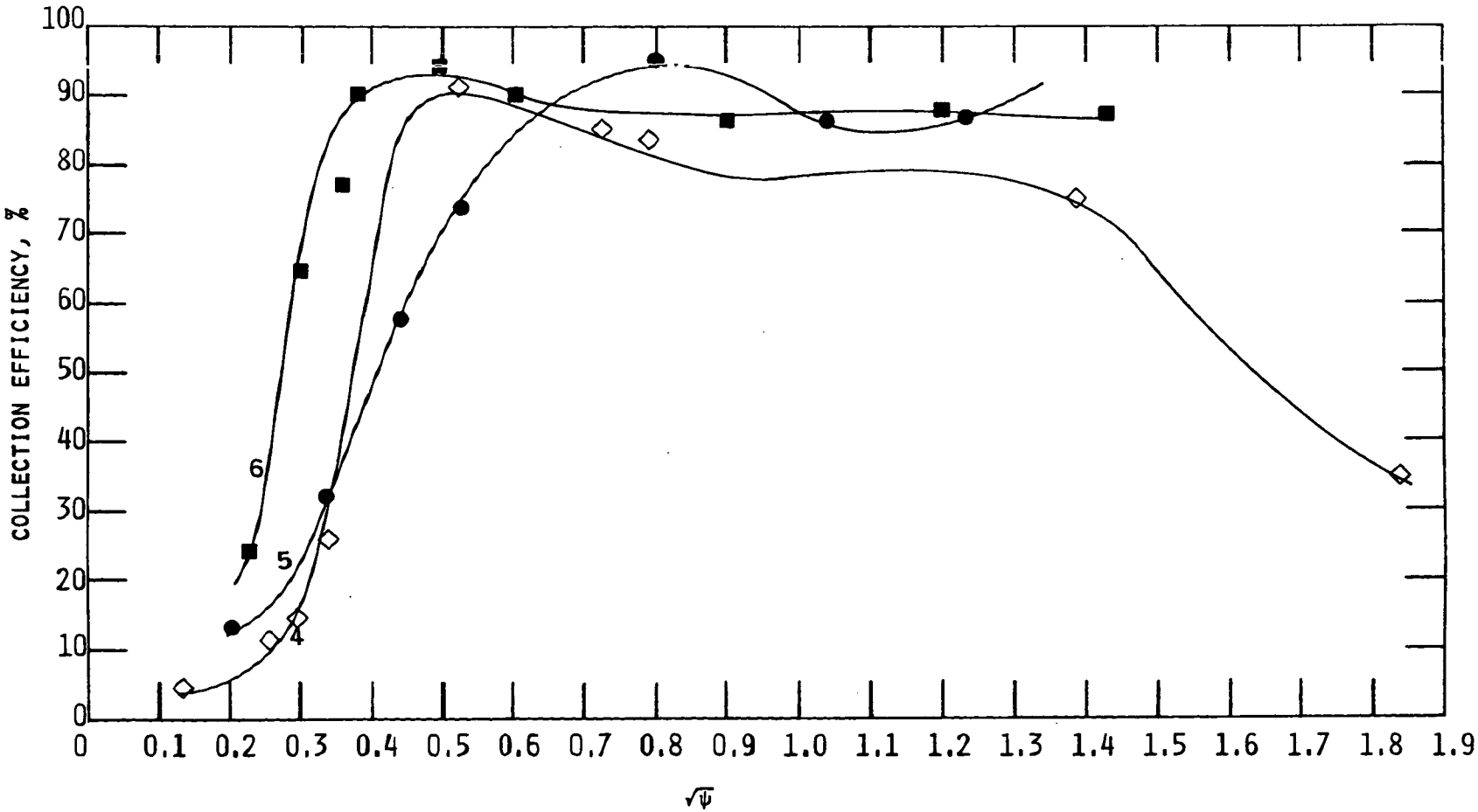

Figure 16. Collection Efficiency (%) Versus $\sqrt{\psi}$
Modified Brink BMS-11 Cascade Impactor
Stage 4 - Stage 6 (Glass Fiber Substrates)
Uncorrected for Wall Losses

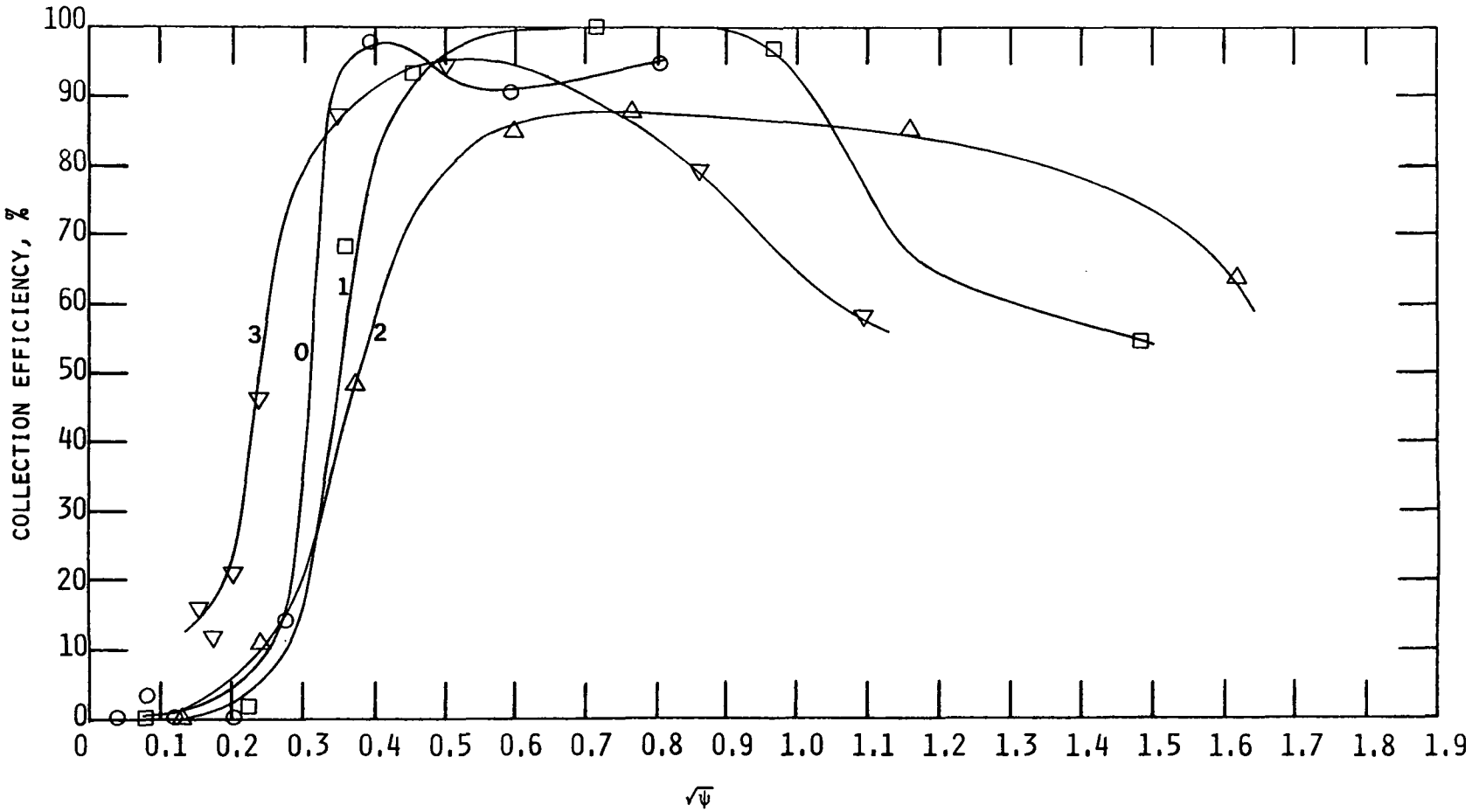

Figure 17. Collection Efficiency (%) Versus $\sqrt{\psi}$
Modified Brink BMS-11 Cascade Impactor
Stage 0 - Stage 3 (Greased Collection Plates)
Uncorrected for Wall Losses

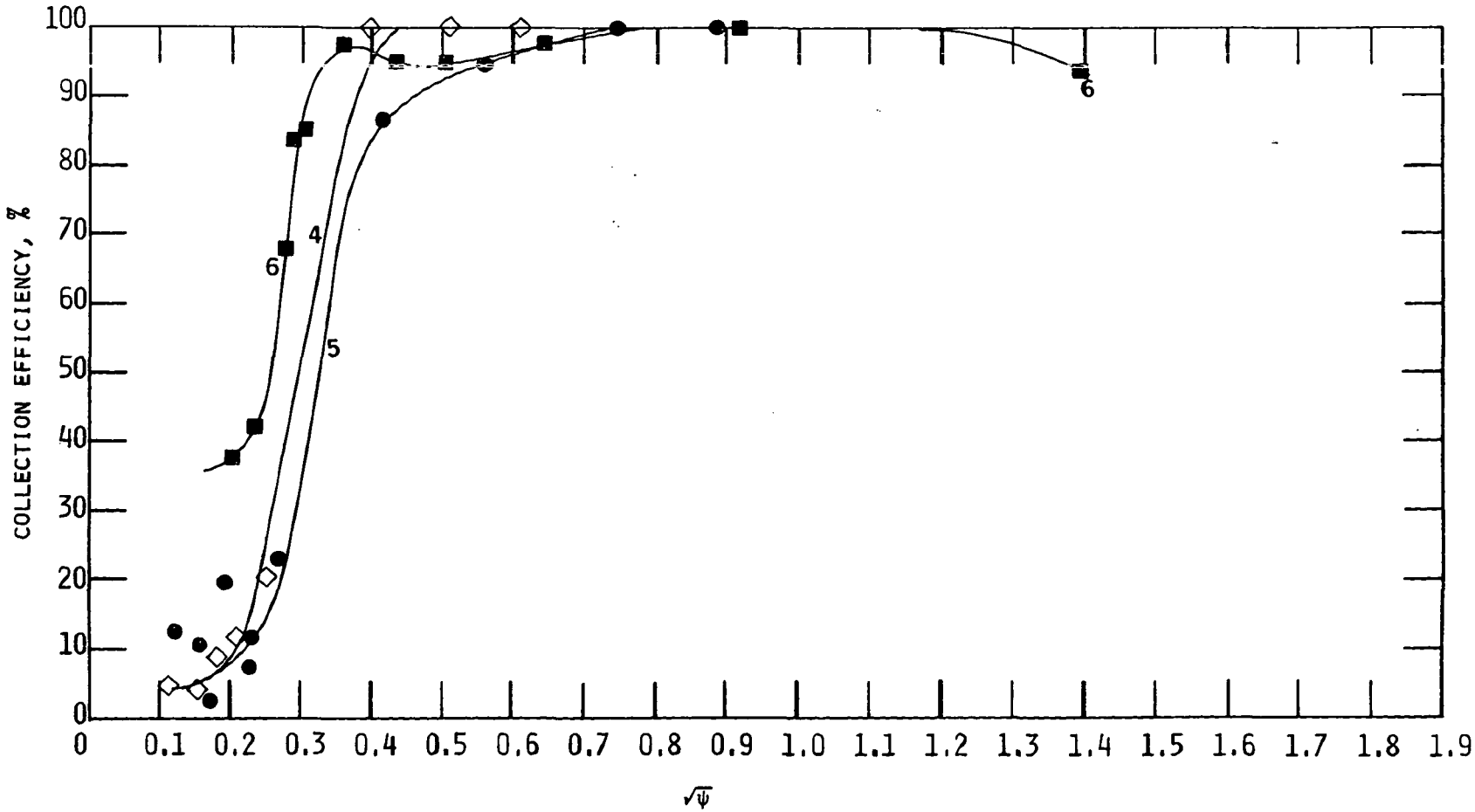

Figure 18. Collection Efficiency (%) Versus $\sqrt{\psi}$
Modified Brink BMS-11 Cascade Impactor
Stage 4 - Stage 6 (Greased Collection Plates)
Uncorrected for Wall Losses

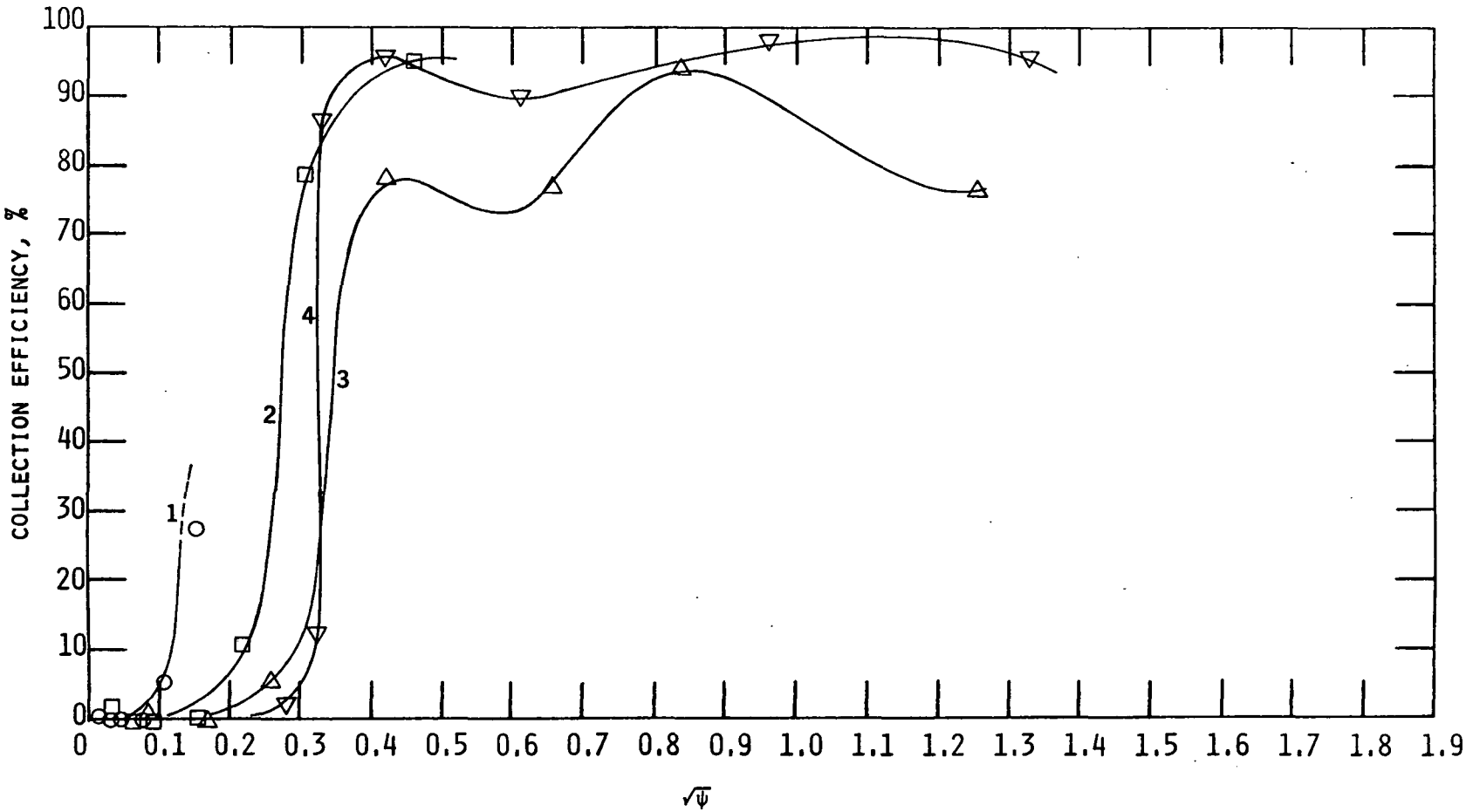

Figure 19. Collection Efficiency (%) Versus $\sqrt{\psi}$
MRI Model 1502 Inertial Cascade Impactor
Stage 1 - Stage 4
Uncorrected for Wall Losses

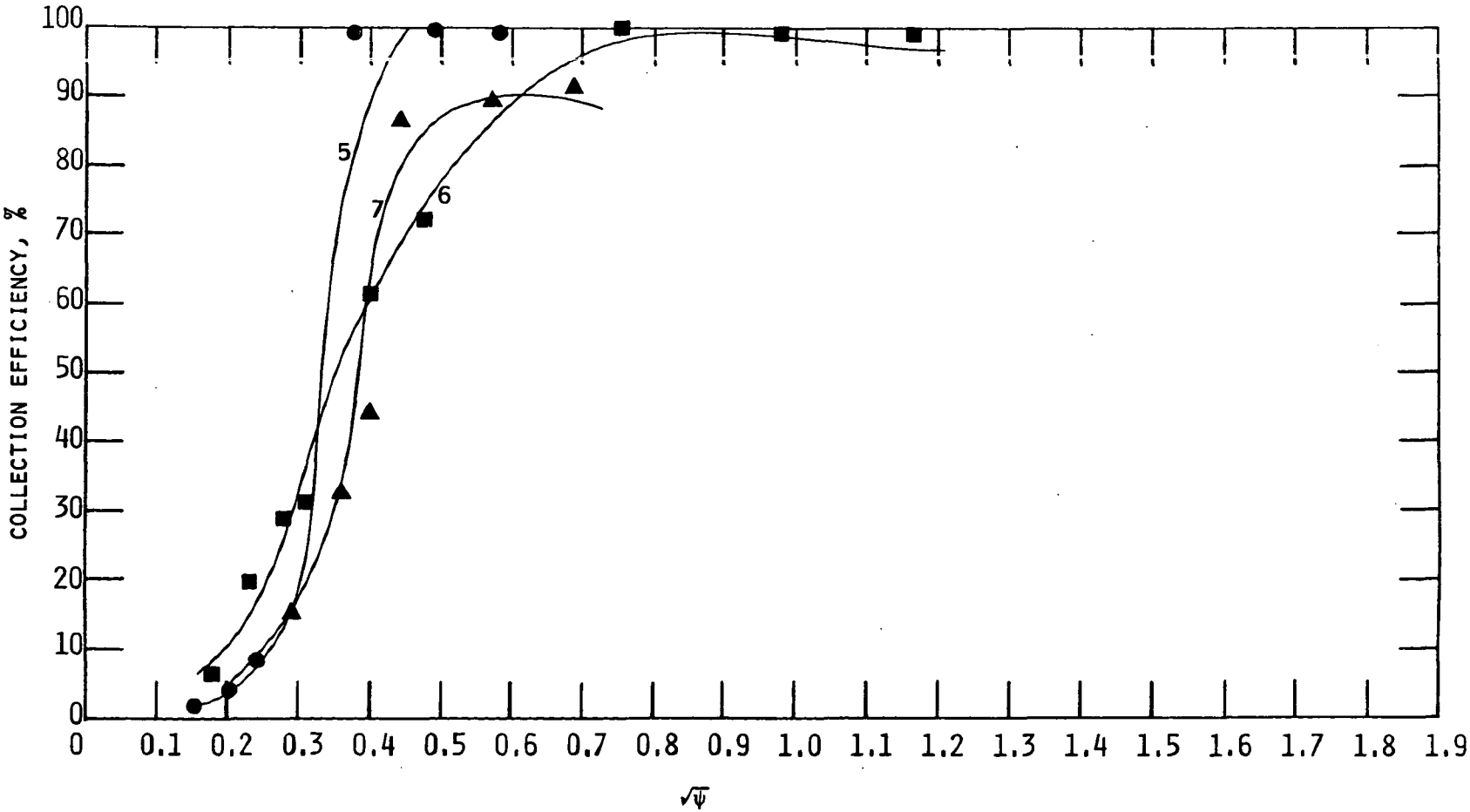

Figure 20. Collection Efficiency (%) Versus $\sqrt{\Psi}$
MRI Model 1502 Inertial Cascade Impactor
Stage 5 - Stage 7
Uncorrected for Wall Losses

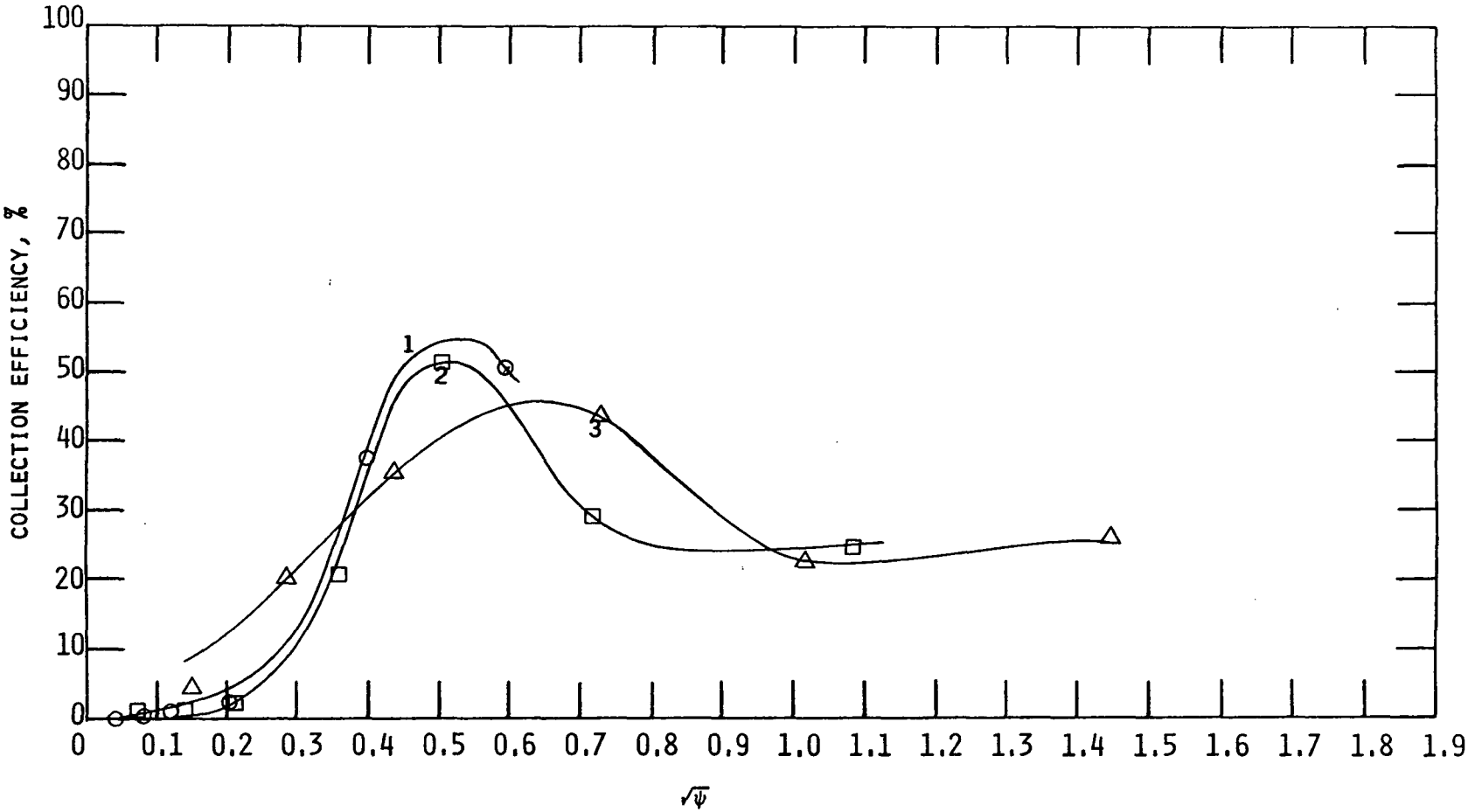

Figure 21. Collection Efficiency (%) Versus $\sqrt{\psi}$
Sierra Model 226 Inertial Cascade Impactor
Stage 1 - Stage 3 Flowrate = 14 LPM
Uncorrected for Wall Losses

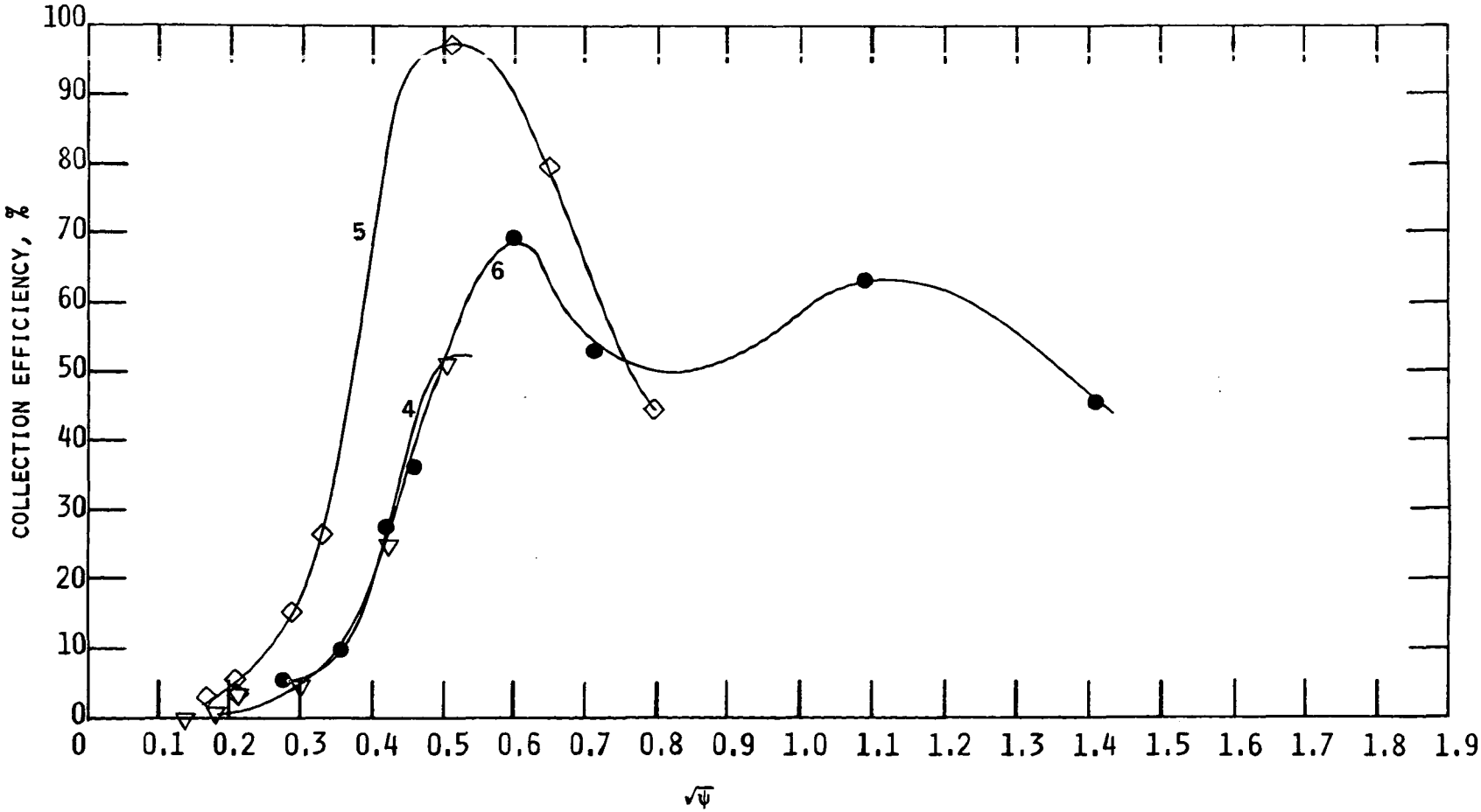

Figure 22. Collection Efficiency (%) Versus $\sqrt{\psi}$
Sierra Model 226 Inertial Cascade Impactor
Stage 4 - Stage 6 Flowrate = 14 LPM
Uncorrected for Wall Losses

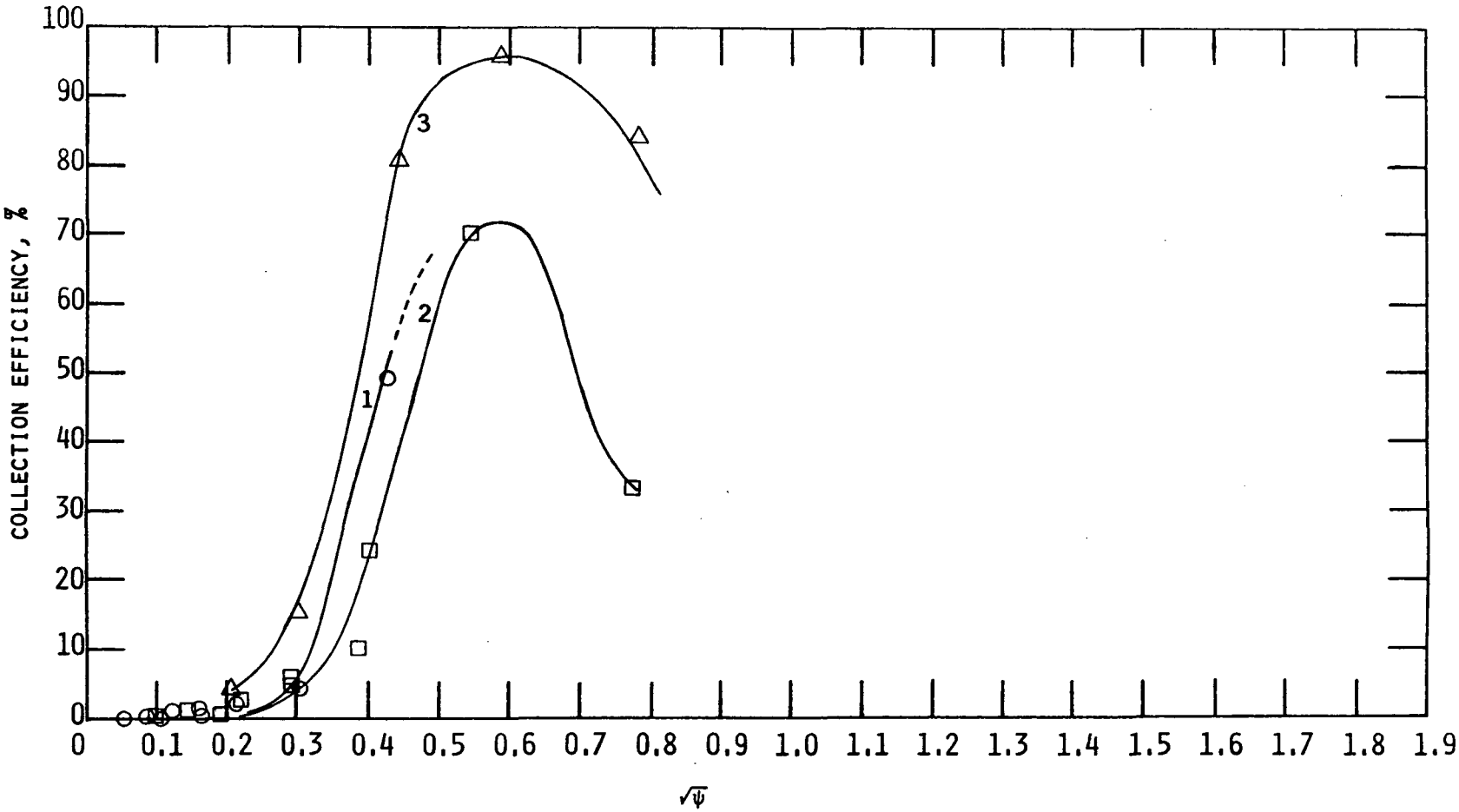

Figure 23. Collection Efficiency (%) Versus $\sqrt{\psi}$
Sierra Model 226 Inertial Cascade Impactor
Stage 1 - Stage 3 Flowrate = 7 LPM
Uncorrected for Wall Losses

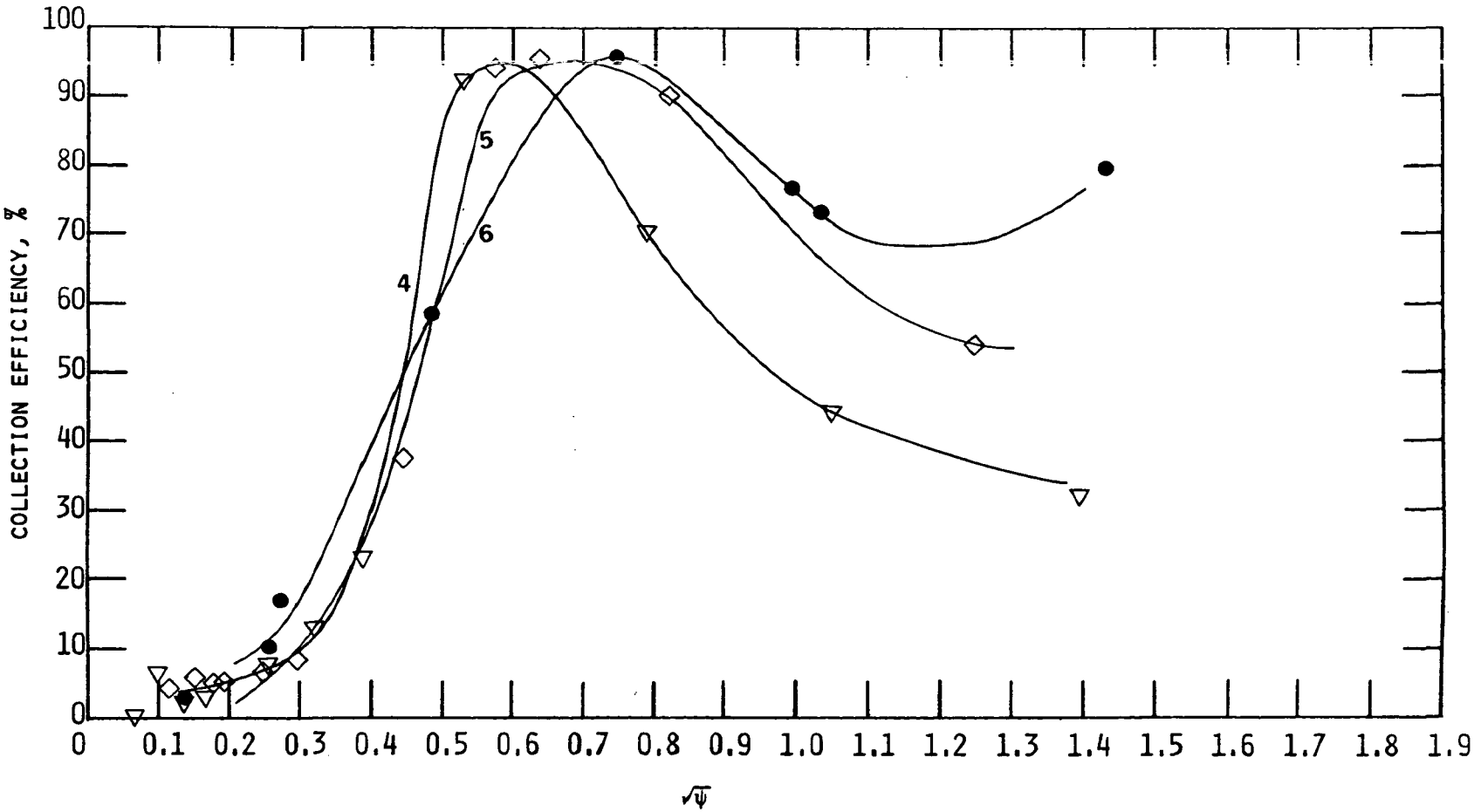

Figure 24. Collection Efficiency (%) Versus $\sqrt{\Psi}$
Sierra Model 226 Inertial Cascade Impactor
Stage 4 - Stage 6 Flowrate = 7 LPM
Uncorrected for Wall Losses

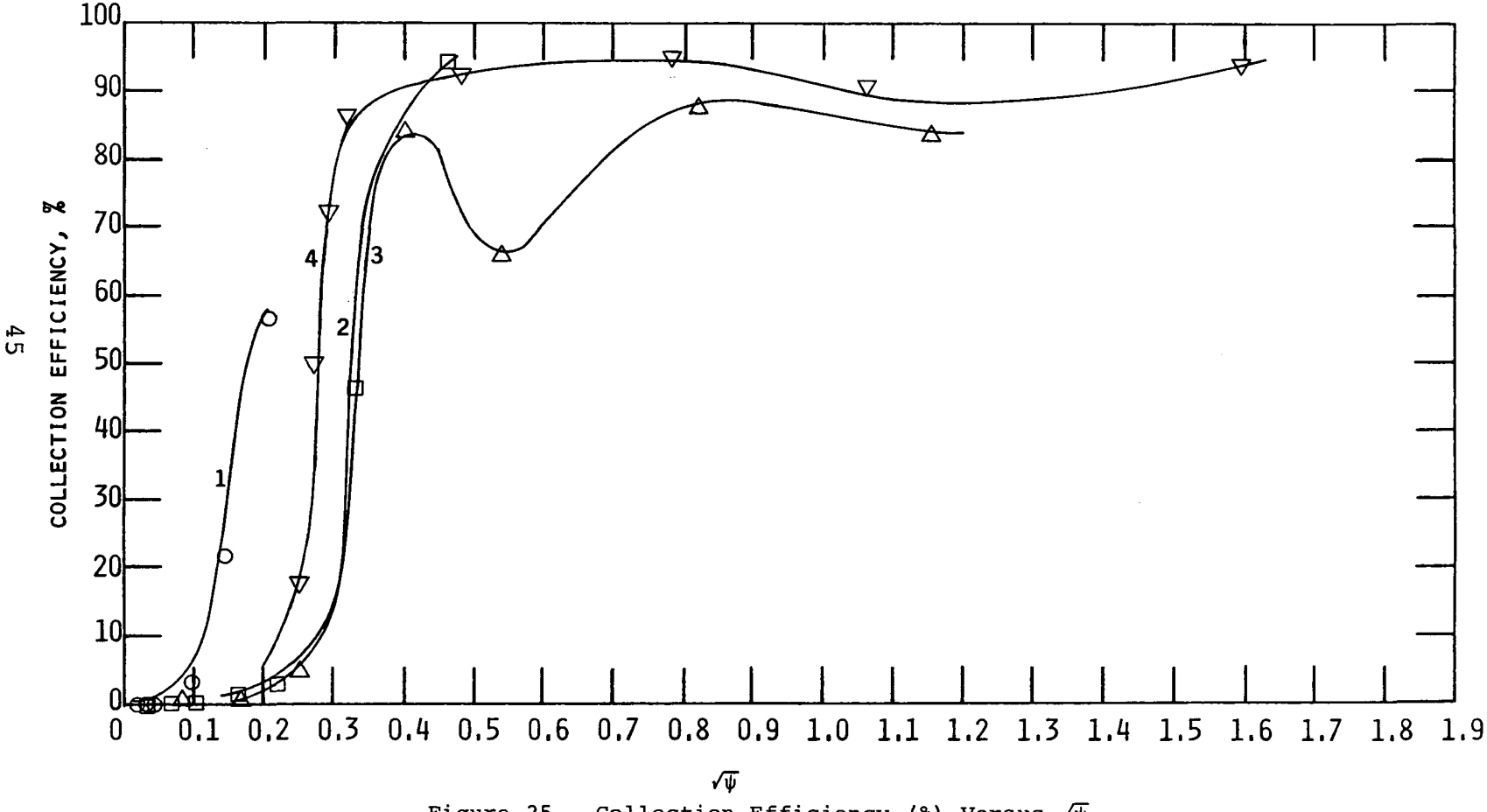

Figure 25. Collection Efficiency (%) Versus $\sqrt{\psi}$
University of Washington Mark III Cascade Impactor
Stage 1 - Stage 4
Uncorrected for Wall Losses

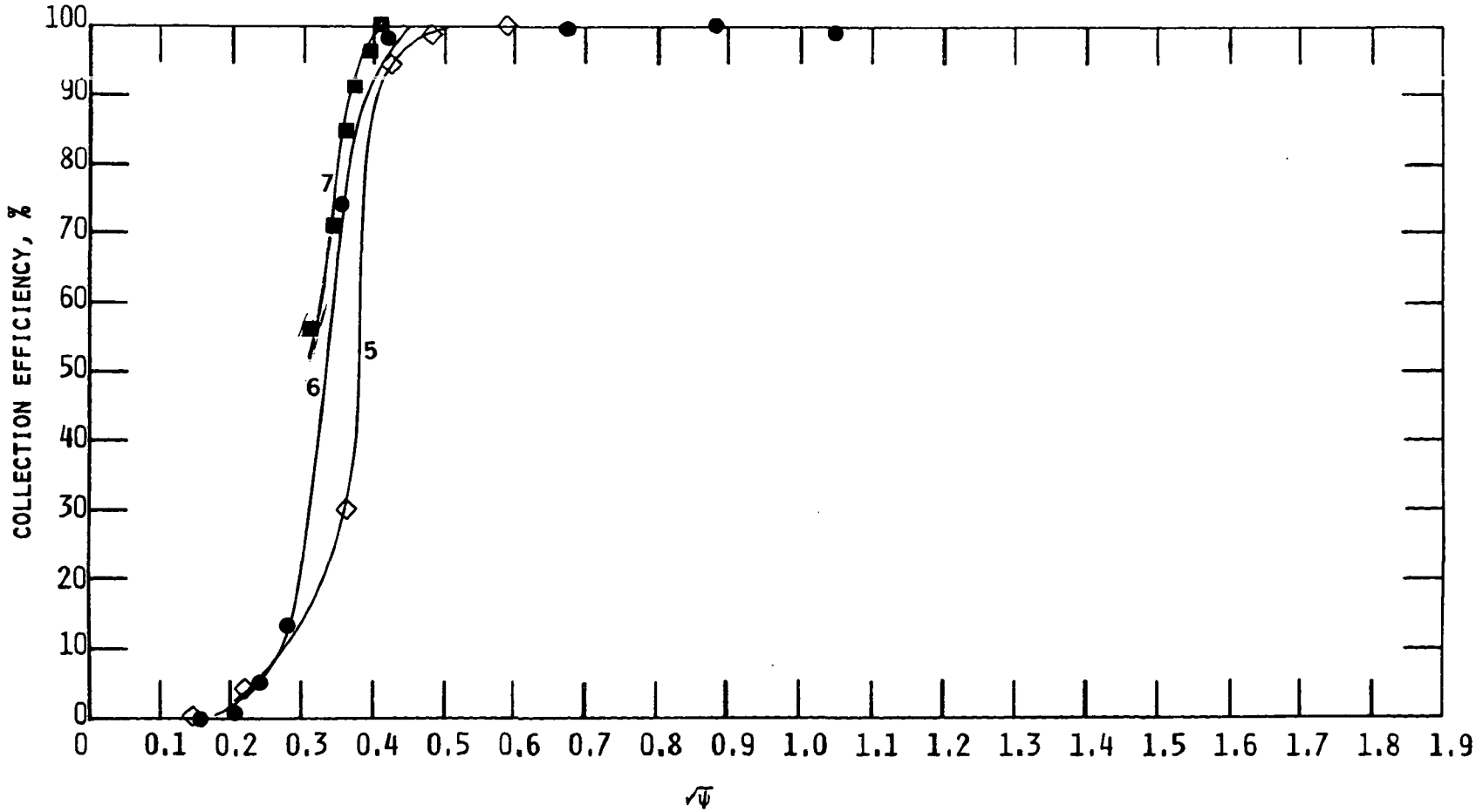

Figure 26. Collection Efficiency (%) Versus $\sqrt{\psi}$
University of Washington Mark III Cascade Impactor
Stage 5 - Stage 7
Uncorrected for Wall Losses

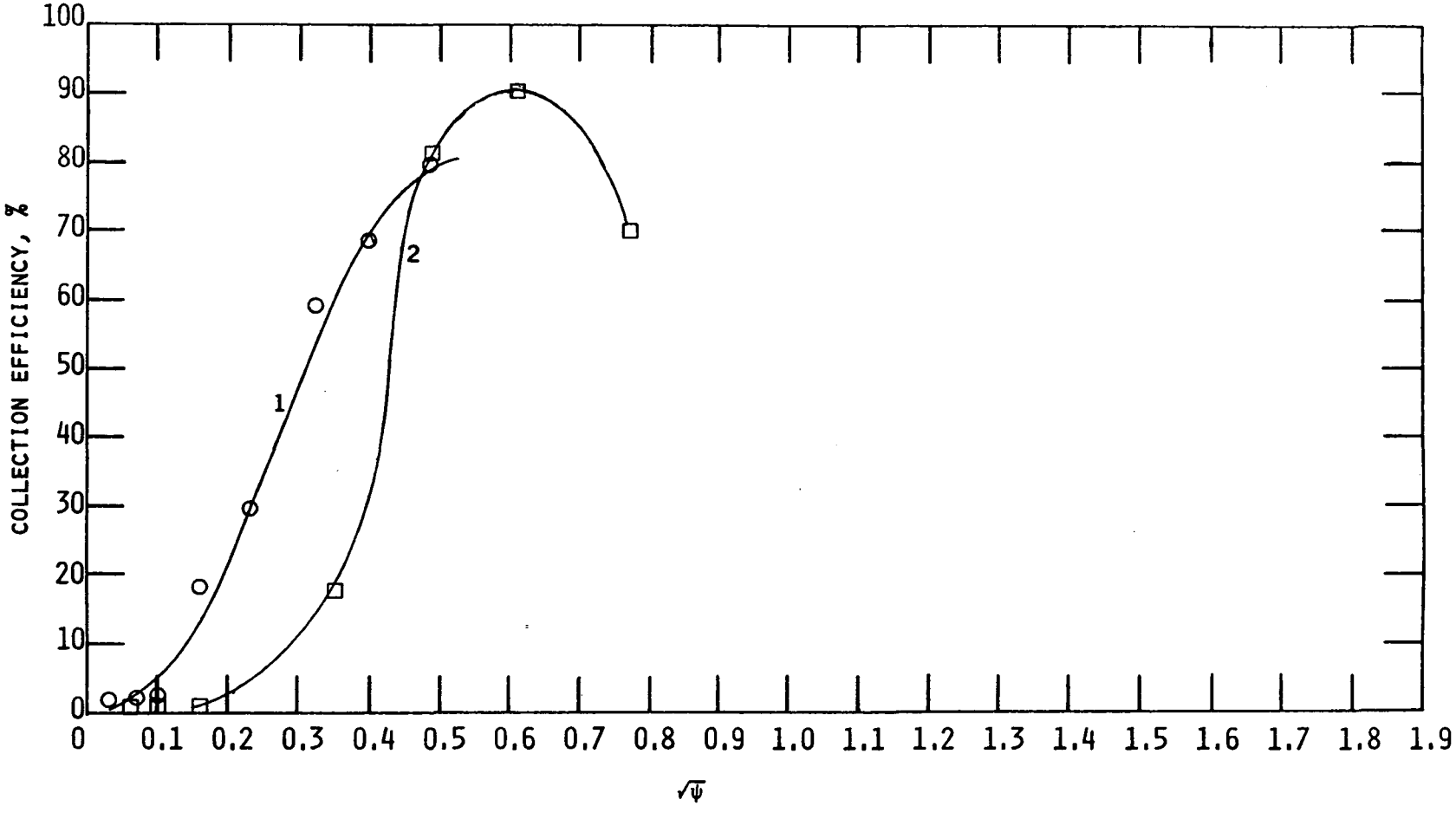

Figure 27. Collection Efficiency (%) Versus $\sqrt{\psi}$
Andersen Mark III Stack Sampler
Stage 1 - Stage 2
Corrected for Wall Losses

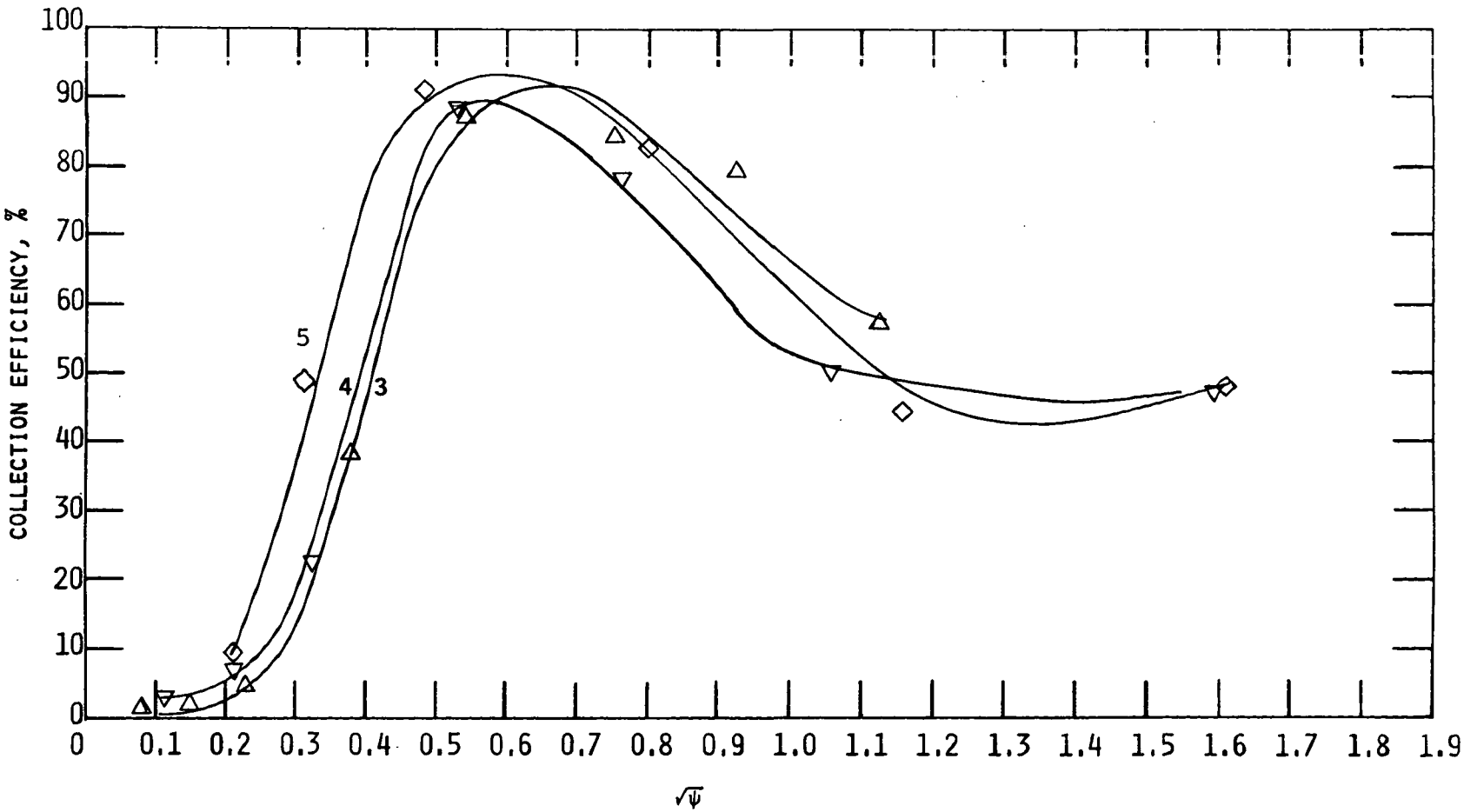

Figure 28. Collection Efficiency (%) Versus $\sqrt{\psi}$
Andersen Mark III Stack Sampler
Stage 3 - Stage 5
Corrected for Wall Losses

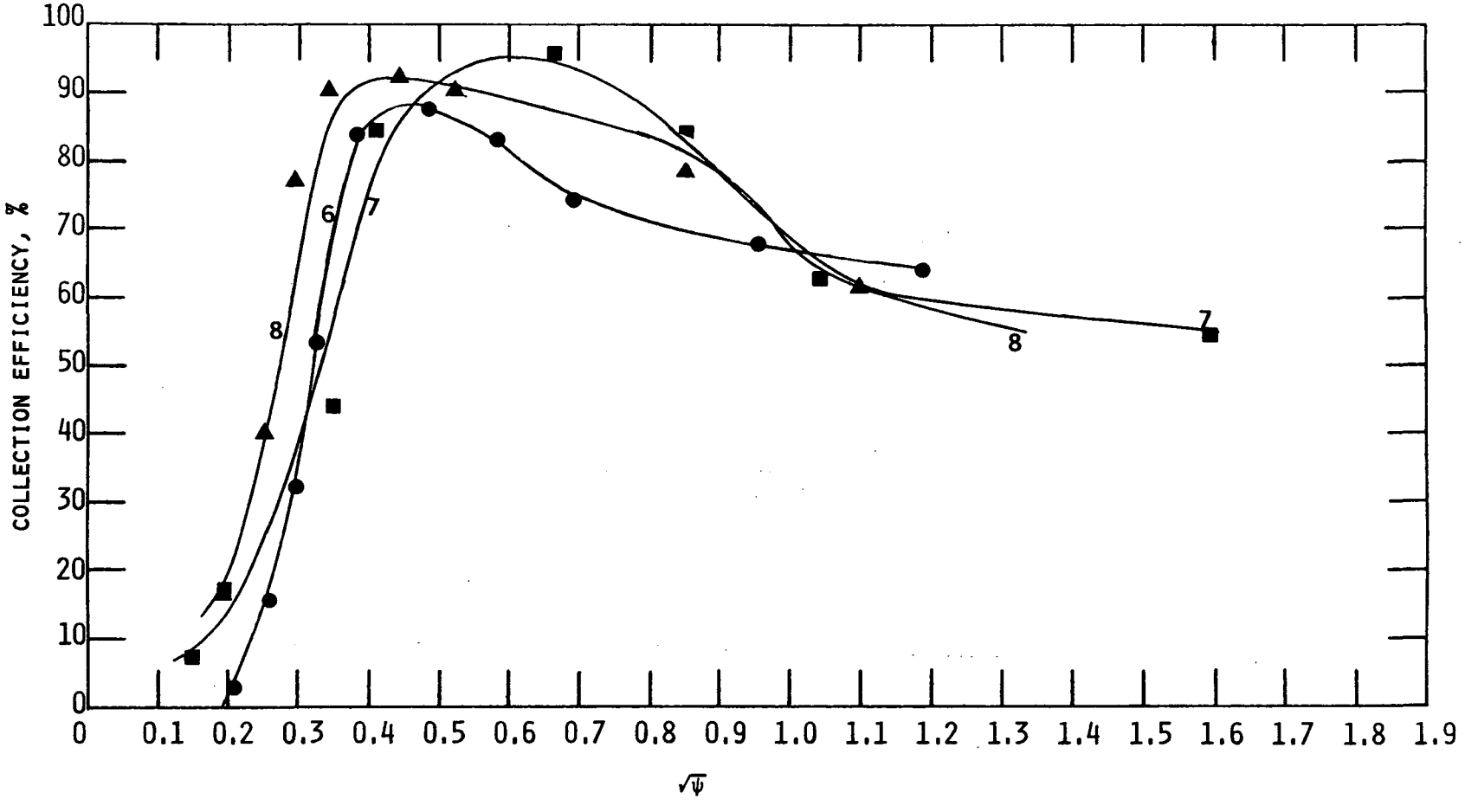

Figure 29. Collection Efficiency (%) Versus $\sqrt{\psi}$
Andersen Mark III Stack Sampler
Stage 6 - Stage 8
Corrected for Wall Losses

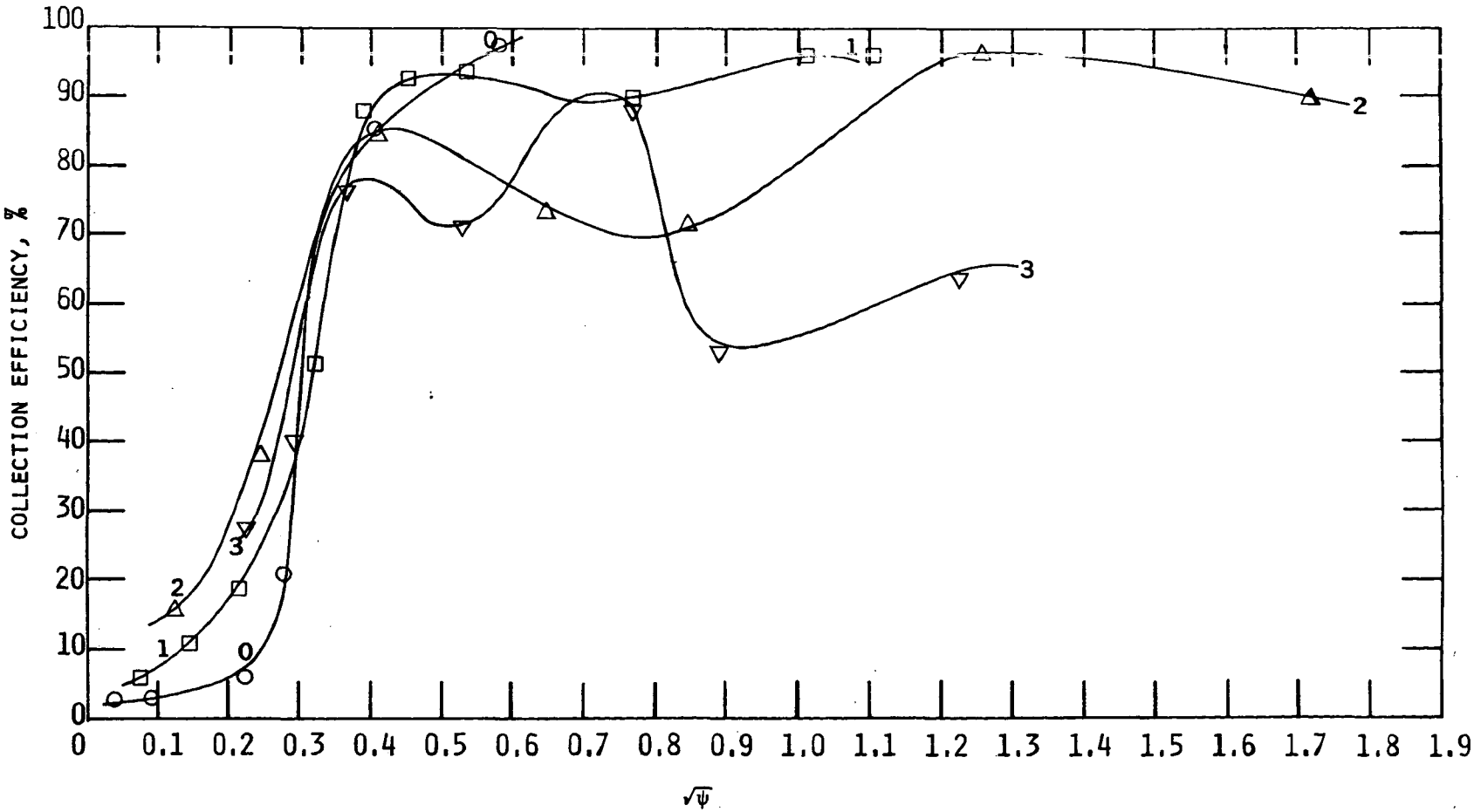

Figure 30. Collection Efficiency (%) Versus $\sqrt{\psi}$
Modified Brink BMS-11 Cascade Impactor
Stage 0 - Stage 3 (Glass Fiber Substrates)
Corrected for Wall Losses

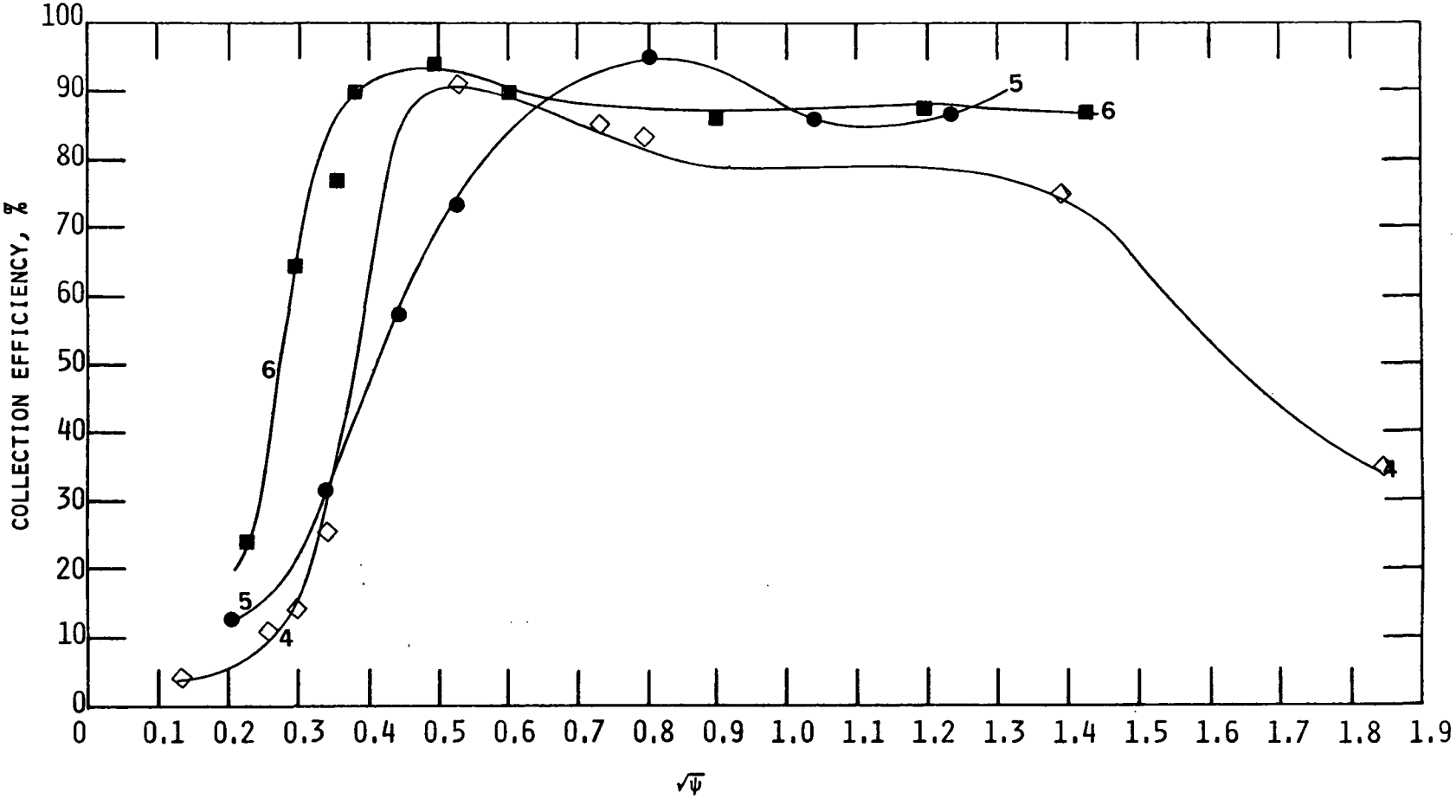

Figure 31. Collection Efficiency (%) Versus $\sqrt{\psi}$
Modified Brink BMS-11 Cascade Impactor
Stage 4 - Stage 6 (Glass Fiber Substrates)
Corrected for Wall Losses

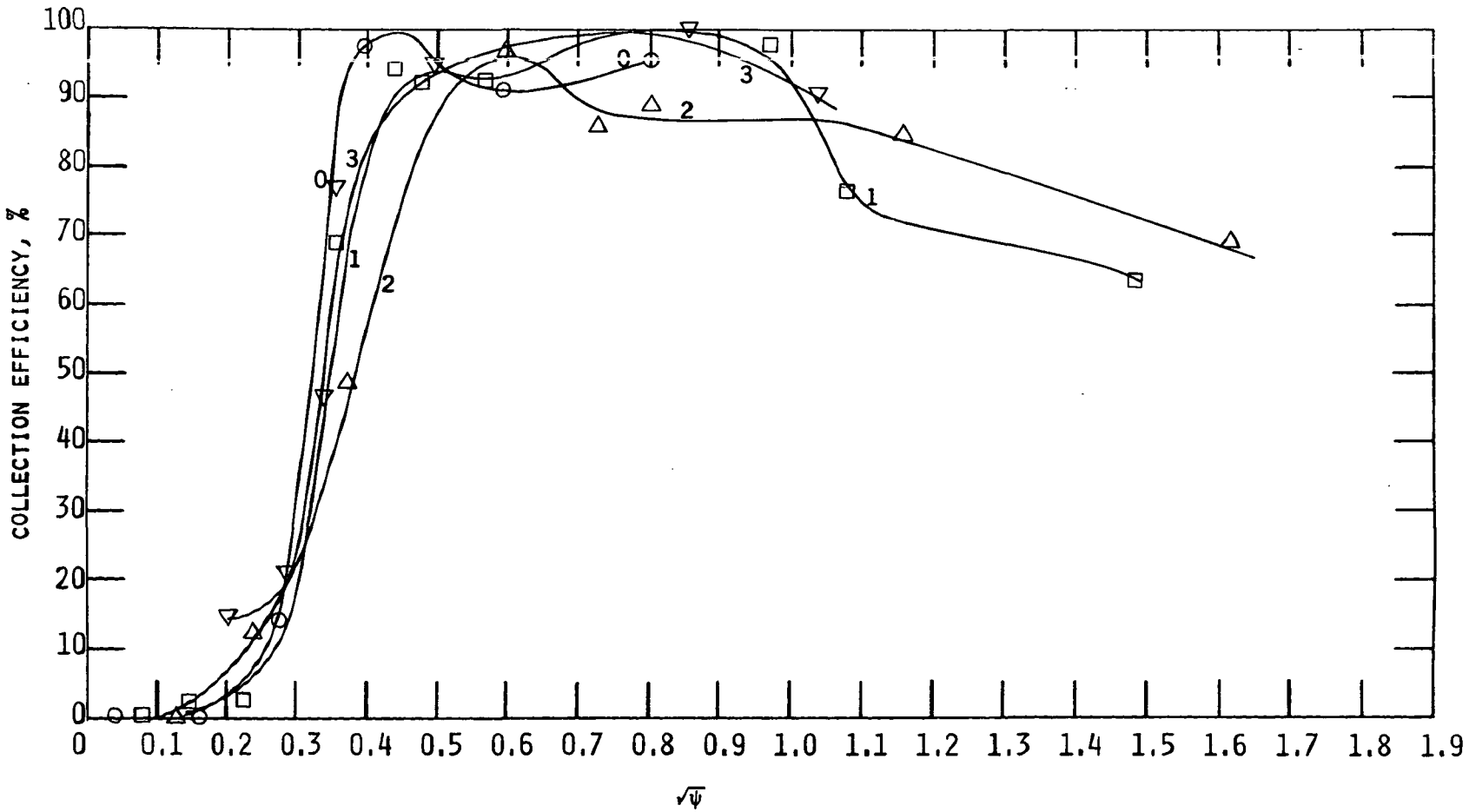

Figure 32. Collection Efficiency (%) Versus $\sqrt{\psi}$
Modified Brink BMS-11 Cascade Impactor
Stage 0 - Stage 3 (Greased Collection Plates)
Corrected for Wall Losses

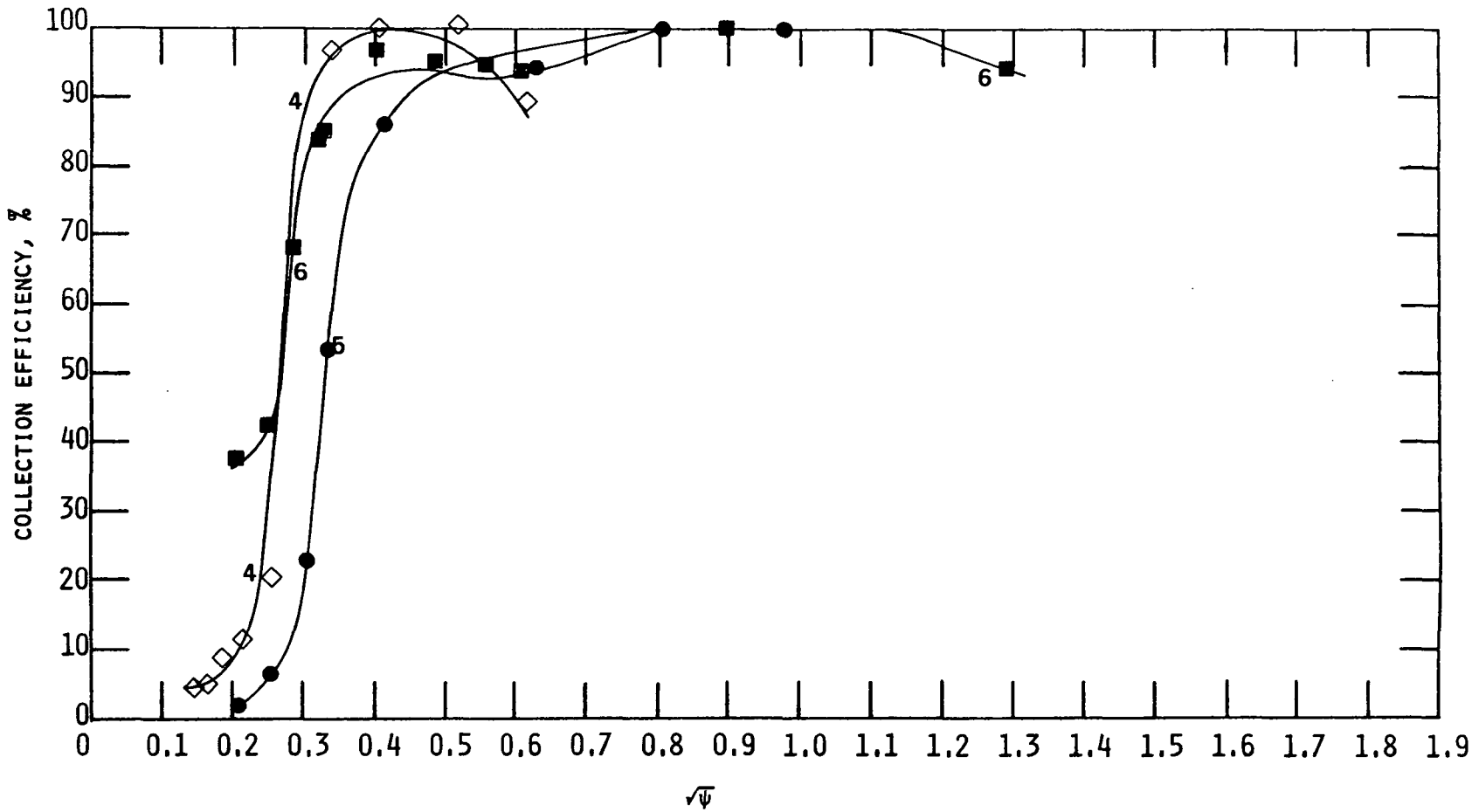

Figure 33. Collection Efficiency (%) Versus $\sqrt{\psi}$
Modified Brink BMS-11 Cascade Impactor
Stage 4 - Stage 6 (Greased Collection Plates)
Corrected for Wall Losses

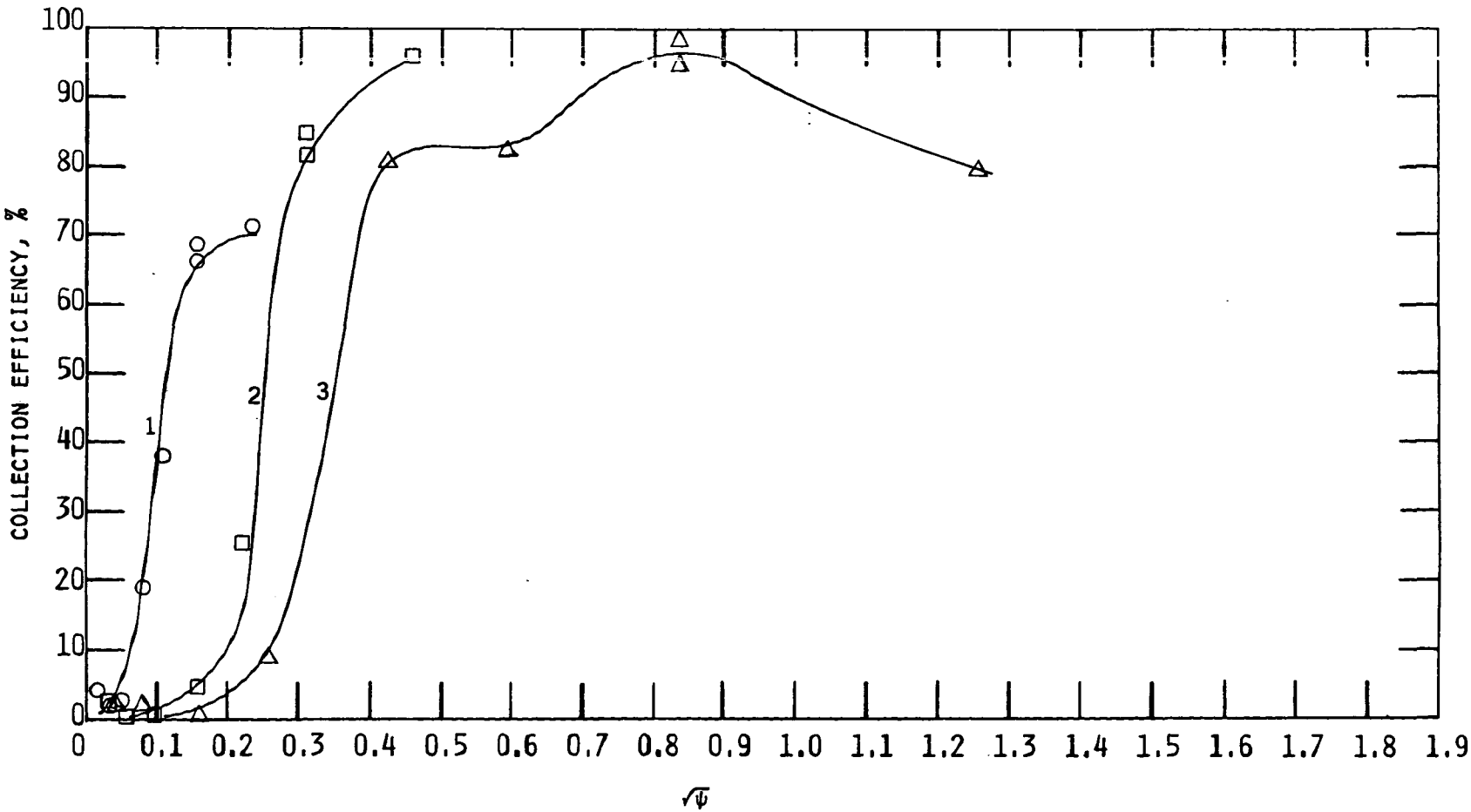

Figure 34. Collection Efficiency (%) Versus $\sqrt{\psi}$
MRI Model 1502 Inertial Cascade Impactor
Stage 1 - Stage 3
Corrected for Wall Losses

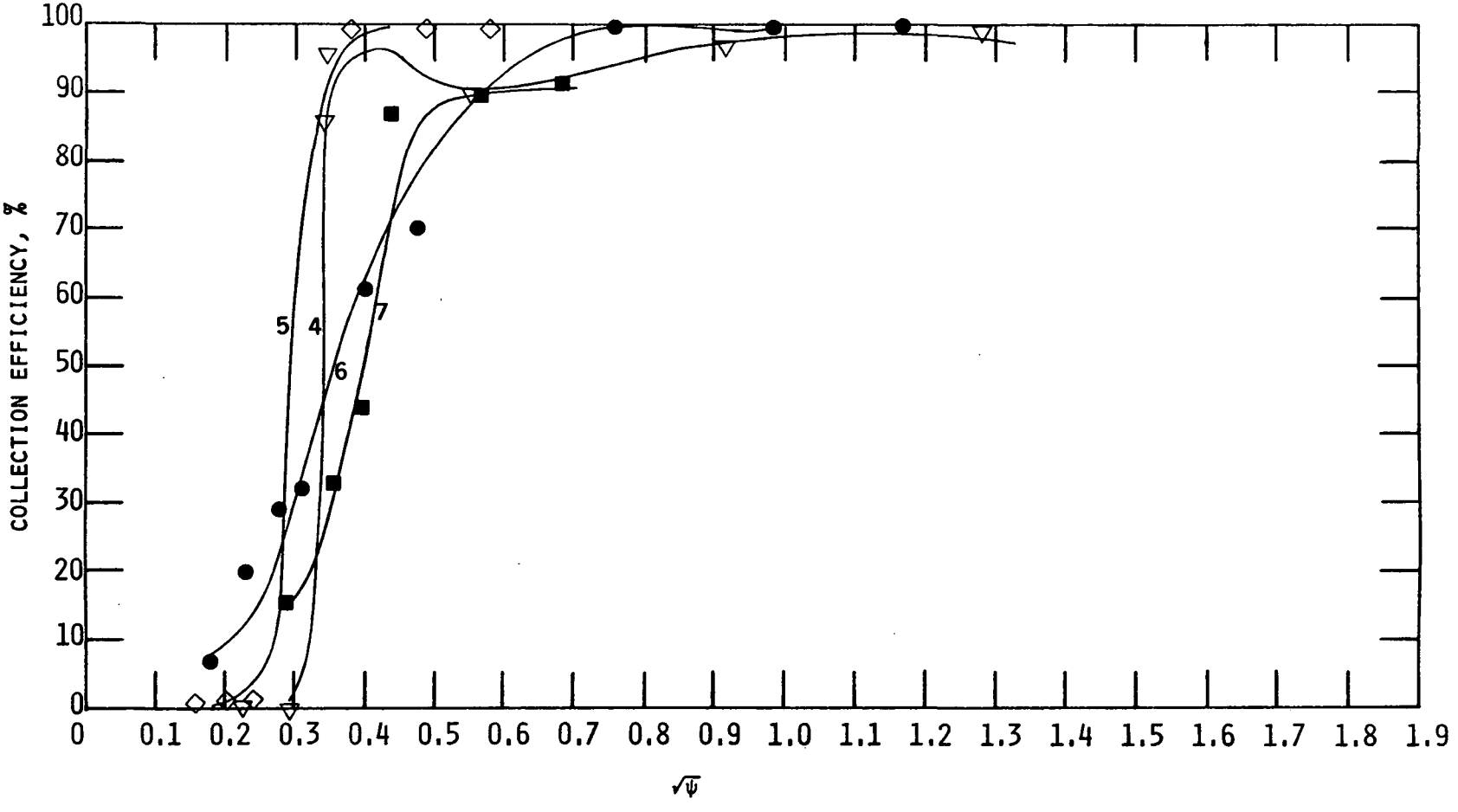

Figure 35. Collection Efficiency (%) Versus $\sqrt{\psi}$
MRI Model 1502 Inertial Cascade Impactor
Stage 4 - Stage 7
Corrected for Wall Losses

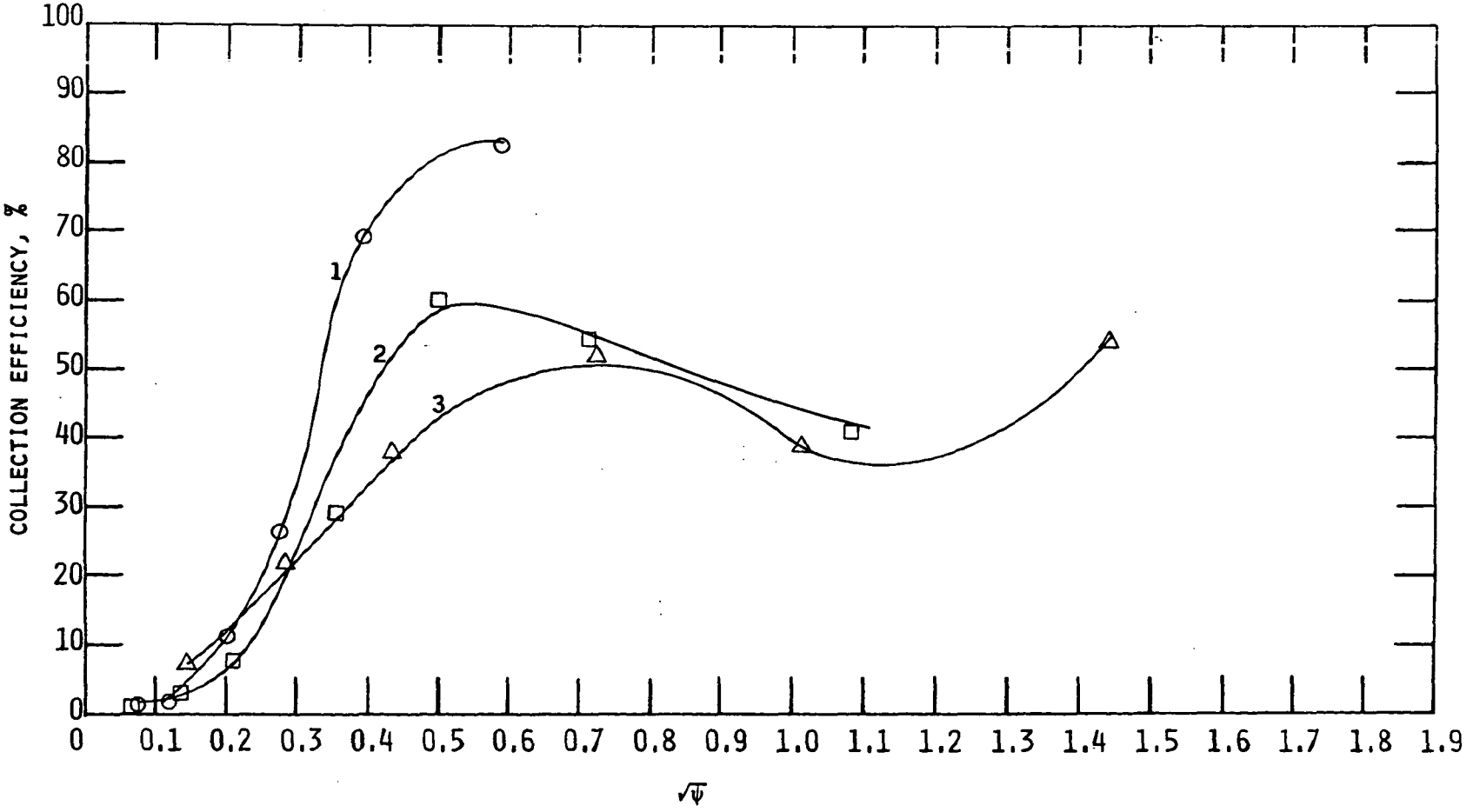

Figure 36. Collection Efficiency (%) Versus $\sqrt{\psi}$
Sierra Model 226 Inertial Cascade Impactor
Stage 1 - Stage 3 Flowrate = 14 LPM
Corrected for Wall Losses

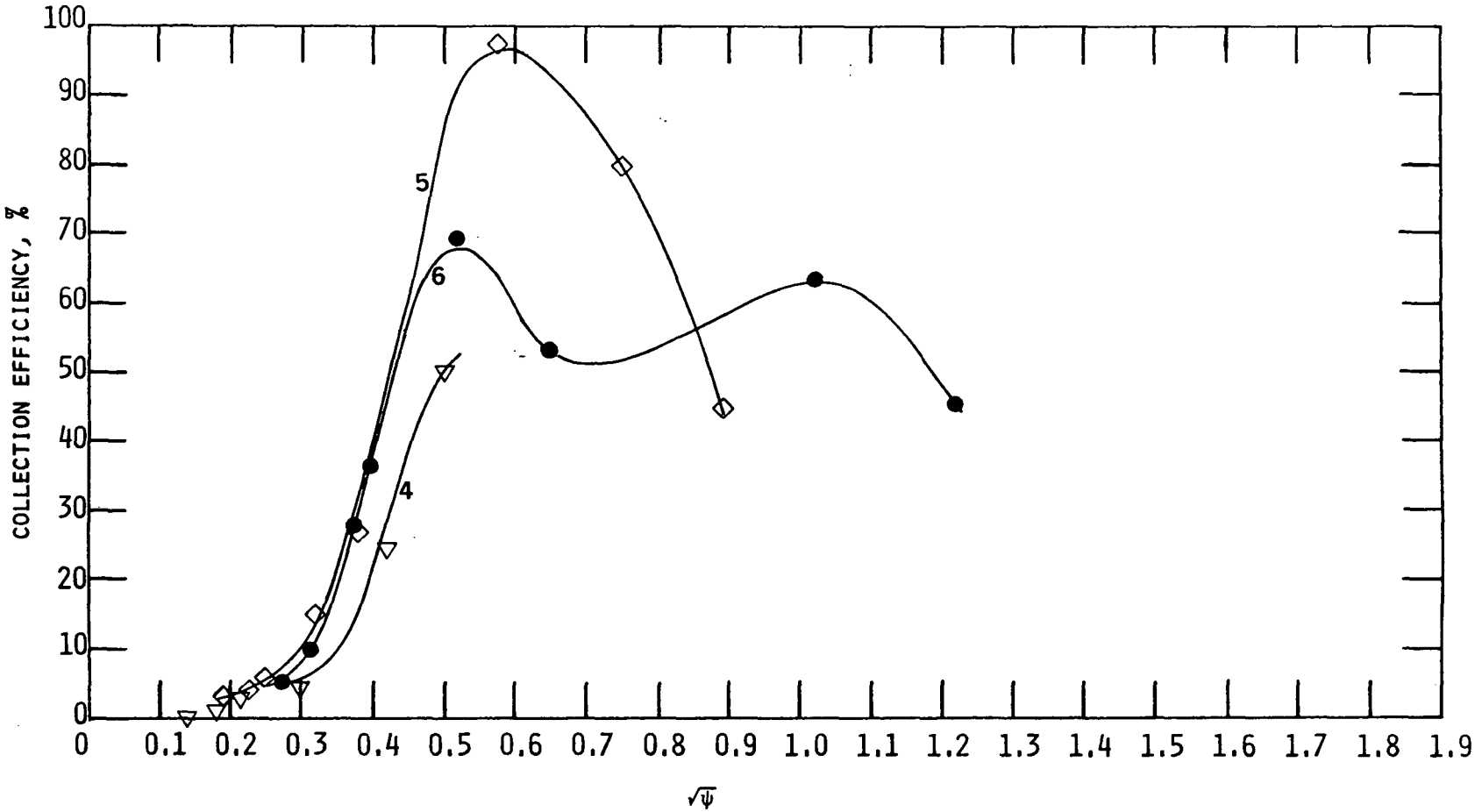

Figure 37. Collection Efficiency (%) Versus $\sqrt{\psi}$
Sierra Model 226 Inertial Cascade Impactor
Stage 4 - Stage 6 Flowrate = 14 LPM
Corrected for Wall Losses

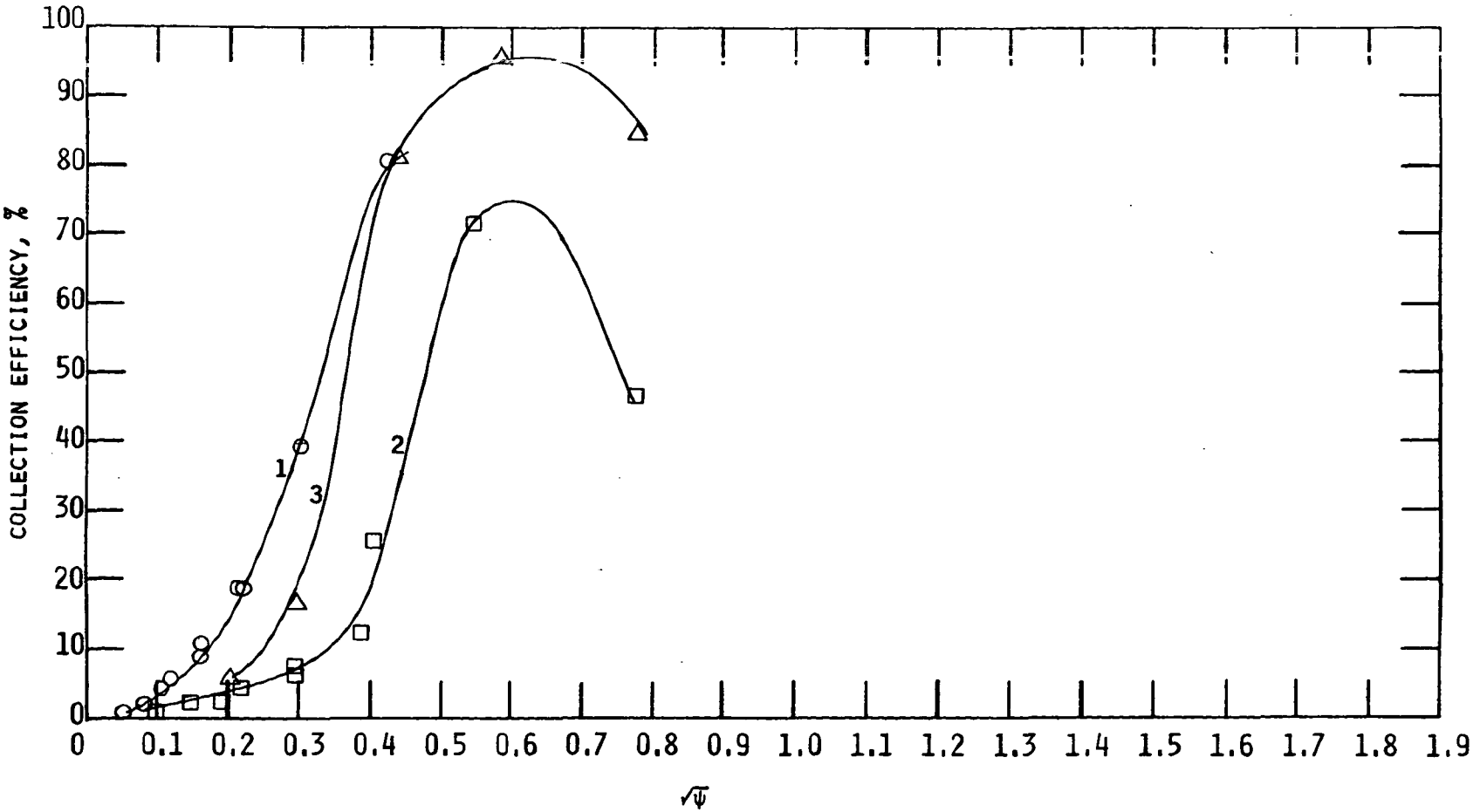

Figure 38. Collection Efficiency (%) Versus $\sqrt{\Psi}$
Sierra Model 226 Inertial Cascade Impactor
Stage 1 - Stage 3 Flowrate = 7 LPM
Corrected for Wall Losses

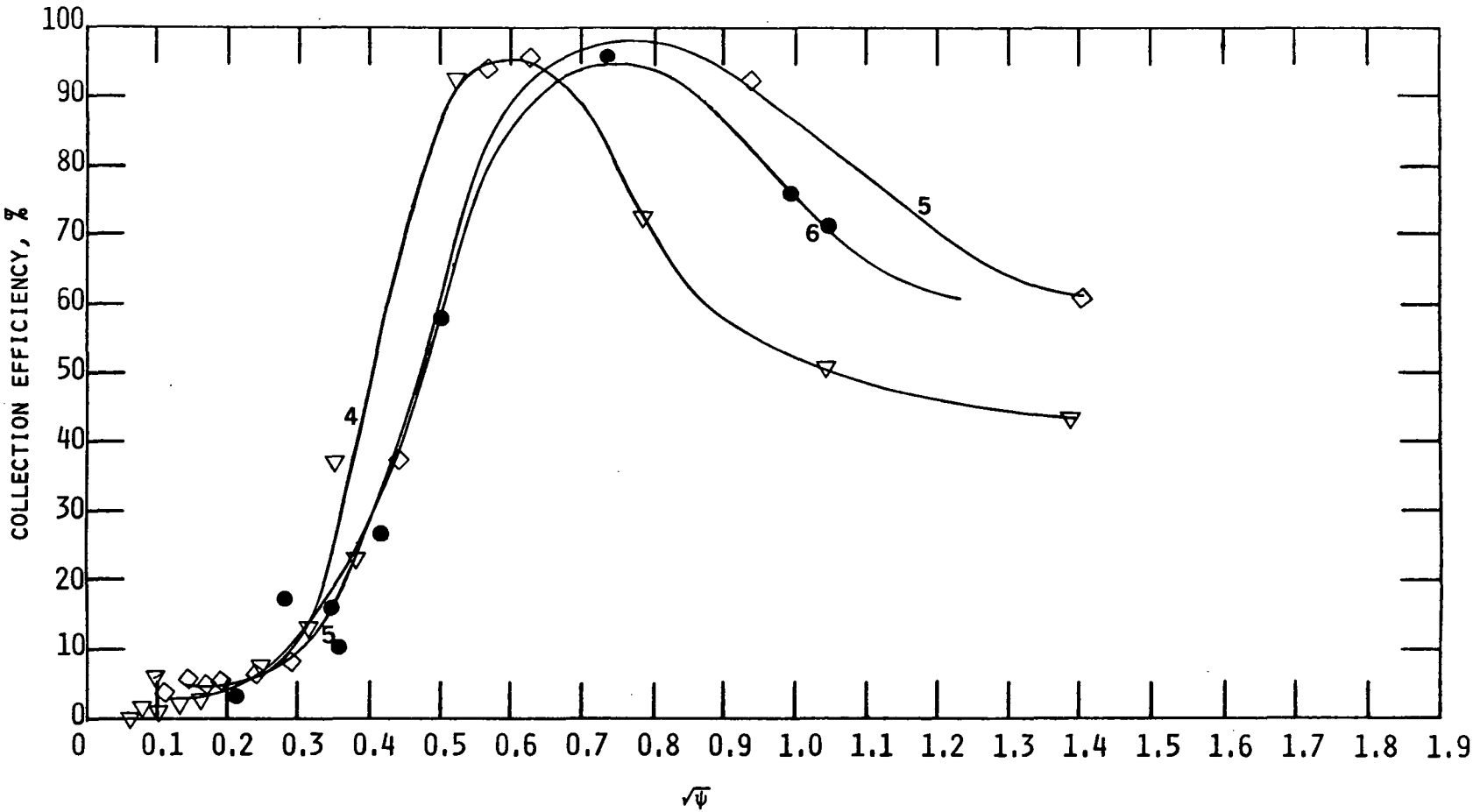

Figure 39. Collection Efficiency (%) Versus $\sqrt{\psi}$
Sierra Model 226 Inertial Cascade Impactor
Stage 4 - Stage 6 Flowrate = 7 LPM
Corrected for Wall Losses

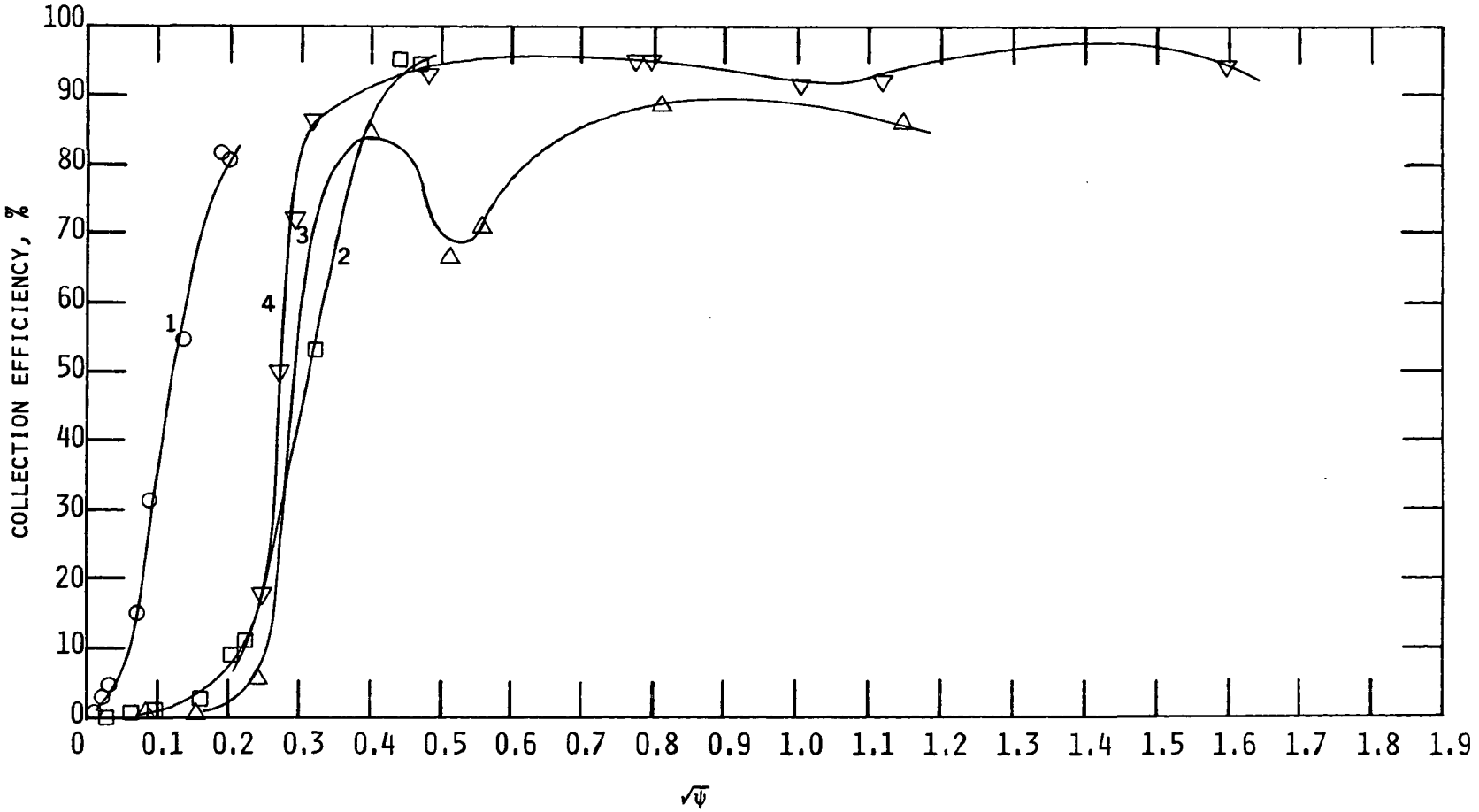

Figure 40. Collection Efficiency (%) Versus $\sqrt{\psi}$
University of Washington Mark III Cascade Impactor
Stage 1 - Stage 4
Corrected for Wall Losses

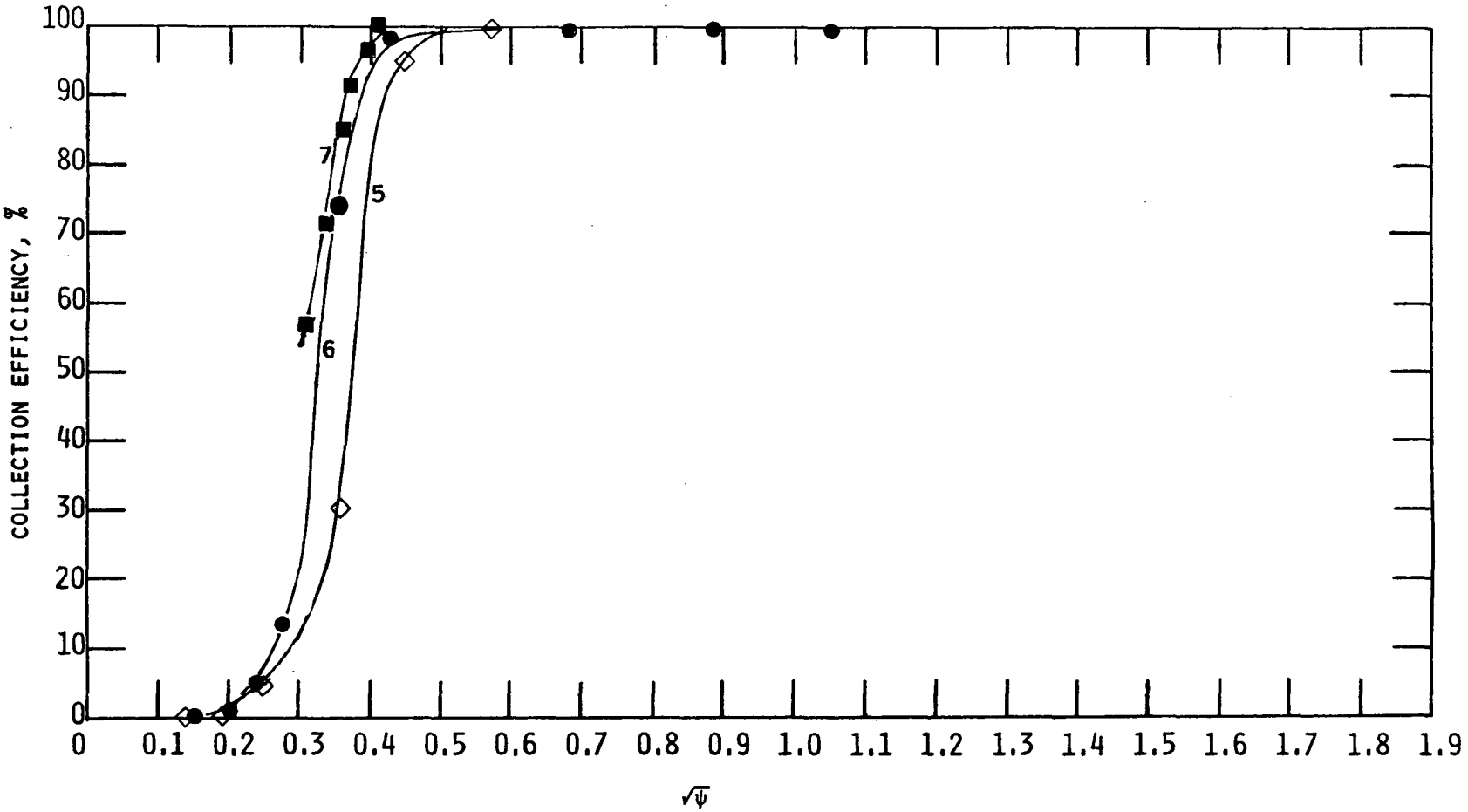

Figure 41. Collection Efficiency (%) Versus $\sqrt{\psi}$
University of Washington Mark III Cascade Impactor
Stage 5 - Stage 7
Corrected for Wall Losses

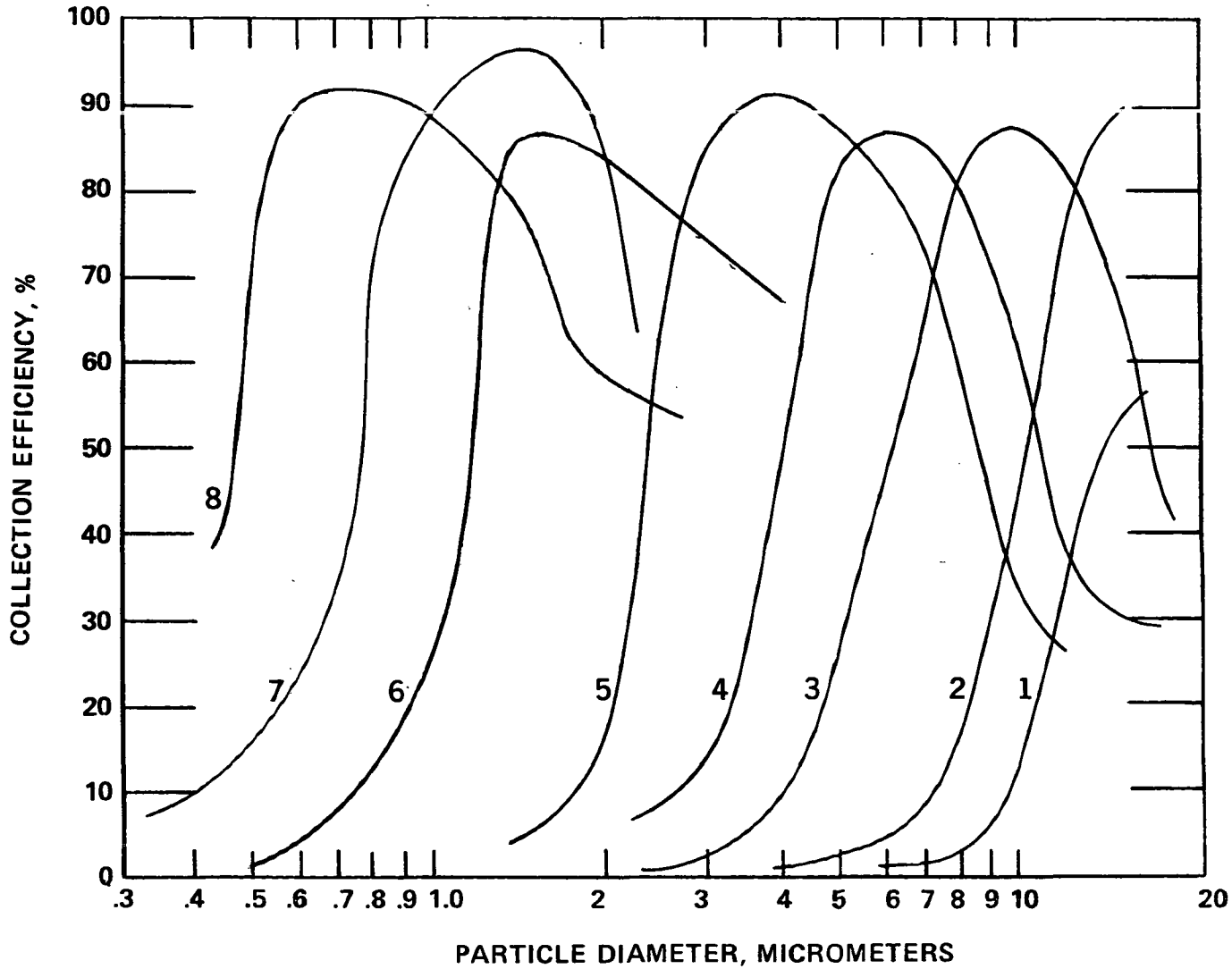

Figure 42. Collection Efficiency (%) Versus Particle Size Andersen Mark III Stack Sampler (Stage 1 - Stage 8) Uncorrected for Wall Losses (14 LPM, 22°C, 29.5"Hg, 1.00 gm/cm^3)

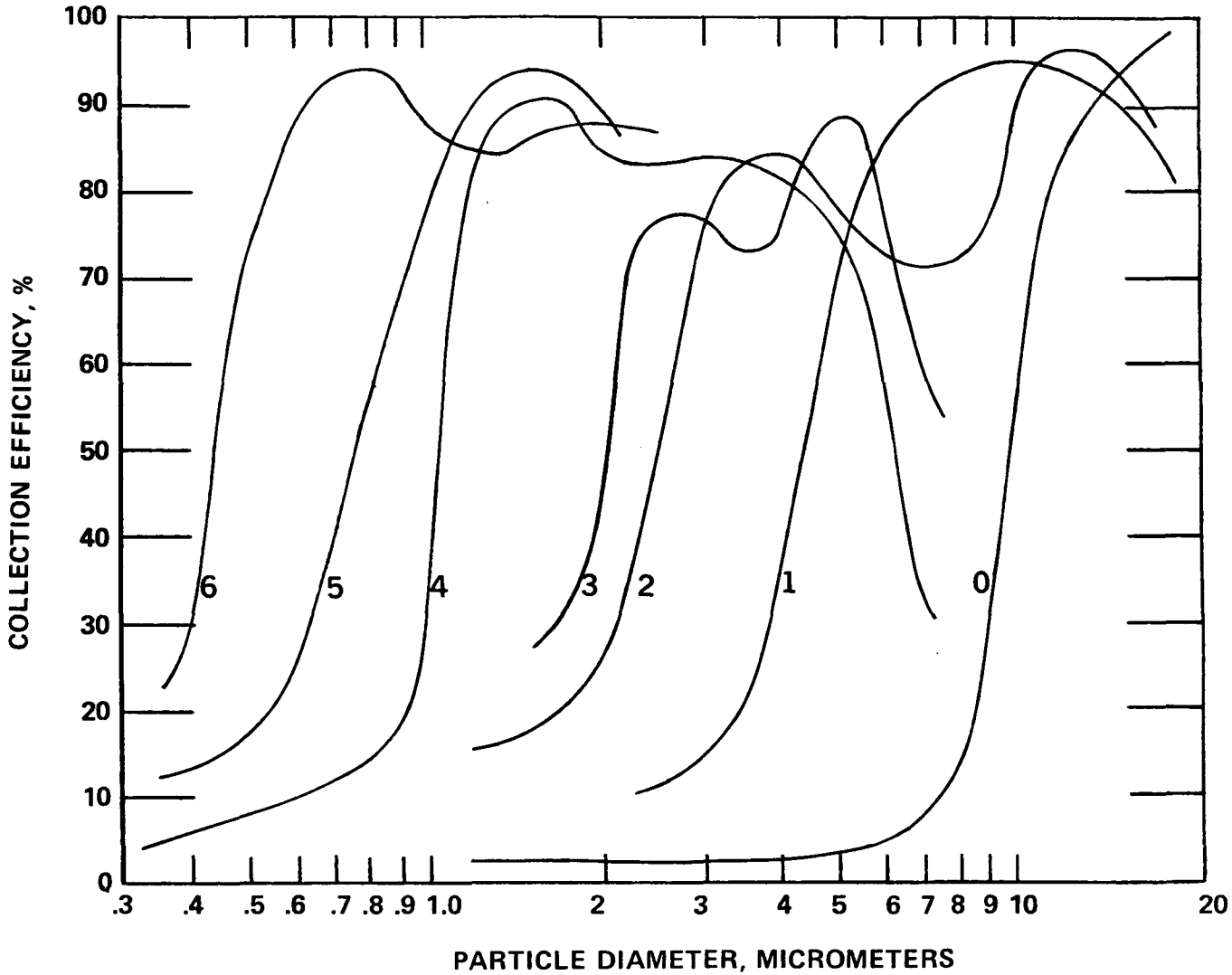

Figure 43. Collection Efficiency (%) Versus Particle Size Modified Brink BMS-11 Cascade Impactor (Glass Fiber Substrates) (Stage 0 - Stage 6) Uncorrected for Wall Losses (0.85 LPM, 22°C, 29.5"Hg, 1.00 gm/cm^3)

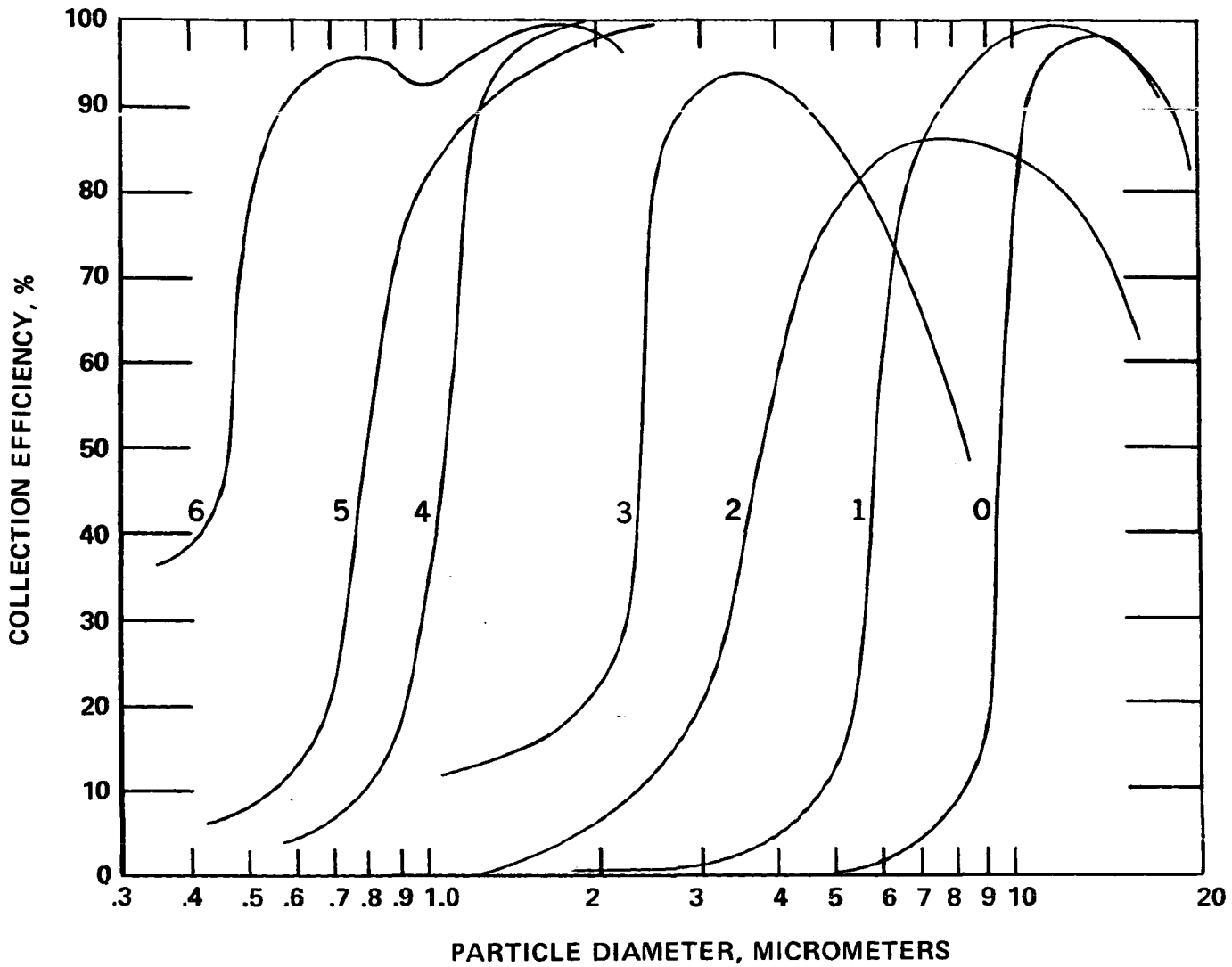

Figure 44. Collection Efficiency (%) Versus Particle Size Modified Brink BMS-11 Cascade Impactor (Greased Collection Plates) (Stage 0 - Stage 6) Uncorrected for Wall Losses (0.85 LPM, 22°C, 29.5"Hg, 1.00 gm/cm^3)

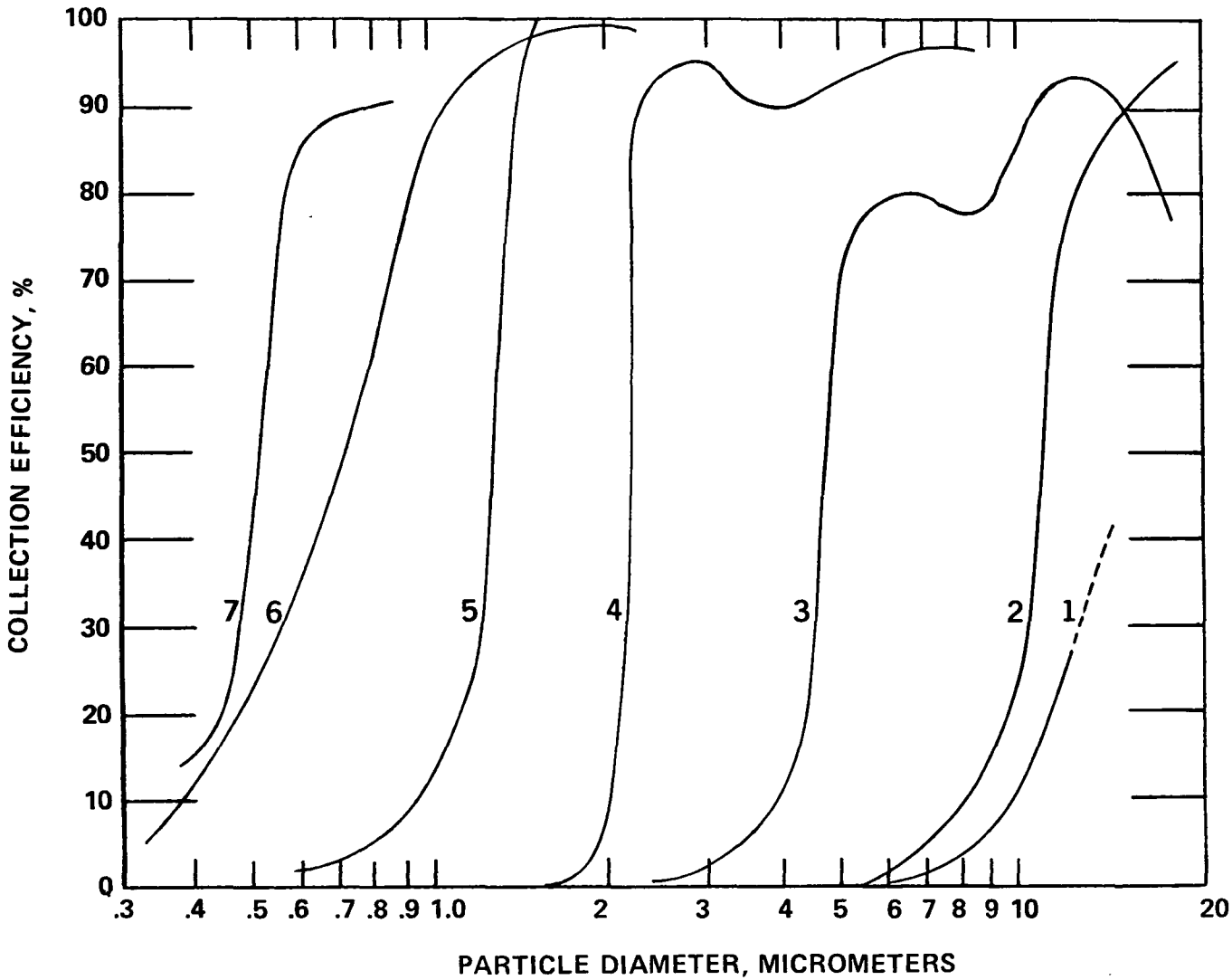

Figure 45. Collection Efficiency (%) Versus Particle Size
MRI Model 1502 Inertial Cascade Impactor
(Stage 1 - Stage 7)
Uncorrected for Wall Losses
(14 LPM, 22°C, 29.5"Hg, 1.00 gm/cm^3)

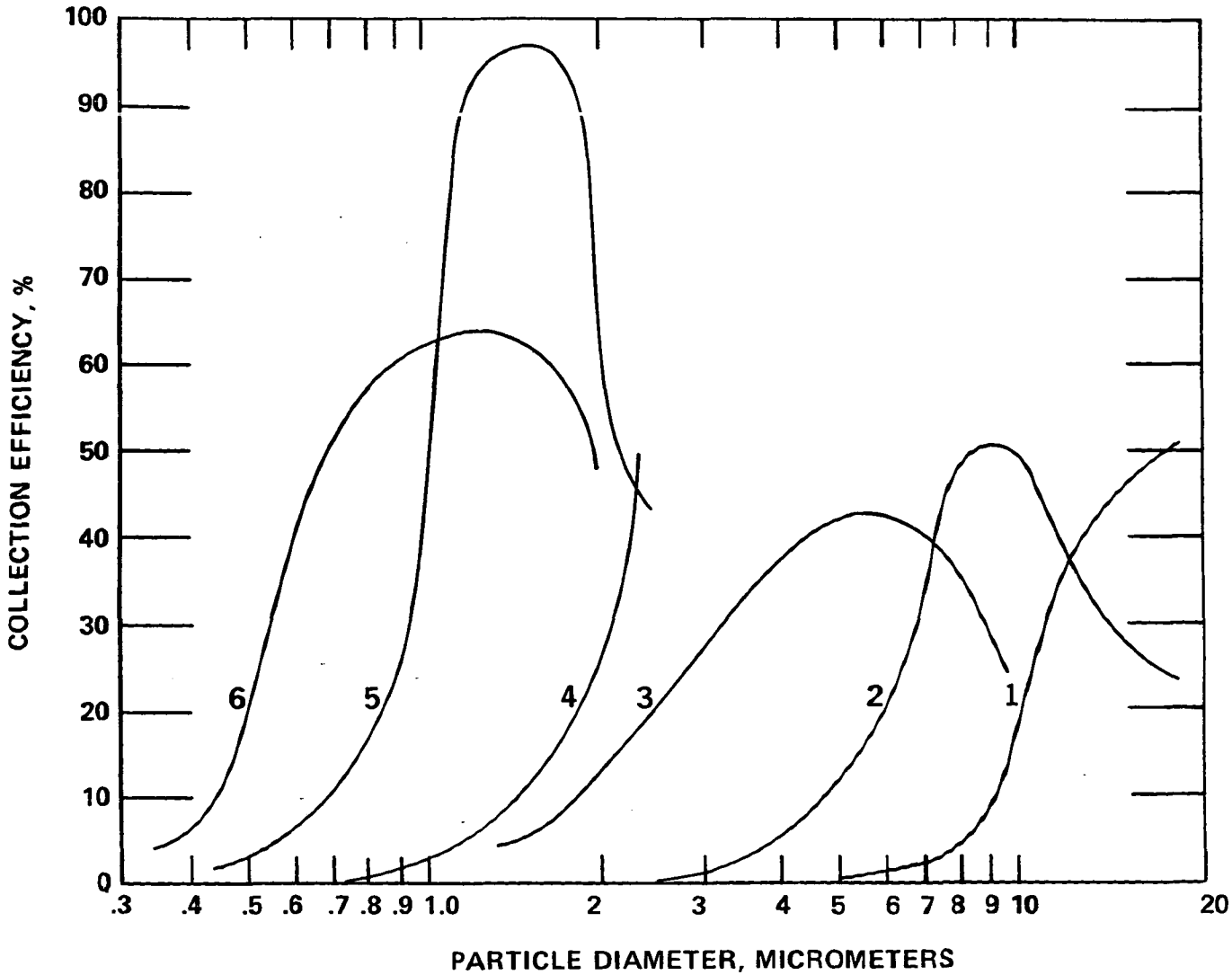

Figure 46. Collection Efficiency (%) Versus Particle Size Sierra Model 226 Source Cascade Impactor (14 LPM, 22°C, 29.5"Hg, 1.00 gm/cm^3) (Stage 1 - Stage 6) Uncorrected for Wall Losses

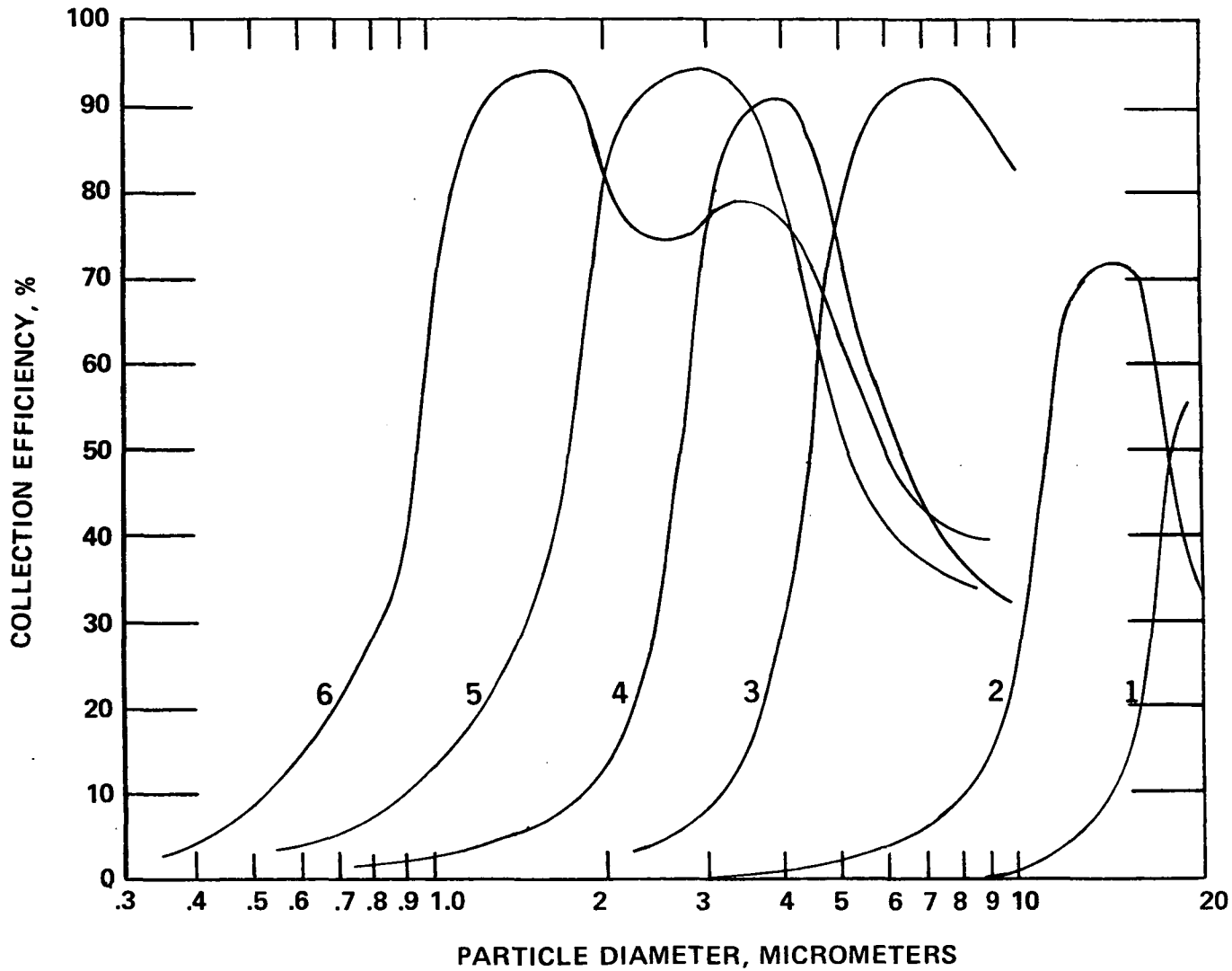

Figure 47. Collection Efficiency (%) Versus Particle Size
Sierra Model 226 Source Cascade Impactor
(7 LPM 22°C, 29.5"Hg, 1.00 gm/cm^3)
(Stage 1 - Stage 6)
Uncorrected for Wall Losses

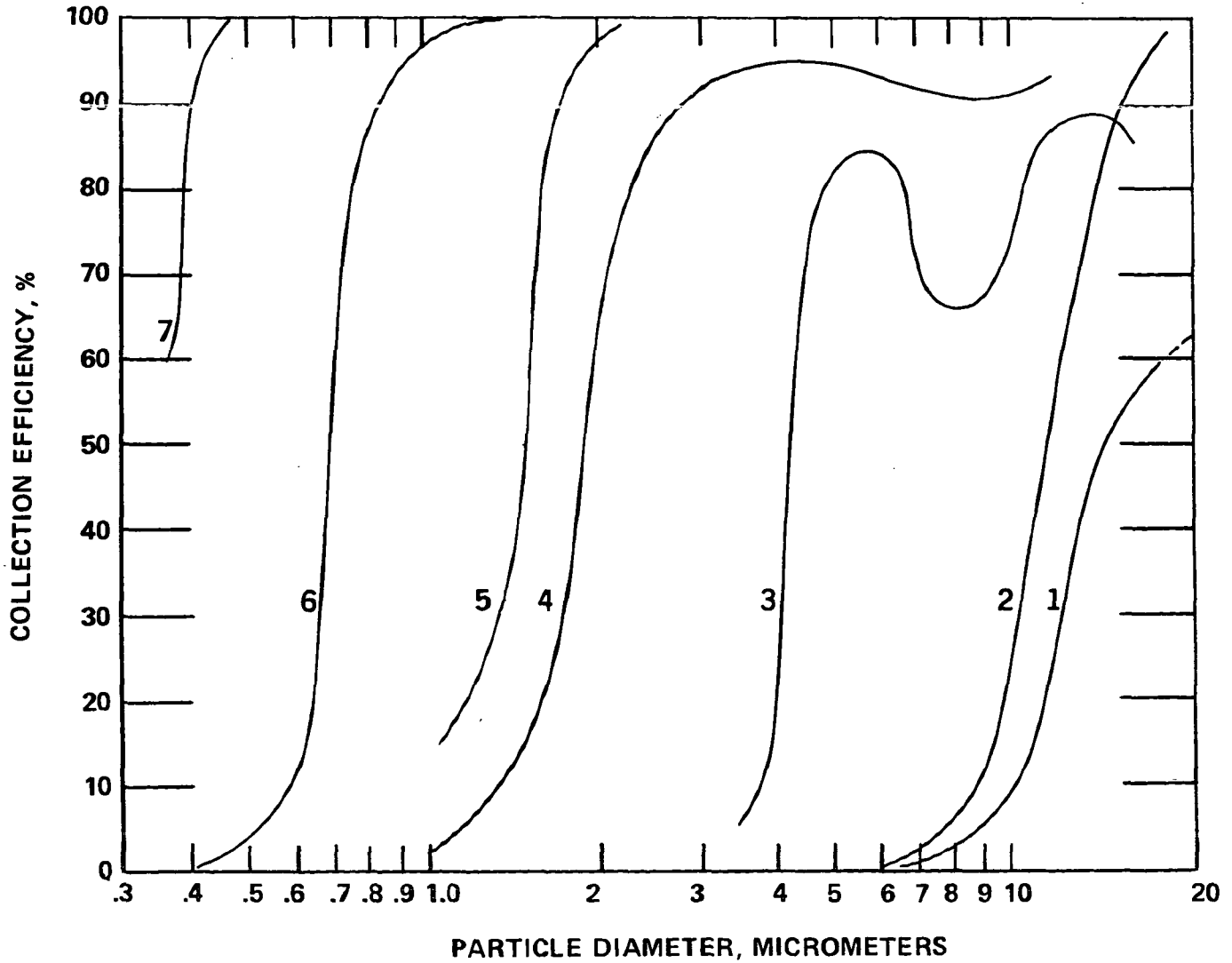

Figure 48. Collection Efficiency (%) Versus Particle Size University of Washington Mark III Cascade Impactor (14 LPM, 22°C, 29.5"Hg, 1.00 gm/cm^3) (Stage 1 - Stage 7) Uncorrected for Wall Losses

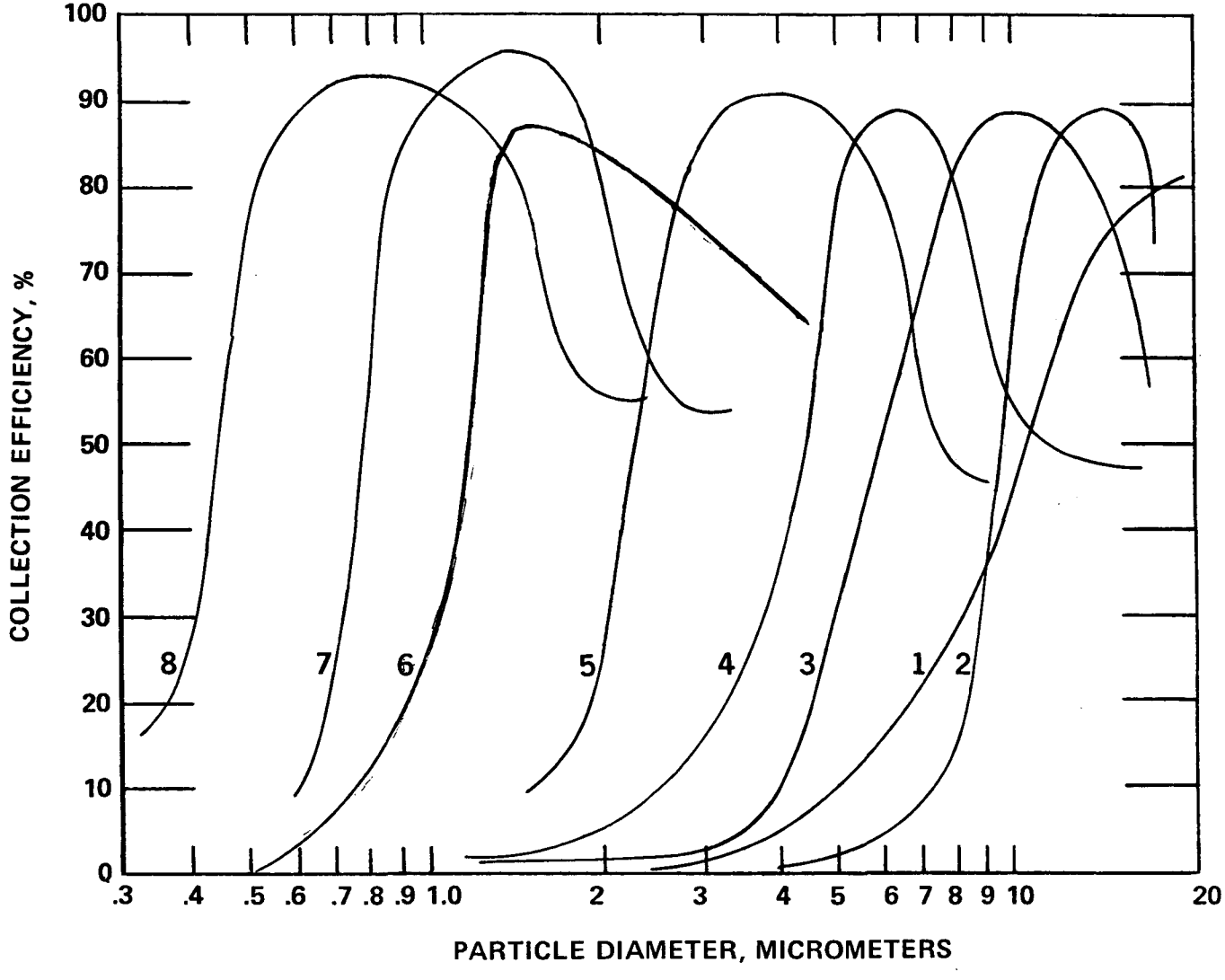

Figure 49. Collection Efficiency (%) Versus Particle Size Andersen Mark III Stack Sampler (Stage 1 - Stage 8)
Corrected for Wall Losses
(14 LPM, 22°C, 29.5"Hg, 1.00 gm/cm^3)

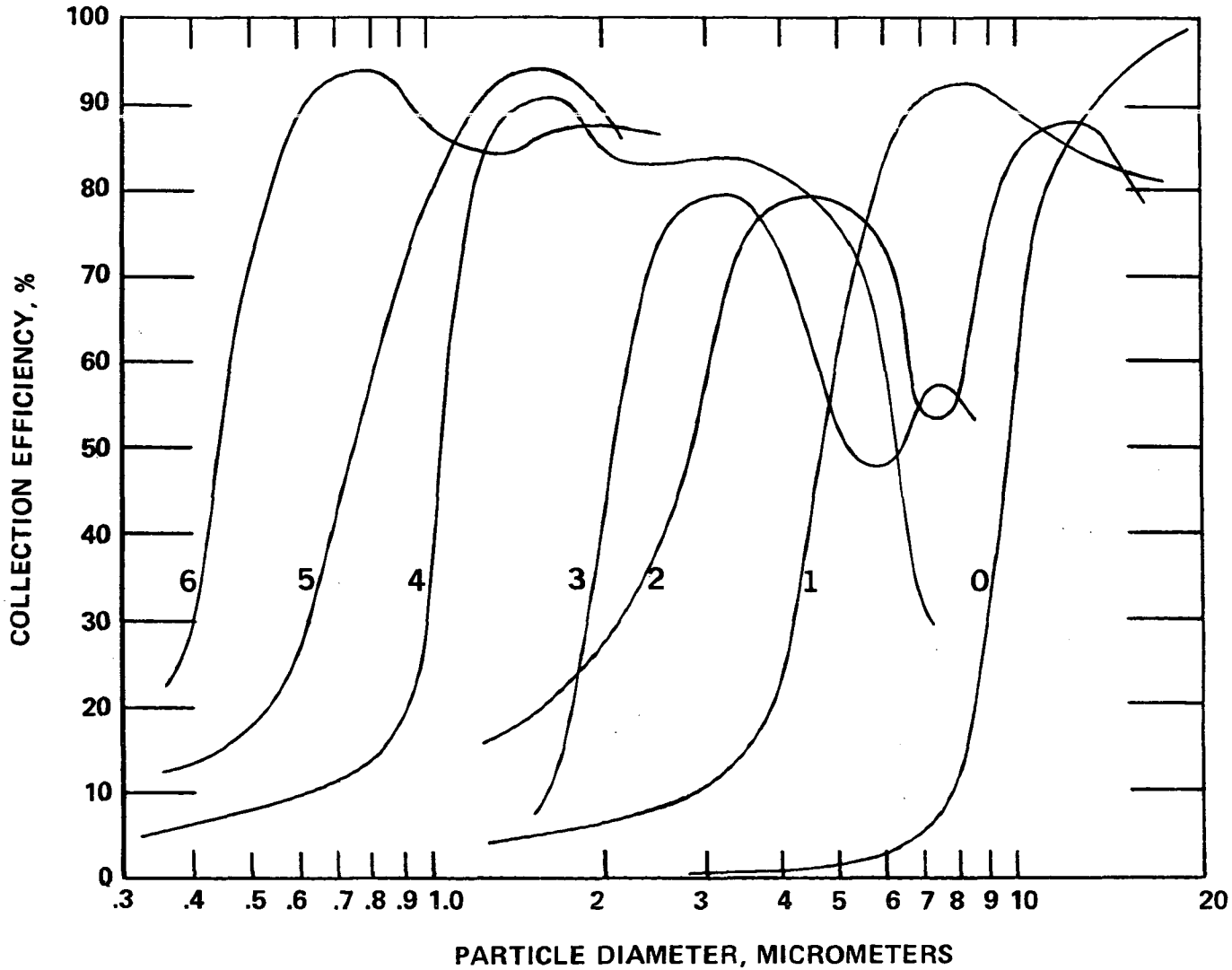

Figure 50. Collection Efficiency (%) Versus Particle Size Modified Brink BMS-11 Cascade Impactor (Glass Fiber Substrates) (Stage 0 - Stage 6) Corrected for Wall Losses (0.85 LPM, 22°C, 29.5"Hg, 1.00 gm/cm^3)

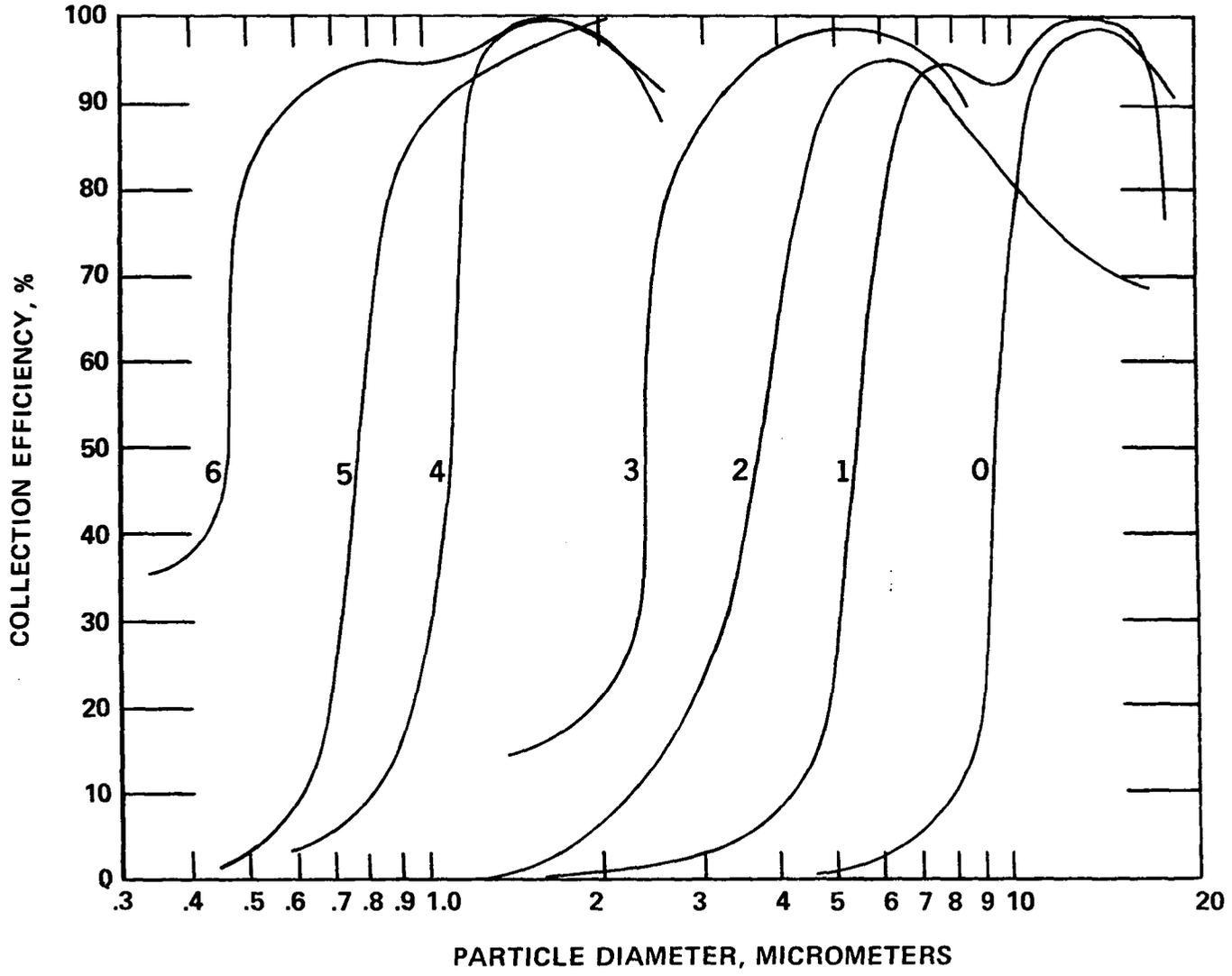

Figure 51. Collection Efficiency (%) Versus Particle Size Modified Brink BMS-11 Cascade Impactor (Greased Collection Plates) (Stage 0 - Stage 6) Corrected for Wall Losses (0.85 LPM, 22°C, 29.5"Hg, 1.00 gm/cm^3)

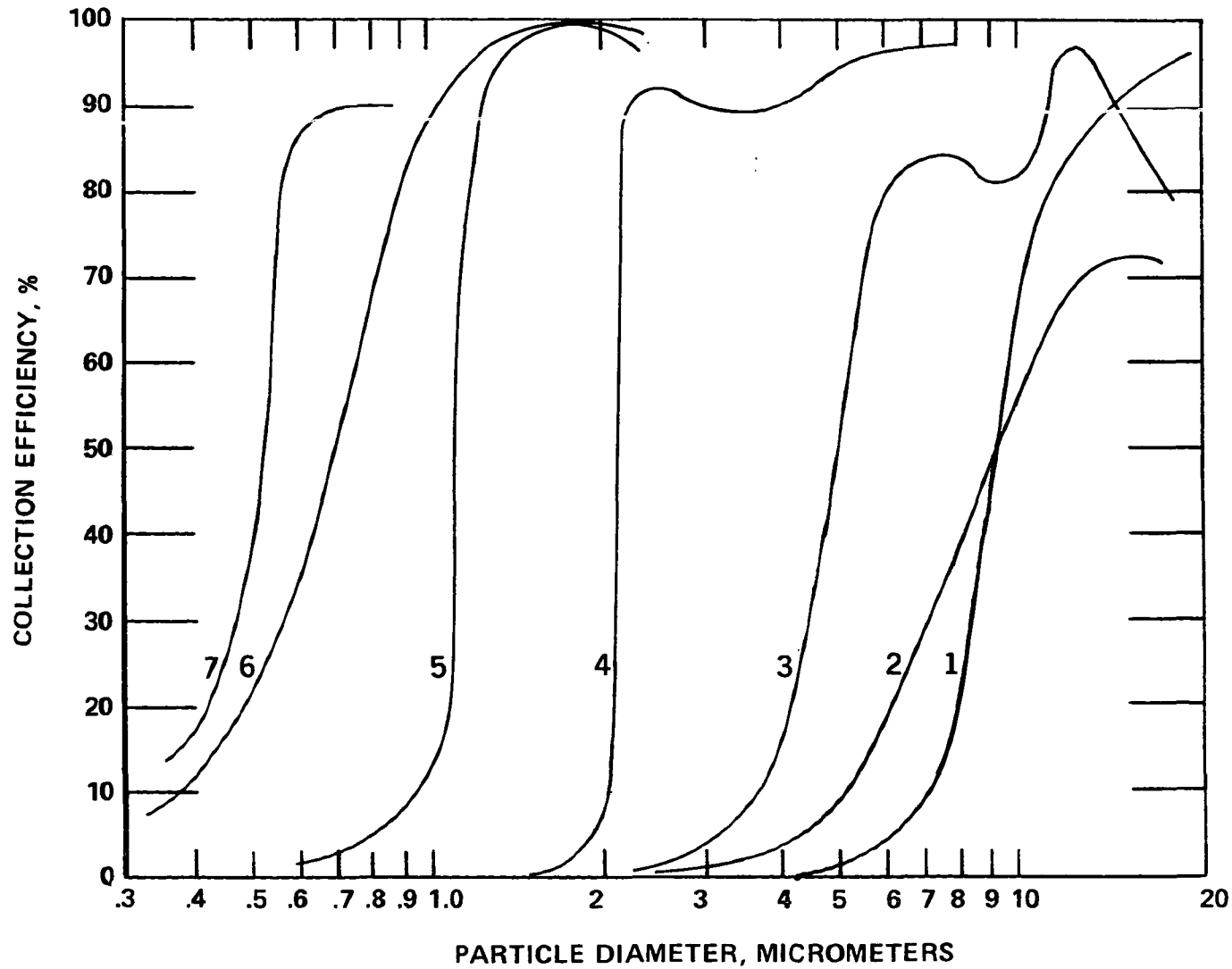

Figure 52. Collection Efficiency (%) Versus Particle Size MRI Model 1502 Inertial Cascade Impactor (Stage 1 - Stage 7) Corrected for Wall Losses (14 LPM, 22°C, 29.5"Hg, 1.00 gm/cm^3)

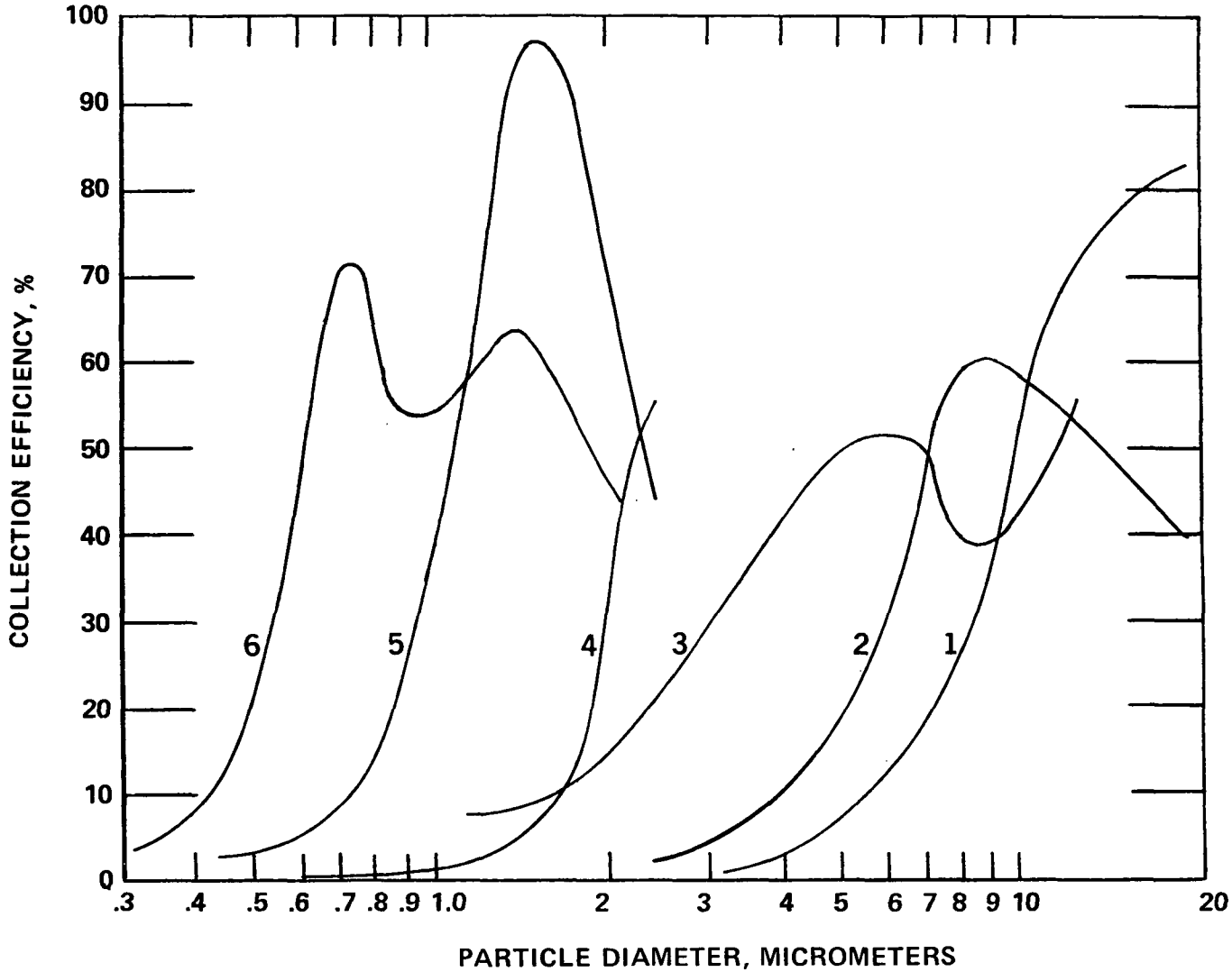

Figure 53. Collection Efficiency (%) Versus Particle Size Sierra Model 226 Source Cascade Impactor (14 LPM, 22°C, 19.5"Hg, 1.00 gm/cm^3) (Stage 1 - Stage 6)
Corrected for Wall Losses

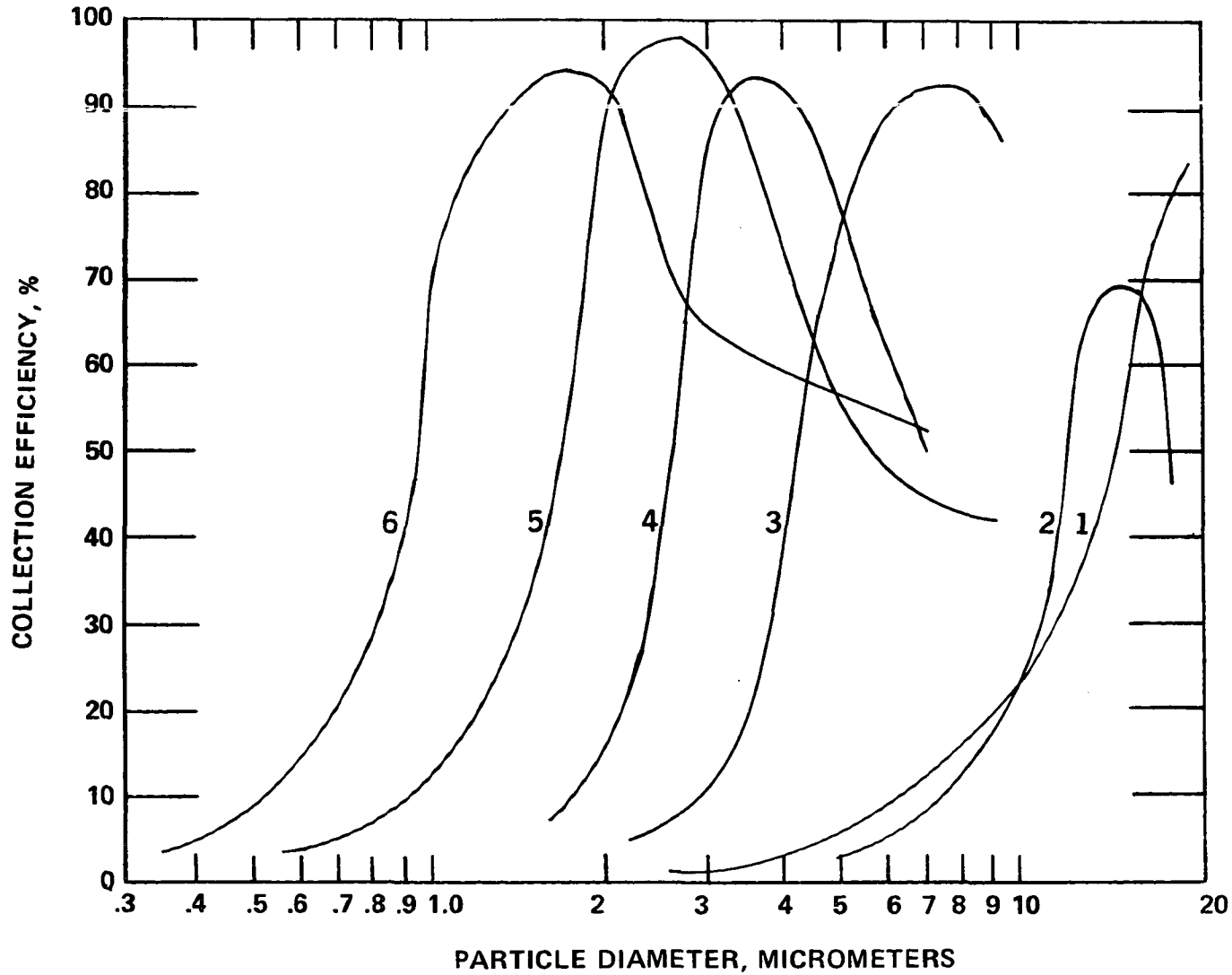

Figure 54. Collection Efficiency (%) Versus Particle Size Sierra Model 226 Source Cascade Impactor (7 LPM, 22°C, 29.5"Hg, 1.00 gm/cm^3) (Stage 1 - Stage 6) Corrected for Wall Losses

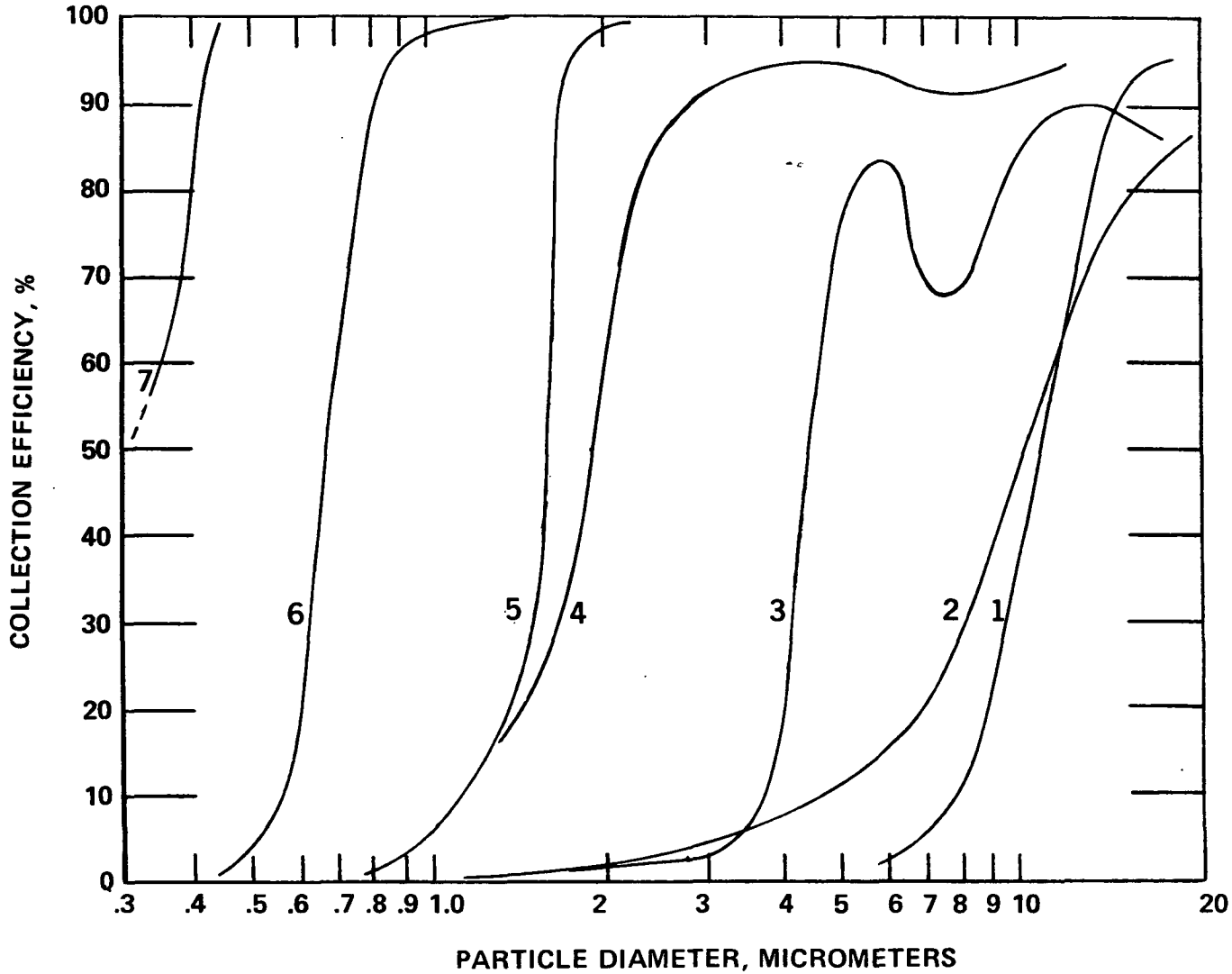

Figure 55. Collection Efficiency (%) Versus Particle Size University of Washington Mark III Cascade Impactor (14 LPM, 22°C, 29.5"Hg, 1.00 gm/cm^3) (Stage 1 - Stage 7) Corrected for Wall Losses

TABLE 7

Square Root of the Stokes Number at 50% Collection Efficiency, $\sqrt{\psi_{50}}$

Uncorrected for Wall Losses

Stage	0	1	2	3	4	5	6	7	8
Andersen		.41	.43	.41	.39	.34	.32	.34	.29
Brink (Glass Fiber)	.31	.28	.27	.38	.37	.40	.27		
Brink (Grease)	.31	.35	.38	.24	.29	.32	.26		
MRI		-	.27	.34	.32	.33	.35	.38	
Sierra (14 LPM)		.44	.47	-	.49	.49	.37		
Sierra (7 LPM)		.42	.47	.36	.44	.46	.44		
U. of W.		.17	.32	.33	.27	.38	.33	-	

Corrected for Wall Losses

Stage	0	1	2	3	4	5	6	7	8
Andersen		.31	.43	.41	.39	.33	.32	.33	.28
Brink (Glass Fiber)	.30	.32	.27	.29	.38	.41	.27		
Brink (Grease)	.32	.35	.38	.34	.26	.33	.27		
MRI		.11	.25	.35	.34	.29	.35	.40	
Sierra (14 LPM)		.33	.42	.65	.49	.42	.43		
Sierra (7 LPM)		.33	.48	.36	.40	.47	.47		
U. of W.		.12	.31	.29	.27	.37	.35	.30	

TABLE 8

Particle Diameter (Micrometer) at 50% Collection Efficiency, D_{p50} for the Conditions Stated in Table 1

Uncorrected for Wall Losses

Stage	0	1	2	3	4	5	6	7	8
Andersen		14.0	10.4	6.1	4.0	2.35	1.20	.76	.46
Brink (Glass Fiber)	9.7	4.3	2.45	2.00	1.05	.76	.43		
Brink (Grease)	9.3	5.8	3.7	2.30	1.05	.78	.46		
MRI		-	11.0	4.7	2.20	1.25	.31	.50	
Sierra (14 LPM)		17.0	8.2	-	2.30	1.00	.67		
Sierra (7 LPM)		18.0	11.0	4.4	2.65	1.70	.95		
U. of W.		14.0	11.2	4.1	1.86	1.57	.67	-	

Corrected for Wall Losses

Stage	0	1	2	3	4	5	6	7	8
Andersen		10.5	9.4	5.8	4.4	2.20	1.20	.70	.43
Brink (Glass Fiber)	9.7	4.7	2.80	2.10	1.05	.75	.44		
Brink (Grease)	9.3	5.4	3.7	2.35	1.10	.76	.46		
MRI		9.1	9.2	4.9	2.10	1.10	.69	.52	
Sierra (14 LPM)		9.8	7.0	5.0	2.20	1.10	.60		
Sierra (7 LPM)		14.5	12.0	4.2	2.55	1.65	.95		
U. of W.		10.5	10.0	4.4	1.86	1.60	.66	.30	

REFERENCES

1. Ranz, W.D., and J. B. Wong. Impaction of Dust and Smoke Particles, Ind. and Eng. Chem., 50, No. 4 (April, 1958).

2. Willeke, K. Performance of the Slotted Impactor. Am. Ind. Hygiene Assoc. J., 683-691, September, 1975.

3. Rao, A. K. Sampling and Analysis of Atmospheric Aerosols. Particle Tech. Lab. Publ. No. 269, Department of Mechanics Engineering; University of Minnesota, Minneapolis, Minnesota 55455, June 1975.

4. Fuchs, N. A. (1964) The Mechanics of Aerosols, Pergamon Press, New York.

5. Marple, V. A. A Fundamental Study of Inertial Impactors. Ph.D. Thesis, Mechanical Engineering Department, University of Minnesota, Minneapolis, Minnesota 55455, 1970.

6. Berglund, R. N., and B.Y.H. Liu. Generation of Monodisperse Aerosol Standards. Environmental Science and Technology, Vol. 6, No. 2, 1973.

7. Lindblad, N. R., and J. M. Schneider. Production of Uniform-Sized Liquid Droplets. J. Sci. Instru., Vol. 42, 1965.

8. Strom, L. The Generation of Monodisperse Aerosols by Means of a Disintegrated Jet of Liquid. Rev. Sci. Instr., Vol. 40, No. 6, 1969.

9. Stober, W., and H. Flachsbart. An Evaluation of Ammonium Fluorescein as a Laboratory Aerosol. Atmos. Environ. Vol. 7, 1973.

10. Calvert, S. Cascade Impactor Calibration Guidelines. EPA-600/2-76-118, U. S. Environmental Protection Agency, Research Triangle Park, N.C., 1976.

11. Jaericke, R., and I. H. Blifford. The Influence of Aerosol Characteristics on the Calibration of Impactors. Journal of Aerosol Science, 5(5):457-464, 1974.

TECHNICAL REPORT DATA
(Please read Instructions on the reverse before completing)

1. REPORT NO.	2.	3. RECIPIENT'S ACCESSION NO.
EPA-600/2-76-280		

4. TITLE AND SUBTITLE	5. REPORT DATE
Particulate Sizing Techniques for Control Device Evaluation: Cascade Impactor Calibrations	October 1976
	6. PERFORMING ORGANIZATION CODE: SORI-EAS-76-653
7. AUTHOR(S): Kenneth M. Cushing, George E. Lacey, Joseph D. McCain, and Wallace B. Smith	8. PERFORMING ORGANIZATION REPORT NO.
9. PERFORMING ORGANIZATION NAME AND ADDRESS: Southern Research Institute, 2000 Ninth Avenue, South, Birmingham, Alabama 35205	10. PROGRAM ELEMENT NO.: 1AB012; ROAP 21ADM-011
	11. CONTRACT/GRANT NO.: 68-02-0273
12. SPONSORING AGENCY NAME AND ADDRESS: EPA, Office of Research and Development, Industrial Environmental Research Laboratory, Research Triangle Park, NC 27711	13. TYPE OF REPORT AND PERIOD COVERED: Final; 3/73-7/76
	14. SPONSORING AGENCY CODE: EPA-ORD

15. SUPPLEMENTARY NOTES: IERL-RTP project officer for this report is D. B. Harris, 919/549-8411 Ext 2557, Mail Drop 62. EPA-650/2-74-102a was previous report in this series.

16. ABSTRACT: The report gives results of a calibration study to determine sizing parameters and wall losses for five commercially available cascade impactors. A vibrating-orifice aerosol generator was used to produce monodisperse ammonium fluorescein aerosol particles 15 to 1 micrometers in diameter. A pressurized Collison Nebulizer system was used to disperse Dow Corning polystyrene latex (PSL) spheres 2 to 0.46 millimeters in diameter. When ammonium fluorescein was used, the mass collected by each impactor surface was determined using absorption spectrophotometry of washes from the various surfaces. When sizing with the PSL spheres, a Climet Instruments Model 208A Particle Analyzer was used to determine particle number concentrations at the inlet and the outlet of the test impactor. Results are reported showing stage collection efficiency as a function of the square root of the Stokes number, stage collection efficiency as a function of particle size, and impactor wall losses (total, nozzle, and inlet cone) as a function of particle size. It has been determined that the values of the Stokes number for the 50% collection efficiency are not generally the same for each impactor stage. A table of these values is presented. Published theories do not successfully predict these values, so empirical calibration is required before these devices can be used accurately in the field or laboratory.

17. KEY WORDS AND DOCUMENT ANALYSIS

a. DESCRIPTORS	b. IDENTIFIERS/OPEN ENDED TERMS	c. COSATI Field/Group
Air Pollution Aerosols Dust Measurement Calibrating Impactors Stokes Law (Fluid Mechanics)	Air Pollution Control Stationary Sources Particulates Cascade Impactors	13B 07D 20D 11G 14B

18. DISTRIBUTION STATEMENT	19. SECURITY CLASS *(This Report)*	21. NO. OF PAGES
Unlimited	Unclassified	94
	20. SECURITY CLASS *(This page)* Unclassified	22. PRICE

EPA Form 2220-1 (9-73)